LEABHARLANN CHOLÁISTE NA TRÍONÓIDE, BAILE ÁTHA CLIATH | TRINITY COLLEGE LIBRARY DUBLIN
Ollscoil Átha Cliath | The University of Dublin

**Terms and Conditions of Use of Digitised Theses from Trinity College Library Dublin**

**Copyright statement**

All material supplied by Trinity College Library is protected by copyright (under the Copyright and Related Rights Act, 2000 as amended) and other relevant Intellectual Property Rights. By accessing and using a Digitised Thesis from Trinity College Library you acknowledge that all Intellectual Property Rights in any Works supplied are the sole and exclusive property of the copyright and/or other IPR holder. Specific copyright holders may not be explicitly identified. Use of materials from other sources within a thesis should not be construed as a claim over them.

A non-exclusive, non-transferable licence is hereby granted to those using or reproducing, in whole or in part, the material for valid purposes, providing the copyright owners are acknowledged using the normal conventions. Where specific permission to use material is required, this is identified and such permission must be sought from the copyright holder or agency cited.

**Liability statement**

By using a Digitised Thesis, I accept that Trinity College Dublin bears no legal responsibility for the accuracy, legality or comprehensiveness of materials contained within the thesis, and that Trinity College Dublin accepts no liability for indirect, consequential, or incidental, damages or losses arising from use of the thesis for whatever reason. Information located in a thesis may be subject to specific use constraints, details of which may not be explicitly described. It is the responsibility of potential and actual users to be aware of such constraints and to abide by them. By making use of material from a digitised thesis, you accept these copyright and disclaimer provisions. Where it is brought to the attention of Trinity College Library that there may be a breach of copyright or other restraint, it is the policy to withdraw or take down access to a thesis while the issue is being resolved.

**Access Agreement**

By using a Digitised Thesis from Trinity College Library you are bound by the following Terms & Conditions. Please read them carefully.

I have read and I understand the following statement: All material supplied via a Digitised Thesis from Trinity College Library is protected by copyright and other intellectual property rights, and duplication or sale of all or part of any of a thesis is not permitted, except that material may be duplicated by you for your research use or for educational purposes in electronic or print form providing the copyright owners are acknowledged using the normal conventions. You must obtain permission for any other use. Electronic or print copies may not be offered, whether for sale or otherwise to anyone. This copy has been supplied on the understanding that it is copyright material and that no quotation from the thesis may be published without proper acknowledgement.

# Perception of True Linear Self-Motion using Vestibular Stimulation in Humans: A Mathematical Electrophysiological Analysis

PhD Thesis

Hugh Nolan

Student Number 08129207

Supervisor

Professor Richard Reilly

I declare that this thesis has not been submitted as an exercise for a degree at this or any other University, and it is entirely my own work.

I agree that the Library may lend or copy the thesis upon request.

Thesis 10308

# Summary

In humans, the percept of motion is a combination of multiple sensory modalities, primarily involving vestibular, visual and somatosensory (Ohmi, 1996). The ability to properly perceive motion enables us to function normally within society; conversely, impaired motion processing puts people at risk of falls and injury (Warren et al., 1989). The integration of vestibular information happens at multiple hierarchical levels from brainstem to cortex. Our understanding of the neural substrates which underlie vestibular processing and motion perception is limited (Blanke and Lopez 2010). Multisensory integration is known to be inefficient in fallers (Setti et. al, 2011) while vestibular organs degrade and produce less reliable information, inducing compensatory mechanisms which rely on multisensory integration (Pfaltz, 1983; Sadeghi et al., 2011). The interaction between ageing and processing of vestibular information is not straightforward or fully understood.

The main aim of this thesis was to provide a basis for further study of vestibular processing and the neural substrates underlying this, using true motion stimulation. This was achieved using high-density electroencephalography (EEG) to record the neural responses during motion stimuli. EEG allows for recording with high temporal precision, and using a high-density setup increases spatial resolution such that the responses recorded can be viewed in the context of previous literature. True movement is a more ecologically natural motion stimulus – the use of a Stewart platform with 6 degrees of freedom (Stewart, 1966) for motion simulation allowed participants to experience true motion stimuli, and to target linear motion processing. The use of EEG was a key part in this setup, as the equipment was small enough to mount on a table in the simulator.

To assess the feasibility of the concept, the first experiment investigated the influence of using a Stewart motion platform on EEG recordings. The task was unrelated to the motion the participants underwent. This enabled the comparison of the effect of various motion conditions on the event-related potentials (ERPs). It was found that there was no significant effect of motion condition on the ERPs recorded, and further analysis of the time-series data did not reveal any unusual effect of the motion, and so it was concluded to be a viable methodology for EEG experimentation.

Following the initial studies, the potential of recording ERPs in response to the motion was investigated. The P3 is a well-known ERP component arising from improbable

events and is considered to occur independently of stimulus modality (Katayama and Polich, 1996; Polich, 2007). This provided a starting tool for exploring the use of true motion as a stimulus in EEG. An experiment was designed using 45° angle non-visual motion stimuli presented in a standard paradigm. The results showed that a readily-identifiable P3 component was evoked and distinguishable. This demonstrates that the neural response to motion stimuli is similar to other stimulus modalities, and also provides an easily accessible biomarker for indexing motion processing on the cognitive level.

Once it had been ascertained that the P3 response recorded was valid, a further experiment designed to evoke the response to non-visual passive self-motion was performed. Participants were translated forwards and backwards on the Stewart platform, and ERPs to both the forwards and backwards motions were computed. The responses were analysed in the time and frequency domains, and back-projected to a prototypical cortex to determine the sources of the neural activity (Pascual-Marqui, 2002). These responses were localized to areas associated with multisensory processing which showed concordance with literature from PET and fMRI studies, and revealed non-linear responses to acceleration.

Throughout the course of the thesis, there was need for a considerable amount of EEG data to be processed, with artifacts of muscle and eye movement due to the vestibular reflex circuits. Thus an automated EEG processing and artifact removal process called FASTER was developed, published, and made available within a popular EEG processing framework.

The aims of the thesis were addressed - EEG has been seen as suitable to record responses to the novel true motion stimulus used, and the responses have been characterised. The P3 has well-known properties and therefore has potential for use as an index of motion processing ability. The responses to the true motion stimuli reveal nonlinear processing in the vestibular system which has intrinsic connectivity with the visual system. The results are in agreement with literature and provide further knowledge of motion processing and the role of vestibular information. Further research based upon the conclusions made is discussed, along with some potential for practical use-cases. A number of novel methods for processing EEG data were also developed during the course of the thesis and have been made publicly available.

# Acknowledgements

This thesis was not a solo effort; help came along the way from many, many people.

First and foremost, I would like to acknowledge the continuing invaluable help and support of my supervisor, Prof. Richard Reilly, whose organisation and dedication enabled this whole project to succeed. I am forever grateful.

My sincere thanks go to Dr. John Butler, for his aid in planning these experiments, setting up the motion platform, and on-going input to the resulting journal papers. I am also indebted to Dr. Robert Whelan, for his help with these experiments and bringing me up to speed with EEG, ERP analysis, and general PhD life.

None of this would have been possible without the use of the motion platform, and so I would like to thank Prof. Heinrich Bülthoff for the kind use of his facilities at the Max Planck Institute for Biological Cybernetics.

I would like to gratefully acknowledge the generous funding provided to me by IRCSET and Trinity College Dublin.

I wouldn't have finished this without Caoimhe, who kept me *balanced* enough to finish it. I couldn't have done it without you. Thank you so much!

To all my friends, fellow students, colleagues and family, thank you all for helping me keep a great social life - especially through the writing process!

**This thesis is dedicated to my parents, who have always done everything possible to support me. I can't ever thank you enough!**

# Table of Contents

Abstract

Chapter 1: Introduction

1.1 Background

1.2 Thesis Aims

1.3 Contributions of the Thesis

1.4 Publications Arising from the Thesis

Chapter 2: Literature Review

2.1 Peripheral Vestibular Anatomy

2.2 Central Vestibular Anatomy

2.3 Clinical Implications of Vestibular Dysfunction

2.4 Neuroimaging of the Vestibular System

2.5 Electroencephalography

2.6 Self-motion Perception

2.7 Questions from Literature Review

Chapter 3: General Thesis Methods

3.1 Linear Motion Stimuli

3.2 EEG Recording

3.3 EEG Pre-processing

3.4 Independent Component Analysis

3.5 sLORETA

3.6 SPM

3.7 Time-Frequency Methods

Chapter 4: FASTER – Fully Automated Statistical Threshold for EEG Artifact Rejection

4.1 Introduction

4.2 Methods for EEG Data Collection

4.3 Methods for Artifact Detection and Removal

4.4 Results

4.5 Discussion

4.6 Appendix A – Additional Methods

4.7 Appendix B – Multiple Sclerosis Studies

4.8 Appendix C – EEG-fMRI

4.9 Appendix D - Electrophysiological Comparison of Vasovagal Syncope in Young and Old Adults

Chapter 5: Acquisition of EEG Data on a Stewart Platform

5.1 Introduction

5.2 Methods

5.3 Results

5.4 Discussion

Chapter 6: Vestibular P3

6.1 Introduction

6.2 Methods

6.3 Results

6.4 Discussion

Chapter 7: True Motion Vestibular Evoked Potential

7.1 Introduction

7.2 Methods

7.3 Results

7.4 Discussion

Chapter 8: Discussion

8.1 Thesis Aims

8.2 Validity of Vestibular Electrophysiology using EEG

8.3 Vestibular Electrophysiology using EEG

8.4 Vestibular Function and Ageing

8.5 Future Work Inspired by the Thesis

8.6 Conclusion

Bibliography

Published Works

# Glossary of terms

| | |
|---|---|
| AMICA | Adaptive Mixture ICA (ICA method) |
| aVOR | Angular Vestibulo-Ocular Reflex |
| BCG | Ballistocardiography |
| BPPV | Benign Positional Paroxysmal Vertigo |
| CCR | Cervico-Collic Reflex |
| EEG | Electroencephalography |
| EMG | Electromyography |
| EOG | Electrooculography |
| ERP | Event-Related Potential |
| ERSP | Event-Related Spectral Perturbation |
| FASTER | Fully Automated Statistical Thresholding for EEG Artifact Rejection |
| FDR | False Discovery Rate |
| FFT | Fast Fourier Transform |
| fMRI | Functional Magnetic Resonance Imaging |
| FWE | Family-Wise Error (control) |
| GVS | Galvanic Vestibular Stimulation |
| HUT | Head-Up Tilt Test |
| IC | Independent Component |
| ICA | Independent Component Analysis |
| IPL | Inferior Parietal Lobule |

| | |
|---|---|
| IPS | Intra-Parietal Sulcus |
| InfoMax | Information Maximization (ICA method) |
| LORETA | Low-Resolution Exact Tomography |
| lVOR | Linear Vestibulo-Ocular Reflex |
| MNI | Montreal Neurological Institute (standardised brain space) |
| MRI | Magnetic Resonance Imaging |
| MS | Multiple Sclerosis |
| MST | Middle Superior Temporal (gyrus) |
| MT | Middle Temporal (gyrus) |
| PCA | Principal Component Analysis |
| PET | Positron Emission Tomography |
| PIVC | Parieto-Insular Vestibular Cortex |
| ROI | Region of Interest |
| SCC | Semicircular Canal |
| sLORETA | Standardized Low-Resolution Exact Tomography |
| SNR | Signal-to-Noise Ratio |
| SPM | Statistical Parametric Mapping |
| SnPM | Statistical Non-Parametric Mapping |
| SPL | Superior Parietal Lobule |
| TWI | Temporal Window of Integration |
| VCR | Vestibulo-Collic Reflex |
| VEP | Visual Evoked Potential |
| VESPA | Visual Evoked Spread Spectrum Analysis |

| | |
|---|---|
| VIP | Ventral-Intraparietal Cortex |
| VOR | Vestibulo-Ocular Reflex |
| VSR | Vestibulo-Spinal Reflex |
| VSyR | Vestibulo-Sympathetic Reflex |
| VVS | Vasovagal Syncope |
| WHO | World Health Organisation |

# Chapter 1

# Introduction

## 1.1 Background

Our sense of position in our environment and our ability to interact with and navigate through the world are core elements of our sense of self, body possession and daily function. Everyday activities such as walking, sitting, standing and talking to others require knowledge of where one's own body is within its environment, and knowledge of the boundaries of the body and its interface with the external world. To co-ordinate these activities, our brain and body must use information incoming from a wide range of sensory systems, at varying time-frames, and stitch them together to portray a cohesive picture of the external world. This function of multisensory integration is a complex computational process that the healthy brain excels at, but is difficult to perform artificially and efficiently in e.g. industrial automation or robotics applications.

To create a representation of the environment and our position in it, sensory input from a range of sensory systems is integrated - the visual, proprioceptive, somatosensory and vestibular systems are the main systems involved. Of particular importance is the vestibular system, which is the sensory system that detects rotational and linear acceleration that the body is undergoing, providing critical information about body movement; it is commonly referred to as the sense of balance. As movement is composed of periods of acceleration, constant velocity and deceleration, the vestibular system provides key information about the motion our body is undergoing. Furthermore, gravity is a constant acceleration our body undergoes at all time,

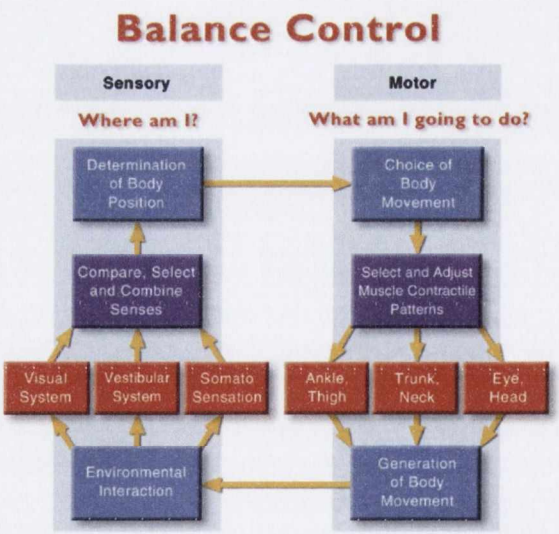


**Figure 1.1. Example of general balance and motor control flow including sensory input and effector output.**

which provides us with an anchor to the ground and the world surrounding us; astronauts require considerable training to habituate to the lack of this constant sensory input. The vestibular sense is not considered to be consciously registered - we do not knowingly perceive the acceleration we are undergoing, but we may viscerally "feel" it as a lurching of the stomach, particularly at high amplitudes (Angelaki et al., 2009). This is due to the vestibular system's highly multisensory nature (Angelaki and Cullen, 2008).

The vestibular system's representation in the brain is currently poorly mapped in humans. Some advances have been made using artificial methods of stimulation, but literature on neural processing of true motion in humans is sparse. As integration of vestibular input is very important for development of internal and external spatial mapping strategies (Brandt et al., 2005; Grabherr et al., 2011), which are fundamental functions for interaction with the environment and for developing and maintaining normal body identity (Yen Pik Sang et al., 2006), furthering our understanding of how the brain processes vestibular input is highly relevant to understanding how humans create a representation of ourselves and how we plan and execute environmental and object interactions.

There is background to compare against in animal literature. Early work primarily involved the investigation of cats' vestibular function at the peripheral organ and brain-stem level. More recently, the work of Angelaki, Gu and DeAngelis has made considerable ground in investigation of cortical areas involved in processing vestibular and visual-vestibular interaction in macaque monkeys during tasks such as representation of motion and detection of direction of motion, or heading. These insights are valuable as they provide templates for comparison of human data; while it is not possible to draw general inference on human cortical architecture based on monkey data, particularly at the functional level, structural homologies between the species are common and can guide research in human neuroimaging studies.

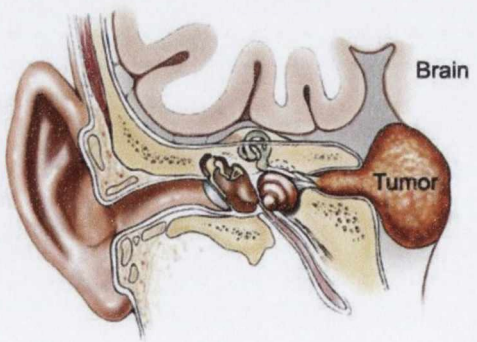


**Figure 1.2. A vestibular schwannoma, also known as an acoustic neuroma, is a benign tumour formed in the vestibulocochlear cranial nerve.**

Disorders of the vestibular system tend to manifest as unusual dizziness, inappropriate sensation of motion and inability to balance. Vestibular loss due to trauma, infection or tumours is relatively common, and research into

effective rehabilitation strategies has proved fruitful. Physiotherapy interventions for facilitating sensory substitution using proprioceptive and visual cues are generally quite successful, and there have been some studies looking into the mechanisms of this substitution in traumatic injury. However, one area which has received relatively little attention is age-related vestibular loss and compensation, which is of growing relevance with the changing global age demographic. As mobility declines with age and issues such as falls and frailty become more problematic, insight into the role vestibular input plays could provide improved routes of rehabilitation or treatment.

The questions regarding age-related vestibular loss and its role in mobility and falls, and even cognitive decline, are becoming more relevant as the global age demographic is shifting. Due to advances in healthcare and longevity research propagating throughout the world, the number of people alive over the age of 65 is increasing rapidly. In Ireland, the annual death rate has decreased by 14.9% from 1987 to 2011, while the birth rate has increased by 22.7%. Population projections from 2006 estimate that by 2041, the number of adults aged 65 or over will have increased to 248% of the 2012 population. Figures are taken from the Central Statistics Office information dissemination service (www.statbank.ie) and the Population and Labour Force Projection 2011 - 2041 report (Central Statistics Office, 2008).

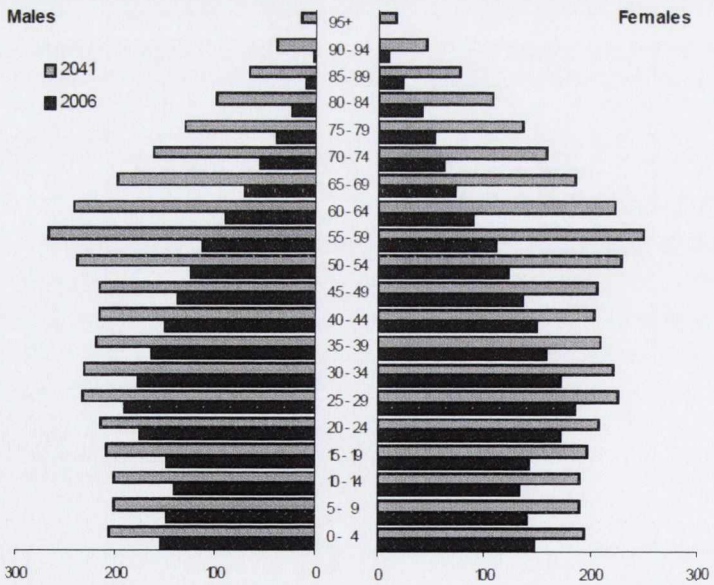


**Figure 1.3. Population estimates in 2041 using an assumption of constant birth rate. The increase in elderly population is high. Using assumptions of lower birth rate reduces the younger population, making the percentage of elderly even higher.**

Falls account for approximately 22,000 overnight admissions per annum (excluding day-cases) – this is 40% of all acute injury-related hospital admissions, with an average hospital stay of seven days, and this average stay steadily increases with age. In the elderly population, 10% require treatment and 2-3% require hospitalisation for injury every year; 75% of these injuries are fall-related. As prevalence of osteoporosis increases with ageing, fractures and breaks are a common result of falls for the elderly, which can necessitate extended hospital stays or carer presence. The cost of healthcare for falls in the elderly population is estimated to be over €400 million, per annum. This could increase to over €2 billion by the year 2030.

The reasons for increased prevalence of falls with age are multi-fold, with components of the musculoskeletal, cardiovascular and neurological systems contributing to the phenomenon. Neurologically, peripheral and central components play a part:

1) The peripheral sensory organs degrade with age; well-known examples are eyesight and hearing, which commonly become worse with age. This is due to degeneration of neurons transmitting information to the central nervous system (CNS), and is a phenomenon seen to exist in multiple sensory systems. This is known to happen within the vestibular organs, whose physical degradation with age is documented (Alvarez et al., 2000). However, the behavioural correlates and mechanisms by which this contributes to falling are not straightforward, and as their output is not cognitively registered, such decline is not directly noticeable.
2) Centrally, both unisensory and multisensory integration of sensory information change and become less efficient with ageing, perhaps as a result of peripheral sensory loss. Unisensory experiments in visual, proprioceptive, and auditory modalities have shown that elderly adults have difficulties modulating unisensory inputs, and inhibiting responses to specific modalities in multisensory tasks. Audio-visual multisensory integration experiments have shown that elderly adults who fall exhibit a longer period of multisensory integration compared to those without falls history. As the vestibular system has been seen to be relevant to self-perception and embodiment, such changes may also bring with them other issues of cognitive or mental health; early intervention in such issues can greatly improve quality of life and independent living for years, along with reducing the financial and personal burden of healthcare.

Of particular interest would be to study whether vestibular cortical processing measures show differences in fallers and non-fallers. It has been observed that processing of vestibular information does adapt with age - in studies by Baloh, elderly patients are tracked longitudinally (Baloh et al., 2003). Vestibular organ degradation was tracked, and standard tests were performed to quantify behavioural changes on gait and balance. Despite physical degradation of the organ, behavioural changes were found in one test only; in other tests of the same organs, performance did not change. Importantly, balance was not seen to be affected. As it is known that adaptation to vestibular damage occurs in traumatic vestibular loss, it can be concluded that processing of vestibular inputs changes with age to compensate for sensory loss. Thus the evidence points towards the possibility that age-related peripheral neuropathy along with subsequent neural plasticity related to processing of sensory information could play a part in the mobility problems and falls. Current knowledge of vestibular multisensory processing in ageing is lacking, particularly in terms of neuroimaging studies, which allow for measurement of neural function and associated areas involved in such processing and thus provide insight into the cortical processes and areas involved.

Moreover, literature is generally lacking neural characterisations of even unisensory vestibular processing in humans, in particular in response to true motion. There have been a number of studies performed investigating vestibular function using simulated vestibular stimuli, and a few investigating very short latency responses to rotational motion, but there is little knowledge of the responses to true motion on a time-scale compatible with multisensory integration at a cortical level. As it is imperative to know details of unisensory processing before investigating multisensory processing, this is a vital step in understanding how cortical reorganisation is relevant to age-related vestibular loss. Furthermore, present methods - which are not based on true motion - only allow investigation of rotational motion, by stimulation of the semi-circular canal organs. They do not allow specific investigation of linear motion processing, which is detected by the otolith organs. As gravity is a linear acceleration, balance and the sense of orientation or upright are strongly affected by the otolith organs. Furthermore, ambulation primarily involves linear motion, so proper otolith function is very important to co-ordinate gait.

The aims of this thesis were thus to remedy this lack of knowledge and to provide a framework for these investigations. To this end, a paradigm was developed to enable recording of neuroimaging data during true motion stimulation using electroencephalography (EEG). Appropriate data processing methods were developed.

Investigations into the neuro-dynamics of linear motion processing were made, a feat which was not possible using previous stimulus generation methods. The results obtained showed concordance with literature on cortical locations of vestibular processing, and provide further temporal information and flexibility of paradigms impossible using large magnetic resonance imaging (MRI) or positron emission tomography (PET) scanners. These results provide a strong groundwork on which to base further investigations into vestibular functional changes in both unisensory and multisensory domains, including tests enabling investigation into age-related cortical changes.

## 1.2 Thesis Aims

The overall aim of the experiments described in this thesis was to facilitate further investigation of falls and ageing by the development of novel methodologies for investigating the neural substrates of vestibular function and processing in humans using electrophysiological measures during true self-motion. To do this, novel EEG paradigms and methods for recording and processing neuroimaging data in humans during true linear motion were developed, and the responses recorded were characterized.

The research questions posed were thus:

- What are the appropriate neuroimaging technologies for investigating vestibular function and decline?
- As the otoliths respond to gravity and mediate balance, they are important for falls. Current stimulus methodologies do not allow specific stimulation of otoliths; real linear motion does. What needs to be done to enact the use of real motion as stimuli for neuroimaging?
- How do the responses of the vestibular system to such motion stimuli manifest, and compare to current imaging results of vestibular function?
- As functional MRI and PET have limited temporal resolution, could the use of imaging modalities with higher temporal resolution advance knowledge of vestibular function?

## 1.3 Contributions of the Thesis

- Description of protocol for recording vestibular EEG responses during true linear motion using a Stewart platform. (Chapters 5 - 7)
- Validation of EEG data quality when recorded on a Stewart platform. (Chapter 5)
- Design of ecological motion stimuli for eliciting vestibular P3 cognitive ERP components. (Chapter 6)
- Confirmation of P3 elicitation and description of spatiotemporal properties, including cortical source analysis. (Chapter 6)
- Design of ecological motion stimuli for eliciting vestibular ERPs. (Chapter 7)
- Description of vestibular ERP components using spatial, temporal, spectral and source analyses. (Chapter 7)
- Proposed separation of onset and continuous responses arising from vestibular stimulation. (Chapter 7)
- Development of a method for fully automated EEG processing, including artifact removal at various stages. (Chapter 4)
- Release of this method as a software package integrated with the popular EEGLAB toolbox. (Chapter 4)
- Continuing application of this method to a longitudinal study of Multiple Sclerosis patients. (Chapter 4)
- Development of quantitative measures for signal quality to measure artifact removal successes. (Chapter 4)
- Application of quantitative methods to clinical data acquired during syncope. (Chapter 4)
- Description of spectral differences in younger and older syncope patients prior to initial symptom onset. (Chapter 4)
- Preliminary development of further statistical processing methods which have seen application to joint EEG-fMRI data. (Chapter 4)

## 1.4 Publications Arising from the Thesis

Peer-Reviewed Journal Papers

- **Nolan H.**, Whelan R., Reilly R.B., "FASTER - Fully Automated Statistical Thresholding for EEG Artifact Rejection". Journal of Neuroscience Methods, 192(1), pp. 152-162, 2010. (**Chapter 4**)
- **Nolan H.**, Butler J., Whelan R., Foxe J., Bülthoff H.H., Reilly R.B., "Neural correlates of oddball detection in self-motion heading: A high-density event-related potential study of vestibular integration". Experimental Brain Research, 219(1), pp. 1-11, 2012. (**Chapter 6**)
- Whelan R., Lonergan R., Kiiski H., **Nolan H.**, Kinsella K., Hutchinson M., Tubridy N., Reilly R.B., "Impaired information processing speed and attention allocation in multiple sclerosis patients versus controls: A high-density EEG study". Journal of the Neurological Sciences, 293(1-2), pp. 45-50, 2010. (**Chapter 4**)
- Whelan R., Lonergan R., Kiiski H., **Nolan H.**, Kinsella K., Bramham J., Reilly R.B., O'Brien M., Hutchinson M., Tubridy N., "A high-density ERP study reveals latency, amplitude, and topographical differences in multiple sclerosis patients versus controls". Clinical Neurophysiology, 121(9), pp. 1420-1426, 2010. (**Chapter 4**)
- Kiiski H., Reilly R.B., Lonergan R., Kelly S., O'Brien M., Kinsella K., Bramham J., Burke T., O'Donnchadha S., **Nolan H.**, Hutchinson M., Tubridy N., Whelan R., "Change in PASAT performance correlates with change in P3 ERP amplitude over a 12-month period in multiple sclerosis patients". Journal of the Neurological Sciences, 293(1-2), pp. 45-50, 2010. (**Chapter 4**)
- Kiiski H., Whelan R., Lonergan R., **Nolan H.**, Kinsella K., Hutchinson M., Tubridy N., Reilly R.B., "Preliminary evidence for correlation between PASAT performance and P3a and P3b amplitudes in progressive multiple sclerosis". European Journal of Neurology, 18(5), pp. 792-795, 2011. (**Chapter 4**)
- Kiiski H, Reilly R.B., Lonergan R., Kelly S., O'Brien M.C., Kinsella K., Bramham J., Burke T., O'Donnchadha S., **Nolan H.**, Hutchinson M., Tubridy N., Whelan R., "Only Low Frequency Event-Related EEG Activity is Compromised in Multiple Sclerosis: Insights From an Independent Component Clustering Analysis". PLoS ONE, 7(9), e45536, 2012. (**Chapter 4**)
- Balsters J., O'Connell R., Galli A., **Nolan H.**, Greco E., Kilcullen S., Bokde A., Lai R., Upton N., Robertson I., "Changes in resting connectivity with age: A

simultaneous EEG/fMRI investigation". Neurobiology of Aging, 34(9), pp. 2194-207, 2013 Sep. (**Chapter 4**)

Peer-Reviewed Conference Papers

- **Nolan H.**, Butler J.S., Whelan R., Bülthoff H.H, Reilly R.B., "Acquisition of Human EEG Data during Linear Self-Motion on a Stewart Platform". 4th International IEEE EMBS Conference on Neural Engineering, Antalya, Turkey, 2009. (**Chapter 5**)
- **Nolan H.**, Butler J.S., Whelan R., Foxe J.J., Bülthoff H.H, Reilly R.B., "Electrophysiological Source Analysis of Passive Self-Motion". 5th International IEEE EMBS Conference on Neural Engineering, Cancún, Mexico, 2011. (**Chapter 7**)
- **Nolan H.**, Butler J.S, Whelan R., Foxe J.J., Bülthoff J.J., Reilly R.B., "Motion P3 Demonstrates Neural Nature of Motion ERPs". 33rd Annual International Conference of the IEEE Engineering in Medicine and Biology Society (EMBC '11), Boston, USA, 2011. (**Chapter 6**)

Peer-Reviewed Conference Abstracts

- **Nolan H.**, Whelan R., Reilly R.B., "A Fully Automated Method for Artifact Detection in High-Density EEG Data". Neuroscience Ireland Conference, Dublin, 2009. (**Chapter 4**)
- **Nolan H.**, Whelan R., Reilly R.B., "Fully Automated Statistical Thresholding for EEG Artifact Reduction (FASTER)". Bioengineering in Ireland, Dublin, Ireland, 2010. (**Chapter 4**)
- **Nolan H.**, Butler J.S., Whelan R., Reilly R.B., 2010. "Multisensory Self-Motion Oddball Evokes a P3 Response". 11th International Multisensory Research Forum (IMRF), Liverpool, UK, 2010. (**Chapter 6**)
- Barnett-Cowan, M., **Nolan H.**, Butler J.S., Foxe J.J., Reilly R.B., Bülthoff H.H., 2010. "Latent reaction time and event-related potentials to passive physical motion". 11th International Multisensory Research Forum (IMRF), Liverpool, UK, 2010. (**Chapter 7**)

- Barnett-Cowan M., **Nolan H.**, Butler J.S., Foxe J.J., Reilly R.B., Bülthoff H.H., "Reaction time and event-related potentials to visual, auditory and vestibular stimuli". Journal of Vision, 10(7), 2010. (**Chapter 7**)
- O'Dwyer C., **Nolan H.**, Rice C., Fan C.W., Langan Y., Connolly S., Reilly R.B., Kenny R.A., "Electroencephalographic (EEG) findings in different age-groups with vasovagal syncope (VVS)". 59th Annual Scientific Meeting of the Irish Gerontological Association, Dublin, Ireland, 2011. (**Chapter 4**)

# Chapter 2

# Literature review

## 2.1 Peripheral Vestibular System

The vestibular organs, located in the inner ear, are the body's means of detecting acceleration. This is used to orient the body to gravity, maintain balance and smooth gaze, and generate the sensation of motion. The vestibular system is phylogenetically old and has a similar morphology among all vertebrates. The organs comprise two sets of **semicircular canals** (SCCs) and two sets of **otolith organs**, one on each side of the head (Highstein et al., 2004).

The semicircular canals respond to angular acceleration. There are three canals, approximately orthogonal to each other, which detect acceleration in each plane. To do so, each canal is filled with endolymph, a viscous fluid, which is able to flow freely around the canal. At the base of each canal is a node called the ampulla, which joins onto the vestibule, the main body of the labyrinth of the ear. The ampulla is filled with cilia – nerve cells whose firing rate is proportional to the amount of bend they are undergoing. These cilia are surrounded by a membrane known as the ampullary cupula. As the head rotates around a given axis, the endolymph flows through the canal, moving the cupula and thus bending the cilia, which changes their firing rate in proportion to the acceleration the head is undergoing. The cilia synapse with the vestibular section of the vestibulocochlear nerve (cranial nerve VIII) which enters the central vestibular system.

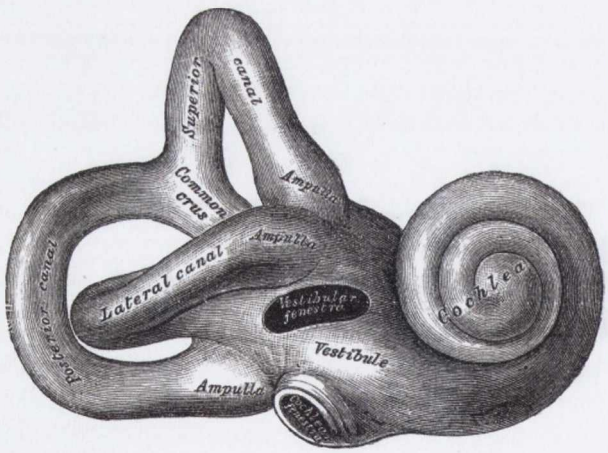

Figure 2.1. Structure of the semicircular canals (Gray, 1918).

The otolith organs, in contrast, respond to linear acceleration. There are two otolith organs, the utricle and the saccule – the utricle responds to vertical acceleration, and the

saccule responds to acceleration in the saggital plane. Both respond to varying degrees to fore-aft acceleration, covering three axes of motion between them. Like the semicircular canals, the otoliths are filled with endolymph; they also contain otoconia (variously named statoconia, otoliths), small crystalline particles which are embedded in the endolymph. The otoliths are lined with cilia, which extend into the otolithic membrane, also known as the cupula. The otoconia lay on the cupula and move within the otolith in response to linear acceleration, and so exert a force on the cilia, bending them and changing their firing rate proportional to the linear acceleration the head is undergoing. The cilia project this information into the central vestibular system via the vestibulocochlear nerve.

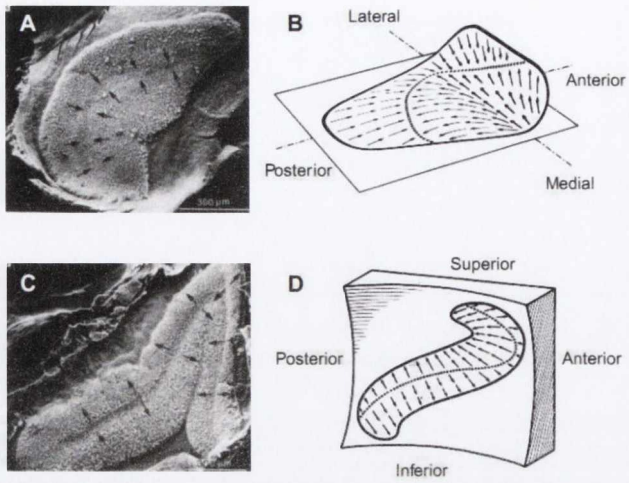


Figure 2.2. The orientation of the hair cells in the utricle (A and B) and the saccule (C and D), (Highstein et al., 2004).

## 2.2 Central Vestibular System

The vestibulocochlear nerve projects from the peripheral vestibular system to the vestibular nuclei in the brain stem. The vestibular nuclei are split into four sections - inferior, superior, medial and lateral - which connect to different structures such as the abducens nucleus, the cerebellum and the thalamus (Highstein and McCrea, 1988). The vestibular nuclei relay vestibular stimuli to control a number of the body's reflexive control systems. These autonomic processes are short-latency responses which maintain balance, posture and gaze using vestibular information. Within this thesis, the most relevant of the reflexes are the vestibulo-ocular reflexes (VORs) and the vestibulo-collic reflex (VCR).

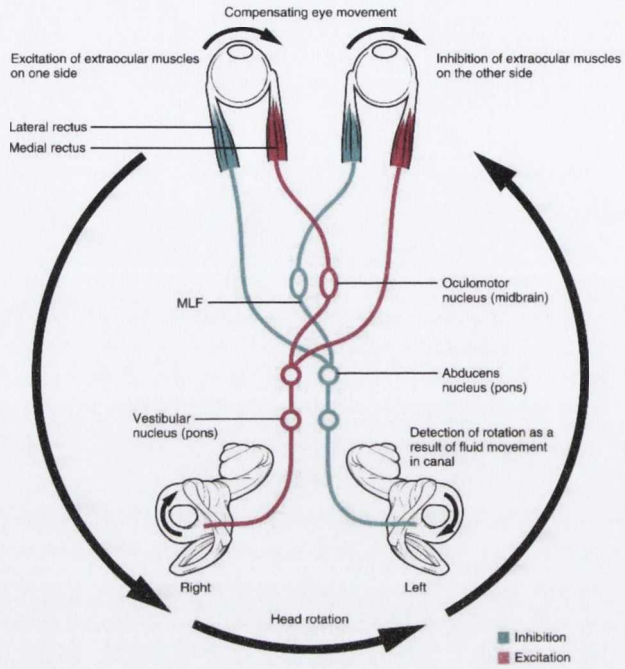


**Figure 2.3. The angular vestibulo-ocular reflex rotates the eyes in opposition to the direction of rotation to maintain a fixation and produce a smooth image.**

The VORs are a set of reflexes which control the movement of the eyes so as to stabilise visual input during motion of the head. The reflexes can be classed into the angular and linear VOR (aVOR/lVOR), depending on the motion experienced. Broadly speaking, the aVOR is controlled by the SCCs and the lVOR by the otoliths. The VORs are the most commonly studied aspect of the vestibular system, and many studies have investigated their properties across a multitude of stimulus inputs. As input and output are often closely related, the VORs are often described in control theory terms as an impulse response, with amplitude and phase responses plotted against frequency and amplitude of input.

The aVOR rotates the eyes in the opposite direction to the head during rotational acceleration, in order to provide momentary fixation upon a focal point. This process is mainly controlled by the SCCs. The reflex acts upon the extraocular muscles to rotate the eyes contralateral to the direction of rotation, to maintain a smooth image. The dynamics of this reflex have been studied numerous times, both experimentally and computationally (e.g. Paulin et al., 1989; Raphan and Cohen, 2002) - the impulse response of the aVOR can be approximated by a high-pass filter of angular acceleration (Ramat and Bertolini, 2009); its phase properties vary from leading at low frequencies to lagging at higher. A so-called velocity storage mechanism tracks velocity over time, which leads to a relatively long time constant for this response (Bertolini and Ramat, 2011). Further factors which contribute to the aVOR are demonstrated when it is suppressed by fixation, which is controlled by cortical projections to the VOR reflex (Naito et al., 2003), suppressed by anticipation (Barnes and Paige, 2004), and suppressed due to plasticity over longer periods of modulated input (Cohen et al., 1992).

The lVOR shares some properties with the aVOR (Paige and Seidman, 1999), however it necessitates a higher degree of visual integration to maintain target fixation (Angelaki, 2004). The lVOR acts against vergence (convergence and divergence of the eyes to obtain fixation on an object) based on vestibular projections and optic flow information to maintain fixation on a target which is translating with respect to the observer. This is considerably more complicated than the rotational case, especially when both subject and object motion is involved - processing separate subject and object motion is required to properly maintain fixation. The main vestibular contribution to the lVOR comes from the otoliths, as they are responsive to linear accelerations, but it has been seen that the SCCs also contribute to a smaller extent (Green and Angelaki, 2003). This is partially due to ambiguity in the resolution of tilt vs. head translations. The lVOR also displays high-pass filter dynamic (Merfeld et al., 2005), and also exhibits habituation over periods of continued stimulation (Anastasio, 2001).

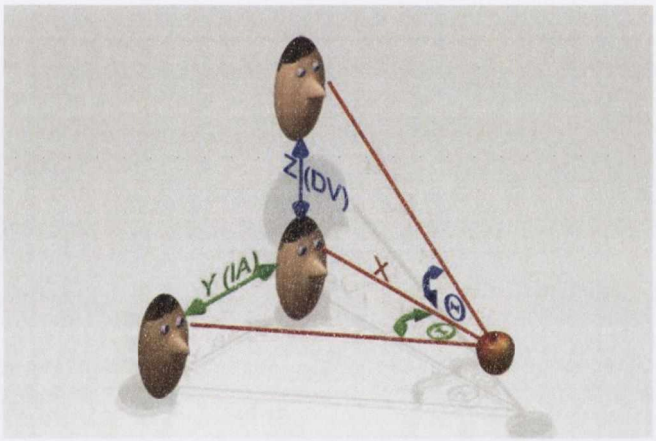


**Figure 2.4. The linear vestibulo-ocular reflex rotates the eyes to maintain fixation on a target during translation, depending on factors such as gaze angle and target distance.**

The VORs have been the subject of a number of mathematical modelling studies, as the inputs and outputs have a relatively small number of variables, which facilitates the application of control theory models (Robinson, 1981). The aVOR has been studied to determine its response at various amplitudes and frequencies, and it has been observed that the impulse response models take semicircular canal input (i.e. rotational acceleration) and respond with varying amplitude and phase lag at different frequencies. As stated above, the lVOR has more complex properties, requiring integration of vestibular and visual information; thus control models are more complex. Several models have been developed which combine responses to both linear and rotational acceleration to predict ocular velocity (Merfeld and Zupan, 2002; Mergner and Glasauer, 1999; Paige and Seidman, 1999; Raphan and Cohen, 2002); the single-axis model detailed by Paige 1999 includes a thorough literature review, as does the paper by Raphan and Cohen 2002. From these models it has been concluded that there is considerable interaction between the lVOR and aVOR. It should be noted that these

models take input as acceleration and use integrators to calculate velocity responses; the notion that jerk, or the time-derivative of acceleration is also included has been discussed previously (Angelaki et al., 1993), and included in Mergner's 1999 model as the product of a differentiator. In this model it is utilised to derive the head's angular velocity - it is not discussed in the context of linear acceleration. Further models could include cortical efferent signals which mediate the VOR, or VOR adaptation - a simple model for this exists without details of the VOR model itself (Menzies et al., 2010).

The vestibulo-collic (VCR) and vestibulo-spinal reflexes (VSR) are reflexes which stabilise the neck and spine, respectively, in response to vestibular input (Wilson, 1991; Wilson et al., 1995). The VCR is effective in counteracting the head's inertia and keeping its position static relative to the body during movements. The main muscle groups involved are the trapezius and sternocleidomastoids (Ferber-Viart et al., 1997). The VSRs control a wider range of muscles the along the trunk. The VCR has also been seen to be affected by task (Keshner et al., 1992), and also by repeated stimulation (Blouin et al., 2003). During true motion, the cervico-collic reflex (CCR) also plays an interlinked role, modulating neck tone in response to muscle stretch. Interaction with the CCR is seen to be approximately additive (Dutia and Price, 1987), but the CCR is also modified by expectation of stimulus (Kuramochi et al., 2004).

Vestibular information is projected from the vestibular nuclei into the cortex primarily via the thalamus (Lopez and Blanke, 2011), although there are also more direct connections from the vestibular nuclei as discussed in Dieterich et al., (2003). The cortical areas which receive these projections from the thalamus are varied. The range of their roles is widespread, from providing contextual information for the mediation of the VOR and other reflex paths (Israel et al., 1995), to providing a sense of subjective vertical and movement through the environment (Redfern et al., 2001).

## 2.3 Clinical Implications of Vestibular Dysfunction

As vestibular information is central to the maintenance of balance and posture, dysfunction of the vestibular system can be distressing and debilitating. Furthermore, due to its control of eye movement via the VOR, vision can also be affected. Typical symptoms of vestibular disorders include persistent dizziness and the sensation of spinning (vertigo), difficulty maintaining balance, persistent nystagmus while at rest or inability to focus visually

during movement (Dix and Hallpike, 1952; Sharpe and Johnston, 1990). Some medical conditions associated with vestibular dysfunction include:

- Benign paroxysmal positional vertigo (BPPV), which occurs when otoconia become dislodged from the endolymph and migrate into the semicircular canals, disrupting the cilia and causing inappropriate sensation of movement (Hughes and Proctor, 1997).
- Ménière's disease is an idiopathic disease – by definition, its cause is unknown – but it is thought to be caused by excessive endolymph building up in the labyrinth. Its symptoms include unpredictable attacks of rotational vertigo (Friberg et al., 1983).

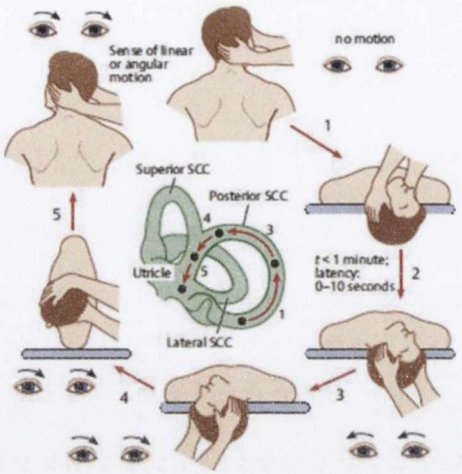


**Figure 2.5. The Epley manoeuvre for treating BPPV. This manoeuvre aims to move the migrated otoconia back towards the ampulla.**

- Stroke or traumatic brain injury can damage the vestibular system (Brandt et al., 1995), and rehabilitation can be very effective in such cases, demonstrating the cortical plasticity available to vestibular processing.
- Loss of vestibular organ function may occur unilaterally or bilaterally; unilateral vestibular loss is seen to be more distressing than bilateral loss, due to the sensory conflict occurring (Curthoys and Halmagyi, 1995; Rinne et al., 1998).
- Neurovascular conditions such as migraine are also known to affect vestibular function or perception (Jeong et al., 2010).

Further to these acute conditions, vestibular function is known to degrade with age – reduction in the numbers of cilia (Peterka et al., 1990) along with morphological changes in their structure (Anniko, 1983) lead to decreased responsivity. Deterioration of balance during aging is also a known phenomenon; falls become more common, with prevalence of up to 25% per annum over the age of 65. Vestibular function often tends to be associated with falling in the elderly, as could be expected (Agrawal et al., 2010; Kristinsdottir et al., 2000; Serrador et al., 2009). Significant vestibular system impairment is common in a cohort of elderly patients referred for assessment of falls risk, and elderly adults with chronic vestibular disorders show a proportional relationship between severity of the condition,

functional capacity and falls (Macias et al., 2005; Sousa et al., 2011). However, this relationship is not entirely straightforward - in (Baloh et al., 2001) and (Baloh et al., 2003) vestibular functional decline is measured longitudinally in older adults but is not associated with changes in functional balance tests; thus compensatory mechanisms are being employed. A large cross-sectional study by (Peterka et al., 1990) shows that trends for VOR parameters do not follow the normalised anatomical trends of sensory decline. Mallinson and Longridge also show that slow-phase caloric vestibular tests do not change with age (Mallinson and Longridge, 2004), and (Sloane et al., 1989) has some discussion on the unproven connection between falls and vestibular function.

Dizziness is commonly used as an evaluative and predictive factor, but this is often due to orthostatic hypotension - which may lead to syncope and falling - rather than vestibular dysfunction or deterioration (McIntosh et al., 1993). However, these may not necessarily be completely separable issues, as the vestibular deterioration affects the vestibulosyompathetic reflex, which may play a part in orthostatic tension (Ray and Monahan, 2002a). In general it is seen that both cardiovascular and vestibular issues can cause dizziness. Furthermore, as discussed in Matheson et al., (1999), the nervous system compensates for these slow declines - it is only when the deterioration is such that it cannot compensate any more that dysfunction occurs. A recent study (Jeka et al., 2010) showed that elderly adults show slower reweighting of visual information in visual-vestibular tasks related to posture. It is also known that multisensory integration changes with aging (Laurienti et al., 2006), and that fallers have a higher level of inefficient audio-visual multisensory integration than non-fallers (Setti et al., 2011). It has been observed that adding cognitive load or sensory reweighting requirements considerably affects postural performance in (Teasdale and Simoneau, 2001; Toulotte et al., 2006). Therefore while peripheral vestibular deterioration is known to happen during aging and plays a part in falling, central and cognitive components involved in multisensory integration, top-down control and self/environment representation must also be considered.

## 2.4 Neuroimaging of the Vestibular System

In order to document and classify the connectivity of the vestibular system from the peripheral organs through the brain stem to the cerebral cortex, imaging of the system in live animals or humans must be performed. In animal studies, intracellular recordings are

common and are highly informative of neuronal activity in specific brain sites. Such recordings have been made at many points during vestibular stimulation from the semicircular canal and otoliths to the vestibular nuclei (Menzies et al., 2010; Newlands et al., 2009; Ris et al., 1995; Roy and Cullen, 2003), cerebellum (Amat, 1982; Lau et al., 1998; Sheliga et al., 1999; Simpson et al., 1974), motoneurons (Baker and Highstein, 1978; Maeda et al., 1972; Straka and Dieringer, 1993; Wilson and Yoshida, 1969) and thalamus (Blum et al., 1979; Deecke et al., 1974; Liedgren and Schwarz, 1976; Meng et al., 2007), providing good coverage of the early stages of vestibular processing and the reflex arcs. These recordings become more divergent as connections multiply while entering the cortex and combining with afferents from other sensory systems (Akbarian et al., 1992; Bremmer et al., 1999a; Chen et al., 2010; Grüsser et al., 1990). Subcortical vestibular anatomy is quite similar within vertebrates (Demêmes et al., 1990; Muller, 1994; Straka et al., 2005). However, the differences in cortical morphologies and intra-cortical connectivity between species mean that we must look to primates for the most relevant human comparisons (Grefkes and Fink, 2005). The parieto-insular vestibular cortex (PIVC) is considered in monkeys to be one of the most important vestibular cortical areas (Akbarian et al., 1992; Chen et al., 2010; Grüsser et al., 1990); this brain area is proposed to be part of an "inner vestibular circle" or vestibular hub, which is a highly interconnected network of regions involved in processing incoming vestibular information (Dieterich et al., 2005; Lobel et al., 1998; zu Eulenburg et al., 2012). Recent work has also investigated the representation of linear motion in macaques, in particular in

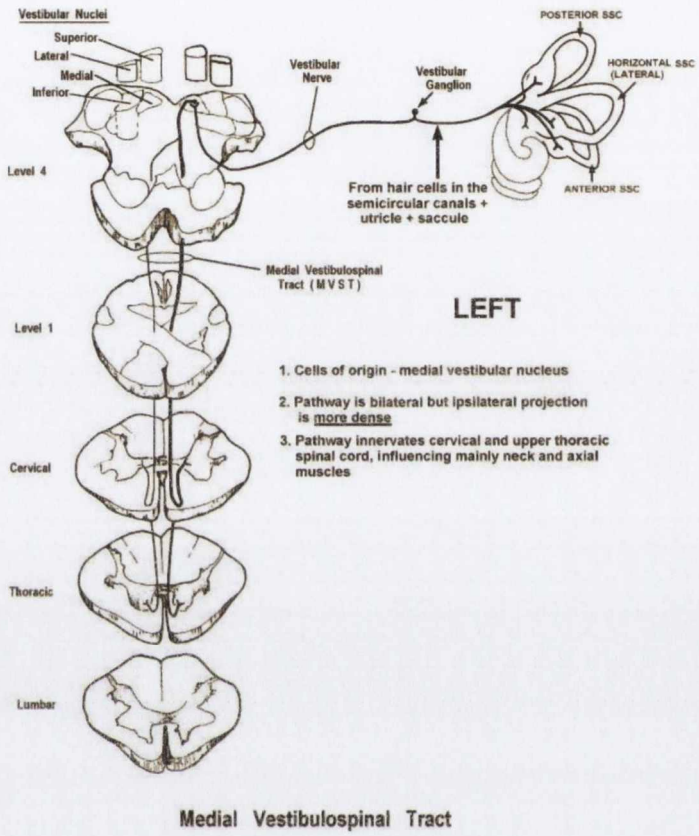


**Figure 2.6. The medial pathway from the semicircular canals through the vestibular nerve and vestibular nucleus to the spinal column, which acts upon the neck and core muscles to maintain posture and balance.**

middle superior temporal cortex (MST) (Bremmer et al., 1999b) and ventral intraparietal (VIP) areas (Schlack et al., 2002).

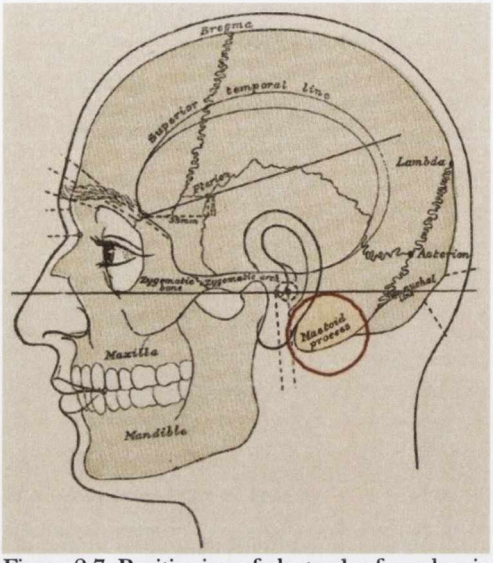

Figure 2.7. Positioning of electrodes for galvanic vestibular stimulation on the mastoid

Human imaging studies follow quite a different pattern, as intracellular recordings are rare in humans for ethical reasons. Recent literature consists of mainly PET (Bottini et al., 1994; Brandt and Dieterich, 1999) and fMRI studies (Dieterich and Brandt, 2008; Eickhoff et al., 2006; Lobel et al., 1998). These imaging methodologies require the use of large machinery, which makes them unsuitable for use during true motion. Instead, these methods use caloric or galvanic vestibular stimulation (GVS) to induce vestibular sensations while the subject remains static. Caloric stimulation involves the irrigation of the ear canal(s) with warm or cold water or air. This methodology is considered to primarily stimulate the semicircular canals (Fetter et al., 1998; Yagi et al., 1992). Galvanic stimulation involves the use of an electrical current applied near the ear in order to electrically stimulate the vestibular organs. This method has been used to stimulate both semicircular canals and otolith organs (Kleine et al., 1999; Wardman and Fitzpatrick, 2002). Thus these methods are able to elicit semicircular canal responses, or simultaneous semicircular canal and otolith responses, but not specifically target otolith responses in general; there is some debate in literature about otolith specificity in GVS at low current densities (Zink et al., 1998), while other research is in conflict with this finding (Séverac Cauquil et al., 2003).

Figure 2.8. Test dummy for caloric stimulation; a warm and/or cold syringe of water is flushed into the ear(s), differentially heating and cooling the endolymph on each side and simulating vestibular stimulation.

The results of human imaging studies show a considerable amount of variability in cortical areas activated during vestibular processing. Two meta-analyses (Lopez et al., 2012; zu Eulenburg et al., 2012) have both shown that the parieto-temporal insular area, which is theorised to map to the primate PIVC, is activated in a

significant number of studies, regardless of stimulation modality. In primates this area is often thought to be a central part of the vestibular network. It receives vestibular information, as well as somatosensory information (Grüsser et al., 1990). It is also hypothesised to be involved in a reciprocal inhibition network with visual processing in the parieto-occipital junction (Brandt et al., 1998), maintaining appropriate weighting of vestibular and visual information for self-motion perception in the cortex. Further areas that have been associated with vestibular stimuli in the cortex include the somatosensory cortex, motor cortex, middle (superior) temporal areas (MT/MST) - these are also known to be involved in motion processing in the visual system (Guzman-Lopez et al., 2011; Seemungal et al., 2013), the inferior and superior parietal lobule (I/SPL), frontal gyrus and occipital cortex. Figure 3 in Lopez and Blanke, (2011) provides a pictorial summary of these areas, with citations, and is reproduced below as Figure 2.13. There is a large amount of variation in these studies and the specifics of the protocols involved may play a part in determining the results.

The use of electroencephalography (EEG) in imaging of vestibular processing was investigated in a number of studies in the 1980s and 1990s. As EEG systems are more portable than fMRI or PET equipment, their use enables imaging during bodily motion. Thus, there are a number of studies investigating the neural responses to high-amplitude rotational stimuli performed using a rotational chair while recording EEG data from a few electrodes (Hofferberth, 1983, 1995; Hood and Kayan, 1985; Kolchev, 1995; Pyykkö et al., 1995; Rodionov et al., 1996; Schneider et al., 1996). They aimed to classify short latency onset responses to vestibular stimuli, and had some success in doing so - their clinical application was discussed in (Hofferberth, 1995), where it was concluded that the equipment necessary relegated the tests to specific, rather than routine, testing, but that they would be useful for investigating the cortical projections of vestibular information. However the above studies' recordings were marred by artifacts from the VOR and VCR, along with possible movement of the electrodes, and mainly targeted rotational motion. One study was performed using a dropping tilt-table to stimulate otoliths (Kast and Lankford, 1986); however the influence of EOG and EMG was not addressed, and as mastoid references were used, EMG interference from sternocleidomastoid muscles was probable which may be time-locked to the stimulus are confound the response. More recently, the EEG response to bone-conducted sound, which is an emerging method for providing vestibular stimulation, has been recorded (Todd et al., 2008). These studies focus on the short-latency evoked potential; they are measures of sensory processing but not necessarily sensory integration,

which takes place later in time. The imaging of people in natural motion, i.e. motion in ranges and patterns which are usually encountered in everyday life, is a new field of study.

## 2.5 Electroencephalography

Electroencephalography (EEG) is a neuroimaging method that involves placing electrodes on the scalp and recording potential differences to determine the underlying neural activity. This method gives high temporal precision (sampling rates > 512Hz), but low spatial precision (a common setup employs 128 electrodes, which has a 4 - 9 $cm^2$ spatial resolution (Ferree et al., 2001)). This is in contrast to fMRI, which has a much lower temporal precision (sampling rates < 1Hz), but higher spatial precision (2 - 3$mm^3$ typical). The advantage of EEG compared to fMRI (or other imaging methods) for the task at hand is the portability of EEG systems, and their fixed position relative to the head. MRI machines are very large, and rigging them for motion would require very large modifications, while the head needs to remain very still within. An EEG system is smaller, considerably less expensive and more portable, can be battery powered and self-contained, and so is suitable for mounting on e.g. a motion platform, allowing for controlled motion while recording neural activity. EEG is also more suitable for patients with claustrophobia, children, or people with physical or mental impairments due to the smaller equipment size.

**Figure 2.8. Biosemi EEG system and cap.**

EEG systems record the electrical activity of the brain through skull and skin. These materials act as spatial filters for the signal and so the underlying neural activity is highly attenuated. This attenuation means that a high level of amplification is needed to detect the signal, which is in the range of 20 - 40 μV. Due to this amplification, other unwanted electrical signals of physical or biological origin get mixed in with the recorded EEG signal. This is a significant problem, as the signal can get swamped by these **artifacts** of higher magnitude than the EEG signal. Such artifacts include recording of electrooculogram (EOG) activity, due to eye movement (Corby and Kopell, 1972), and the recording of electromyogram (EMG) activity, due to subjects moving limbs or clenching muscles (Goncharova et al., 2003). These artifacts can be a particular issue in motion-based research

as the vestibular system's reflex circuits activate both ocular muscles via the VOR and postural muscles via the VSR and VCR.

To extract information from EEG data, one of the most common methods is an Event Related Potential (ERP) study, which consists of recording EEG data from a subject while they are presented multiple times with a stimulus. The EEG data is then split into segments ("epochs" or "trials") of a fixed amount of time before and after each stimulus presentation. The average is taken of each of these segments - this is called the ERP. This isolates the EEG activity which is related to the stimulus presentation, which is usually swamped by the background EEG activity. This background activity is considered zero-mean noise and so tends to zero after averaging, leaving only the ERP. An Evoked Potential (EP) is a type of event-related potential with a short latency that occurs in response to a stimulus and is thought to relate directly to the sensory processing of the object - for example, the early peaks of the visual evoked potential (VEP) have been found to be generated in V1, the primary visual cortex (Russo et al., 2002). Sensory evoked potentials can be contrasted with cognitive potentials, which have longer latencies and reflect the processing and integration of information based upon task or context information - identical sensory stimuli may have different cognitive potential responses based on the experimental context used.

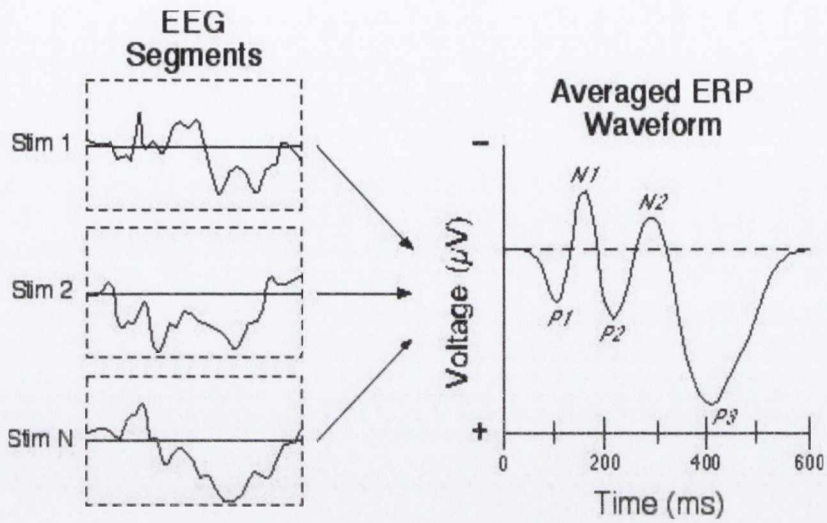

Figure 2.10. Depiction of ERP averaging process.

There is a long-standing question about the generation of ERPs. Two separate mechanisms are proposed which would result in an ERP, and the question is to what extent each contributes to the ERP's generation. The first states that a sensory stimulus activates a brain area which was not previously active, giving rise to a higher level of recorded neuronal activity compared to baseline. The second states that a sensory stimulus resets the phase of an on-going oscillation in that brain area, giving rise to a recorded response which is phase-

locked after the stimulus onset, but with random phase during baseline which will average to zero. Current opinion is that each mechanism has varying contributions (David et al., 2006; Min et al., 2007).

The layers of skull and scalp between the brain and the electrodes act to smear the EEG response across the scalp (Freeman et al., 2003). The spatial smearing that occurs reduces the precision with which neural activity can be localised within the brain. Furthermore the effect of volume conduction means that a signal recorded at an electrode site may lie at some distant point of the brain, and that each electrode records a mix of a large number of signals. To attempt to deal with this problem, source reconstruction methods can be used to indicate where the source(s) of neural activity lie, albeit with limited spatial resolution. A widely-used method for source reconstruction is low-resolution exact tomography (LORETA) and, more recently, standardized LORETA (sLORETA). More details of this method are in Section 3.4.

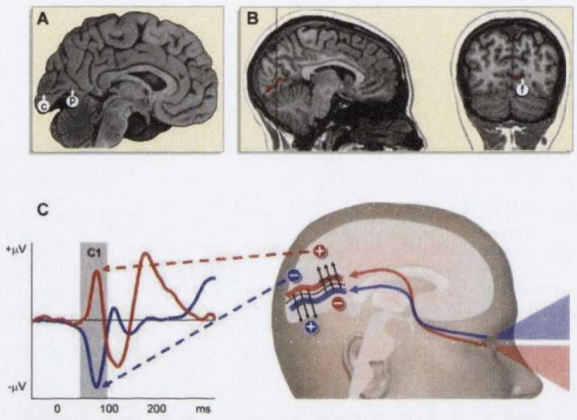


**Figure 2.11. VEP generation by V1, the primary visual cortex, which is located in the occipital region of the brain.**

## 2.6 Self-motion Perception

The perception of self-motion is a phenomenon resulting from the cortical combination of vestibular, visual, proprioceptive and somatosensory information (Jurgens and Becker, 2006). The basic information flow which is known in literature is that the vestibular stimulation is used to very quickly make the body react to accelerations of the head via the vestibular reflexes. This information is combined with proprioceptive information from the neck to determine the orientation of the head to the body and thus integrate this with the body configuration to construct a whole-body representation of acceleration. Proprioceptive reflexes (such as the CCR) constructively or destructively interfere with vestibular reflexes to maintain appropriate body posture (Dutia and Price, 1987). In the cortex, visual information regarding optical flow is then integrated with the incoming vestibular and proprioceptive information (Manchester et al., 1989) - the details of

this process are the subject of a number of recent studies (Berger and Bülthoff, 2009; Butler et al., 2010; Fetsch et al., 2010).

To combine these in the brain, these inputs are weighted and combined together to form a sense of movement. The weighting of integration can be modelled using Bayesian statistics. The changes in instantaneous changes in weighting are based on the reliability of each stimulus at each given point in time (Fetsch et al., 2010). This implies that executive control based on past experience is employed to decipher the likelihood of the cues to control integration. This process in a complex process as information from the various sensory systems takes different amounts of time to reach the brain and go through the cascade of processing. It has been shown that the vestibular-ocular reflex is modulated by cortical feedback (Naito et al., 2003) – intuitively this makes sense as it can be suppressed by concentration. Studies on the suppression of the VOR demonstrated that this modulation is not complete, and that there is a time delay of suppression (Barnes and Paige, 2004). A study showing that VOR suppression affects cognitive tasks (Furman et al., 2003) implies that top-down control is involved, so the time delay of suppression may thus be associated with the longer processing time of visual stimuli, as compared to vestibular stimuli.

The direction of motion, known as heading, is an often-used parameter to investigate the perception of linear self-motion. It is easily manipulated and can be deduced from visual or vestibular sensory information alone (Telford et al., 1995; Warren et al., 1988), allowing for the investigation of sensory integration and weighting. Heading perception requires the processing of sensory information and cognitive judgement based on this (Fetsch et al., 2010). Human behavioural experiments used heading to determine the behavioural weighting strategies of visual and vestibular information (Fetsch et al., 2009), investigate

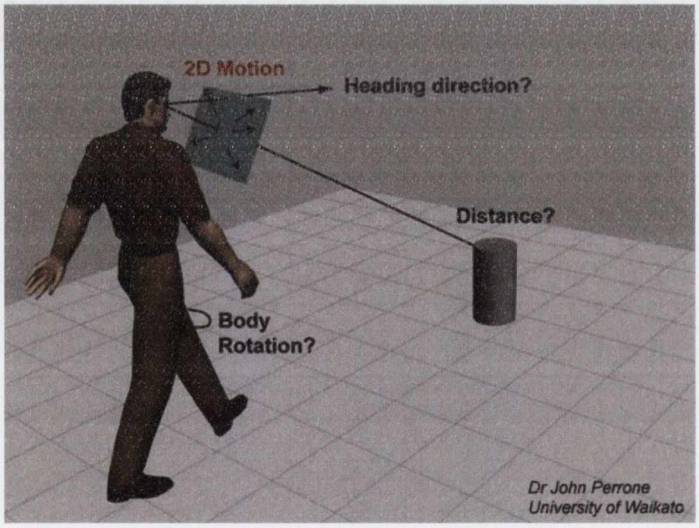


**Figure 2.12. Motion perception integrates current and previous information about the environment, spatial constructs, and sensory information about the body from the visual, proprioceptive and vestibular senses to create an accurate representation of the world around us and our position in it.**

differences in passive and active self-motion (Telford et al., 1995), and determine driving (Wallis et al., 2002) and locomotion (Berard et al., 2009) strategies, among others. In macaques, intracellular imaging during heading experiments is often used to investigate the properties of the MT/MST region. This area exhibits responses to both visual and vestibular motion stimuli (Bremmer et al., 1999a; Duffy and Wurtz, 1991a, b; Lagae et al., 1994) in 3D (Takahashi et al., 2007), as well as integration effects for concurrent stimulation (Gu et al., 2008). Stimulation of the area has been shown to bias heading (Britten and van Wezel, 1998). Heading responses have also been observed in the ventral intraparietal (VIP) area (Bremmer et al., 2002a; Bremmer et al., 2002b; Schlack et al., 2002). In humans, a number of neuroimaging studies of heading using optic flow have been performed. The human area denoted hMT+ (Beauchamp et al., 1997) is often considered to be the human homologue of the primate area MT (Tootell and Taylor, 1995), and thus both can be referred to as MT. Promisingly, this area has been identified a number of times as having involvement in heading (Kovacs et al., 2008; Peuskens et al., 2001; Tootell et al., 1995). Shigemasu et al., (2007) have used BOLD responses from the MT area to reconstruct heading directions, with 90% accuracy. This indicates a functional homology between humans and primates in the perception of motion, which allows us to use conclusions from primate literature as guiding influences in humans. Further to the area MT, the intraparietal sulcus (IPS) (Peuskens et al., 2001) and VIP (Zhang et al., 2004) have also been identified in human heading perception.

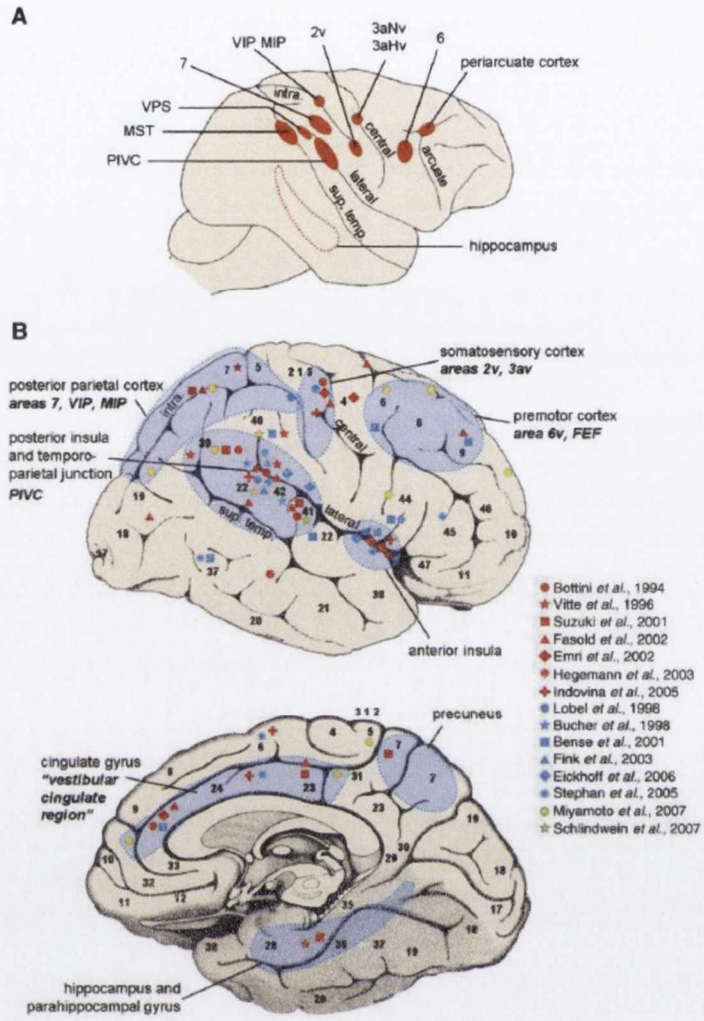


Figure 2.13. Meta-analysis of cortical regions seen to be active during vestibular stimulation in humans. Numerous separate regions are identified in the perception and processing of vestibular information. Taken from Lopez 2011.

In humans, self-motion perception has also been studied in the visual modality. The sensation of self-motion induced using visual cues is called vection - this is a sensation of motion induced using optic flow alone. This is often used as a term to refer to illusory motion, but it is an important component in the perception of real self-motion. As the vestibular system responds to acceleration, it is not responsive at constant velocities. The visual system then provides a representation of motion using optic flow. There are a number of studies which show that the MT/MST regions are involved in the processing of optic flow in monkeys (Britten and van Wezel, 1998, 2002; Duffy, 1998; Duffy and Wurtz, 1991a, b; Lagae et al., 1994; Lappe et al., 1996; Lappe and Grigo, 1999), and humans (Cardin and Smith, 2009; Kovacs et al., 2008). Parts of MT have been demonstrated to respond

selectively to motion direction, which fits with its involvement in heading tasks. MST responds to motion patterns, and its dorsal stream is known to integrate vestibular signals along with visual signals (Duffy, 1998; Fetsch et al., 2007; Gu et al., 2008; Gu et al., 2007; Gu et al., 2006; Takahashi et al., 2007).

Proprioception is the sense of relative position of body parts. This information is used for body awareness constructs (Graziano, 1999; Shenton et al., 2004) and is thus very important in motion perception. It is generally observed that the combination of neck proprioception and vestibular stimulation function to connect head movement with body movement and orientation. In monkeys spatial co-ordinates are represented in separate neural populations in both head-central (vestibular only) and body-central (integrated proprioception and vestibular) reference frames (Fetsch et al., 2007). In humans, some fMRI studies have been performed targeting proprioception in a variety of tasks (Graziano, 1999; Montant et al., 2009; Rausch et al., 1998). A small number of EEG studies have been performed - proprioception evoked potentials have been described (Seiss et al., 2002), and have been investigated in the classification of Huntington's disease and Parkinson's disease (Seiss et al., 2003). The latter study localised the source of the evoked potentials to the pre-motor cortex. Furthermore, a recent study using EEG on a treadmill has shown that numerous joint angles involved in a walking task can be extrapolated from the EEG signals (Presacco et al., 2011).

Other somatosensory influences on the perception of self-motion have been less studied. The trunk and legs receive stimulation during seated acceleration, and thus in theory could be used for motion perception; however, as concurrent vestibular and inertial proprioceptive stimulation occurs, it is difficult to separate this from other sensory information. Walsh, (1961) describes the use of a viscous fluid designed to dampen such somatosensory information. Results showed that acceleration perception thresholds were affected, but not by a significant amount (approximately decreased by a factor of 2.5, but with increased variability). Comparing this to the results of Gu et al., (2007) where labyrinthectomised macaques showed a factor of 50 decrease in task accuracy with the removal of vestibular sensory information, it is clear that somatosensory contributions are not weighted as strongly in motion tasks.

## 2.7 Questions from Literature Review

This review of the literature points to a number of questions which have not been addressed and are pertinent to the aim of understanding the role of central and peripheral vestibular function, particularly in falls:

1) Can EEG measures be used with true motion stimuli to target vestibular responses?
2) Are neural responses to natural motion similar to those evoked using galvanic or caloric vestibular stimulation in humans?
3) Does EEG source analysis of vestibular responses reveal brain areas corresponding to results obtained using fMRI or PET?
4) What is the temporal profile of vestibular information processing?
5) Could EEG be used to investigate the relationships between age-related vestibular decline, changes in multisensory perception, and falls?
6) Would neuroimaging measures be informative for early intervention of people at risk of falls?

In this thesis, questions 1 - 4 will be investigated, and questions 5 and 6 will be discussed in the context of the answers obtained.

# Chapter 3

# General Thesis Methods

This chapter describes methods which are used throughout many or all of the experiments described in the thesis.

## 3.1 Linear Motion Stimuli

In this thesis, a number of experiments recording EEG during true linear motion are described. To perform such experiments, it is necessary to be able to accurately present such motion stimuli in a repeatable fashion. To this end, a Stewart platform (Stewart, 1966) manufactured by Maxcue was employed (von der Heyde, 2001). This is a motion stimulation platform with 6 degrees of freedom – translation and rotation in x, y and z planes – and has a range of 1m movement in all directions. This platform has a motion profile update rate of 100Hz. It is fitted with a large screen with field of view 86°×65° and a resolution of 1400×1050 with a refresh rate of 60 frames per second which can be used to present visual stimuli at a fixed distance from the subject. To remove all visual motion information, the platform was securely covered with a cloth which rendered the environment inside visually static. Subjects were asked whether they could see any movement to ensure the cloth was properly secured, and any trials where visual motion stimuli were reported were repeated after fixing the cloth.

The stimuli provided were thus non-visual motion stimuli. The modalities involved in the perception of the motion stimuli are thus vestibular, proprioceptive and somatosensory. As discussed in Chapter 2, the vestibular contribution to motion perception is considerably more important than the somatosensory input. Proprioceptive changes related to acceleration were minimised, as the subject was seated in a large chair secured with a seatbelt, thus preventing relative body movement. The head was unable to be secured for safety reasons, but was well-supported by a headrest. This allowed a small amount of undesirable movement forwards, but the seatbelt and relatively low amplitude of the motions minimised this. Therefore, the stimuli provided can be concluded to be primarily vestibular

in their nature, and so the ERPs recorded in response to them can be considered to represent vestibular ERPs.

All stimuli used in all experiments were linear motion; this area of motion processing is particularly difficult to study in humans using artificial means. To simulate more natural motion than step profiles which are commonly used in motion studies, as well as to minimize safety risks, a 1Hz 360° sinusoidal acceleration profile was adopted for the main experiments in Chapters 6 and 7, providing a ramp-up to maximum acceleration and ramp-down to zero. The displacement equation for generating motion used was:

$$s(t) = 0.49\frac{(2\pi t - \sin(2\pi t))}{4\pi^2} \qquad 0s \leq t \leq 1s$$

where:

t is time

s(t) is displacement

The maximum displacement was 7.8cm, maximum velocity was 15.6cm/s and maximum acceleration was 49cm/s$^2$. These profiles are pictured in Figure 3.1.

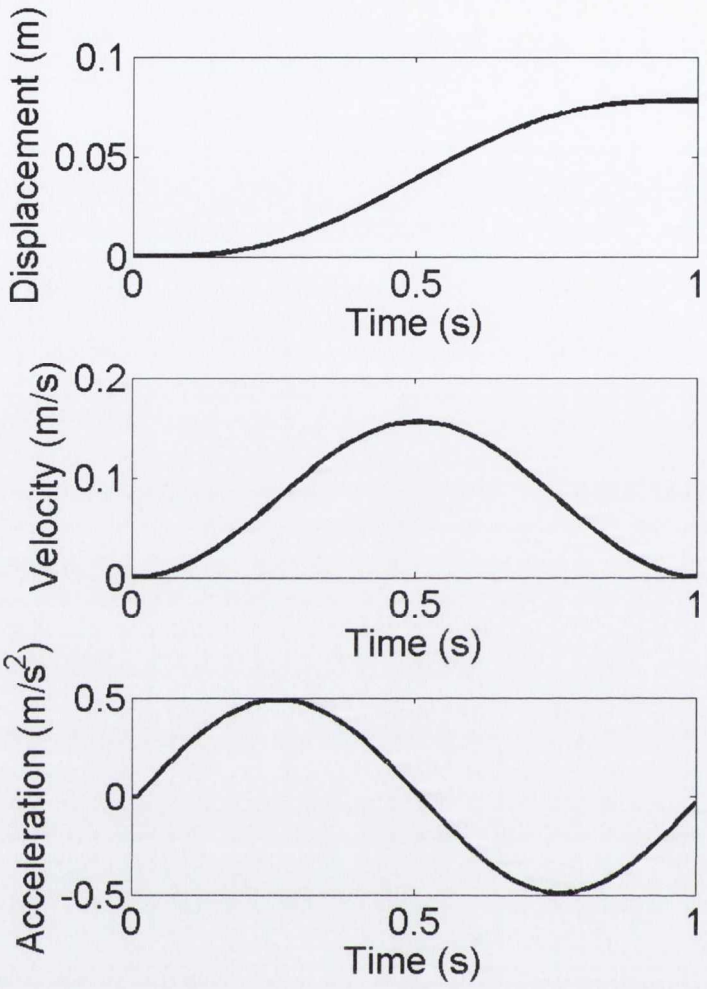


**Figure 3.1. The ideal displacement, velocity and acceleration profiles of the Stewart platform.**

Motion stimuli were constrained to the naso-occipital (NO) and intra-aural (IA) directions. Displacement for each direction can be defined:

$$s_{NO}(t) = s(t)\cos(\theta)$$

$$s_{IA}(t) = s(t)\sin(\theta)$$

The angle $\theta$ is defined as zero for straight-ahead motion.

In Chapter 5, there were four different motion stimuli: static, idle, slow and fast. In the static condition the platform was turned off. In the idle condition the platform was raised to its neutral position then remained idle in this position. In the slow and fast conditions the

platform was moved with a sinusoidal acceleration profile in a fore-aft motion at a frequency of 0.5 Hz for 230 cycles at different maximum accelerations of 0.01G and 0.05G, respectively. The motions were controlled by Virtools™ [1]. This profile was modified to the 1Hz fixed amplitude profile detailed above to reduce the amount of time that subjects were in the motion platform during Chapters 6 and 7.

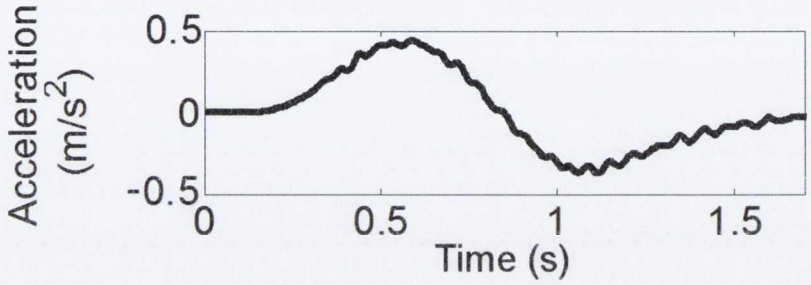


**Figure 3.2. The sinusoidal acceleration profile going forward, as recorded from the Stewart platform. This depicts an average of 50 trials. The variability between trials is small.**

A sample acceleration profile was recorded using a chassis-mounted accelerometer on the Stewart platform; the results are shown in Figure 3.2. As can be seen, the recorded motion profile has a sinusoidal shape, but has a longer length than expected. The input equation specified a one-second long profile, whereas the recording shows that the real length is approximately 1.5s. This is a result of the control systems in the Stewart platform; while it creates a difference from the ideal motion profile, it does not affect the outcome of the experiments in this thesis. However, one error was made during initial results collection in Chapter 7 – a conference paper with inaccurate peak times was published due to an incorrect assumption about the start point of the motion profile. Initially, the start point was approximated as 200ms after the parallel port trigger telling the Stewart platform to move based on initial visualisation of the acceleration profile (Figure 3.2). However, after more rigorous investigation it was seen that there is acceleration during this period, and so the start point was redefined as the parallel port trigger. This resulted in a 200ms difference between peak times as reported in (Nolan et. al 2011a) when compared to those in Chapter 7.

[1] http://www.virtools.com

## 3.2 EEG Recording

In the motion platform, a Biosemi ActiveTwo EEG system[2] was installed. This is an active electrode EEG system which has 128 unipolar scalp electrodes which fit into a cap, along with up to 8 bipolar electrodes which can be mounted on any body part. The cap deforms uniformly keeping the scalp electrodes at known locations for all subjects, based upon the 10-5 system (Oostenveld and Praamstra, 2001). For all experiments, four bipolar electrodes were placed just below and on the outer canthi of each eye, to record EOG activity. Two electrodes were placed on the mastoids, one on the neck approximately placed on the middle of the sternocleidomastoid muscle, and one on the nose, as potential sites for EEG reference and EMG signals. The neck electrode was later found to be unreliable. This system is used for all experiments, except the study described in Chapter 8, where a medical system was employed. For Chapters 6 and 7, EEG data were recorded at 512Hz, with -3dB bandwidth 0 - 102.4Hz[3]. For the validation experiment in Chapter 5, EEG data were recorded at 2048Hz.

A shielded system was also initially used in Chapter 5 - EEG data were recorded using the BrainAmp MRplus™[4] electrode system from 8 scalp electrodes along the scalp midline and one EOG channel, digitized at 5000Hz. The system has a -3dB bandwidth of 0.16Hz to 1000 Hz. The EEG data from the Pz channel were downsampled to 512Hz, bandpass filtered between 2-45Hz, epoched from 1000ms pre-stimulus to 2000ms post-stimulus, and baseline corrected from 500ms before stimulus presentation. Data were manually scanned for obvious artifacts (e.g., muscle twitch).

## 3.3 EEG Pre-Processing

Once the EEG data was recorded, the next step is to condition the data by removing noise and artifacts - signals such as EOG, EMG, electromagnetic interference that are recorded by the EEG system but not of cortical origin. Initially this identification was done manually, but as the volume of data grew, FASTER (Chapter 4) was developed to do this automatically.

The general procedure followed for all event-related potential (ERP) studies was to filter the data to remove irrelevant low- and high-frequency information. The continuous

[2] http://www.biosemi.com
[3] http://www.biosemi.com/activetwo_full_specs.htm
[4] http://www.brainproducts.com

time-series data were then segmented into data portions, commonly known as epochs, which are defined as a set number of time-points preceding and following a stimulus. Epochs containing excessive interference from eye or muscle movement, or other electrical or mechanical artifacts, were removed from the dataset. Any single-channel data containing excessive interference was interpolated from the remaining electrodes using spherical spline interpolation. Independent component analysis (ICA, see below) was used to separate the channels into statistically independent time-series; artifactual components were then rmoved to leave true EEG data remaining (for comprehensive details see Chapter 4). ERPs were computed by averaging across all epochs at each time point; for each run and condition, ERPs were computed for each dataset, and the average of those was taken for each subject to produce a subject average per condition. The grand average of all subjects was then computed across all subject ERPs.

Pre-processing of all EEG data recorded during experiments was performed using EEGLAB (Delorme and Makeig, 2004). This is a free software suite available for the MATLAB environment which provides a comprehensive framework for manipulation and processing of EEG data. Initially processing was performed manually; however as the volume of data increased, the need for an automated method for processing data became apparent. During the course of the thesis, such a method was developed along with corresponding software which works in tandem with EEGLAB; this is detailed in Chapter 4. This method, named FASTER, was applied to data in Chapters 6 and 7, and a preliminary version was used in Chapter 5. FASTER employs independent component analysis (ICA) which is described below. Further methods used in experiments described in Chapters 6 and 7 are standardised low-resolution electrical tomography (sLORETA), statistical parametric mapping (SPM) and time-frequency analysis.

Data processing methods specific to each experiment are detailed in the relevant chapters.

## 3.4 Independent Component Analysis

Independent Component Analysis (ICA) is a general name for a set of methodologies which perform blind source separation (BSS) on multivariate datasets to obtain statistically independent waveforms. The assumptions are that the multivariate data is a linear combination of independent statistical sources. The general process is then to

generate an unmixing matrix - a set of weights that specifies the linear combinations of each univariate data source which produces the statistically independent sources. There are various algorithms implemented for generating these, using different assumptions about the sources, different independence criteria, etc. Some popular methods are fastICA (Hyvarinen, 1999), SOBI (Belouchrani et al., 1997), and Infomax (Bell and Sejnowski, 1995) which is used in FASTER as described in Chapter 4. This is particularly useful for EEG as it can, in theory, separate multiple generating sources of EEG data coming from different brain regions. In practise these are not always robust, particularly across subjects as the recording environment changes from one to the next. However, one particularly useful application of ICA to EEG data is in the field of artifact removal and correction, where it can be used to identify and subtract additive sources of interference such as EOG (Croft and Barry, 2000; Hoffmann and Falkenstein, 2008).

## 3.5 sLORETA

sLORETA is a computational method, with accompanying software[5], used for solving the inverse problem and computing current density maps in the cortex (Pascual-Marqui, 2002). It uses a standardisation procedure which allows exact localization of test sources under no-noise conditions (Pascual-Marqui, 2007, 2009), and has no localisation biases in the presence of measurement and biological noise (Wagner et al., 2004). Its solutions have relatively low spatial resolution (compared to e.g. fMRI), which means that neighbouring voxels will be highly correlated. The general method underlying sLORETA necessitates finding the minimum-norm solution to an ill-posed inverse problem. The software projects EEG data into a 6239 voxel implementation of the Montreal Neurological Institute (MNI) standardised brain space (Evans et al., 1993). Standardisation is performed on each voxel by calculating an estimate of background noise, and current density is then computed as a ratio to the background noise.

Two independent groups, (Sekihara et al., 2005) and (Greenblatt et al., 2005), have shown that the method has no localization bias in the absence of measurement noise. In the presence of measurement noise (but no natural biological noise) they found that sLORETA has a localization bias - however, it is more realistic to consider that the brain in general is always active, thus producing biological noise. Furthermore, sLORETA has recently been

[5] http://www.uzh.ch/keyinst/loreta.htm

validated in several simultaneous EEG/fMRI studies (Mobascher et al., 2009; Olbrich et al., 2009), and in an EEG localization study for epilepsy (Rullmann et al., 2009). The previously developed, related tomography LORETA (Pascual-Marqui et al., 1994) has also received validation from studies combining LORETA with other more established localization methods, such as fMRI (Mulert et al., 2004; Vitacco et al., 2002), structural MRI (Worrell et al., 2000), and PET (Dierks et al., 2000; Pizzagalli et al., 2003; Zumsteg et al., 2005). Further LORETA validation has been based on the localization findings obtained from invasive, implanted depth electrodes, for which there are several studies in epilepsy (Zumsteg et al., 2006a; Zumsteg et al., 2006b; Zumsteg et al., 2006c) and cognitive ERPs (Volpe et al., 2007).

## 3.6 SPM

Statistical parametric mapping is a popular tool for neuroimaging analysis in fMRI, PET and EEG modalities. It is a software suite built on a number of statistical methods and processing tools (Friston and Buchel, 2003). The underlying method involves statistical tests and corrections for multiple comparisons specifically designed for neuroimaging data. For the EEG data in this thesis, the relevant methodologies applied were spatial remapping, statistical testing and family-wise error control (FWE) (Nichols and Hayasaka, 2003).

Data are initially projected from scalp-space into the Montreal Neurological Institute (MNI) standard brain-space using a predefined mapping for the Biosemi 128-channel system. Each sample of scalp EEG data is projected onto a 2D plane. This produces a 3D matrix of pseudo-voxels consisting of two spatial dimensions and one temporal dimension. This is performed on the averaged data of each condition of interest for each subject. Statistical contrasts are then defined and tests are performed on each voxel. The main benefit from the SPM software for EEG comes at this point - FWE correction can be used to define a suitable T-threshold which takes into account spatiotemporal non-independence for a desired type-I error rate, unlike other multiple comparison methods (e.g. Bonferroni correction). Uncorrected p-value thresholds can also be used to explore the data, but are generally less rigorous.

This correction is achieved using aspects of random field theory (Worsley et al., 2004). The Euler characteristic is a topological measure of a shape which, in the context used here, approximately defines the number of above-threshold connected shapes in the voxel space. Its estimated value for a given volume is computed based on a known

smoothing operator applied to the data, to estimate the number of spatially independent elements in the whole volume, and hence calculate the appropriate error rate based on this. It is necessary to apply smoothing to the image prior to computation of the FWE rate to validate the assumptions inherent in the method; this is implemented in SPM using a Gaussian smoothing kernel. The kernel used here was 6 x 6 x 8 voxels at full width, half maximum (FWHM).

sLORETA uses a non-parametric version of SPM called statistical non-parametric mapping (SnPM) to perform statistics, which uses a bootstrapping method to determine the appropriate significance level (Nichols and Holmes, 2002).

## 3.7 Time-Frequency Methods

In Chapters 6 and 7, time-frequency analysis is used to investigate the contribution of different frequency bands to the recorded ERPs. This allowed visualisation of EMG contribution to the ERPs and investigation of alpha-power increases and decreases, among others. To this end, two time-frequency methods were employed:

**FFT-based**. Time-frequency spectrograms were created for ERPs using the short-time Fourier transform on each channel per epoch per file per subject to investigate whether there was any unusual activity in e.g. the gamma band which might correspond to muscle movement. A window length of 128 sample points (0.25s) was used with a FFT size of 256 and 120 point overlap, giving a time resolution of 15.6ms and a frequency resolution of 1Hz. The event-related spectral perturbation was created by averaging these spectrograms for each file and subject and for each frequency dividing the post-stimulus time-frames by the mean value pre-stimulus, to obtain a per-frequency ratio value of increase or decrease from baseline. Band averages for the traditional EEG frequency bands were obtained.

**Wavelet-based.** Wavelet decompositions of ERPs were also created. The "Mexican Hat" wavelet was used for its good time-frequency properties and widespread use in literature. Wavelet decompositions were created at pseudo-frequencies appropriate for the traditional EEG bands delta (1-3Hz), theta (4-7Hz), alpha (8-12Hz), beta (13-35Hz) and gamma (>35Hz). Decompositions were performed at 1Hz intervals for the alpha band, and 2Hz intervals for the gamma band. The instantaneous signal power was computed by

pointwise squaring the signal. Band averages were then taken, and an 8Hz low-pass 2-pole Butterworth filter was applied to reduce the influence of the wavelet carrier signal. The event-related spectral potential (ERSP) plot was computed by subtracting the mean baseline value, and then dividing the whole power signal by the RMS value in the baseline.

For statistical comparison, these time-frequency measures can be then compared to zero or to other conditions at each time-frame and channel using t-tests, with FDR post-correction for multiple comparisons for all values within each frequency band. Further correction can be applied using a "running t-test" method – keeping only p-values with 10 or more consecutively significant time points.

# Chapter 4

# FASTER - Fully Automated Statistical Thresholding for EEG Artifact Reduction

## 4.1 Introduction

During the course of the experiments detailed in Chapters 6 and 7, a large number of EEG recordings were collected. These files were seen to contain normal EEG data without unusual activity arising from the Stewart platform, as verified in Chapter 5. However, normal EEG data is often contaminated with artifacts which occur during recording; furthermore, vestibular stimulation inherently produces EOG from the VOR and EMG from the VCR, both of which are near the scalp and will be mixed into the recorded signal. This chapter outlines a fully automated method which was developed to detect and remove such artifacts from recordings in order to streamline and standardise the processing of data. Automation was desirable to speed up processing, remove subjective variance in classifying artifacts by standardisation, and detect artifacts not noticeable by the human eye. This development enabled faster analysis of data, allowing more time to focus on results of the experiments.

The ERP is computed by averaging EEG epochs. Artifacts such as EOG, EMG, and electrode displacement can be orders of magnitude greater than the ERP, and can thus distort the signal, as the averaging operation is easily biased by outlying values. Throughout the thesis, it has been discussed that the VOR and VCR were induced by the motion stimuli, and thus caused EOG and EMG artifacts to occur. Generally EEG signals are in the order of tens of μV whereas EOG and EMG signals are in the order of hundreds of μV; therefore the EEG can be overpowered by artifact signals if they are not addressed. In addition to EOG and EMG artifacts, poor scalp contact for a particular electrode will produce consistently bad data for the duration of the recording. Other artifacts include spurious electrical activity picked up by the EEG amplifier (such as motor interference, which is discussed in Chapter 5), and electrical drift.

One simple and computationally inexpensive approach to EOG and EMG artifact detection and rejection involves deleting portions of the data with artifacts (e.g., data with amplitudes greater than 75 μV). This can potentially lead to a large loss of data, and consequently reducing the quality of the ERP, particularly during high-amplitude visual stimulation, or long trials which may involve visual fatigue. Electrodes with consistently poor signal quality are typically removed and then recreated using interpolation from the remaining electrodes, which effectively reduces the spatial resolution of the EEG. Therefore, several methods of removing EOG and EMG artifacts while retaining EEG data have been proposed (Croft and Barry, 2000; Moretti et al., 2003; Schlögl et al., 2007).

There are a number of extant methods for detection of artifacts in high-density EEG data, many of which are applicable only to specific artifact types (e.g., EOG artifacts). Some methods for artifact detection have a broader scope, however. For example, the Statistical Control of Artifacts in Dense Arrays Studies (SCADS) method, fully described in (Junghöfer et al., 2000), used thresholding methods to detect artifacts. In this approach, several editing matrices, containing parameters such as standard deviation (SD), maximum gradient, and maximum amplitude value, are constructed for each channel within each epoch. Thresholds are calculated for each parameter across whole epochs, whole channels, and single channels in single epochs using a non-parametric formula to measure the spread of the distribution. Whole channels, whole epochs, or single channels within single epochs whose parameters exceeded the thresholds are removed (epochs) or interpolated (channels).

Another approach to artifact detection involves the use of independent component analysis (ICA), which is made easily available through the EEGLAB software suite (Delorme and Makeig, 2004). ICA is a computational method that separates time-series data into statistically independent component (IC) waveforms. ICA outputs a mixing matrix that transforms EEG data to IC data, and its inverse unmixing matrix to transform IC data back to EEG data. These mixing matrices give information about an IC's spatial location on the scalp, and the transformed data gives information about the IC's temporal activity. Data recorded from scalp electrodes can be considered summations of EEG data and artifact, which are independent of each other: ICA is therefore potentially a useful methodology to separate artifact from EEG signal (Jung et al., 2000; Vorobyov and Cichocki, 2002). There is, however, a need to classify the resulting components as either artifactual or neural (Bian et al., 2006). If detected, artifactual ICs can then be subtracted from the recorded data and the remaining data can be remixed. Several methods for detecting and rejecting artifacts based

on ICA have been described previously in the literature. Some of these approaches can be limited by the requirement for the detection process to be trained from predefined artifacts (i.e. supervised), which are not always available, or may not be generalizable (Delorme et al., 2007; Jung et al., 1998; Schlögl et al., 2007; Yandong et al., 2006). For example, EOG artifacts vary in shape, amplitude and length between subjects. The training procedure is generally carried out manually from visually identified artifacts. Consequently full unsupervised processing is not possible with these methods, reducing the benefits gained from automation.

In short, methods have been developed for removing various types of artifacts from EEG. However, as many are application dependant, or focused on a single type of artifact, it would have been difficult to choose which approach(es) to take. Furthermore, all approaches involved at least some degree of supervision for classification of artifacts. Given the trend towards ever-denser EEG arrays, such artifact rejection methods are time-consuming. Instead, the task was undertaken to develop a general-purpose method which could be used for the data from this thesis and also by the EEG community in general. This method was completed and called Fully Automated Statistical Thresholding for EEG artifact Rejection (FASTER). Raw data are imported, bad channels removed, epochs extracted, artifacts detected and removed using ICA, subjects' data aggregated, and unacceptably noise data sets are removed. This fully automated, unsupervised approach – with raw EEG data as the input and epoched, artifact-attenuated data as the output – was therefore a great asset for processing the data collected in Chapters 6 and 7. The method can also be of use to the many researchers who collect EEG data.

With any new method of processing EEG data, and in particular for a fully automated, unsupervised method, it is essential to quantify the improvement of signal-to-noise and the rate of artifact detection against other established methods. In addition, methods suitable for dense EEG arrays may not be applicable to lower density arrays, and this applicability needs to be tested also. Therefore, FASTER was tested in a number of scenarios, and compared with the SCADS method on 128-, 64-, and 32-scalp electrode arrays of simulated EEG data with simulated artifacts. The advantage of testing an artifact rejection method on simulated data is that the sensitivity and specificity of the detection algorithms can be quantified. While simulated data are useful, however, they often contain artifacts with known properties (e.g., EOG amplitude of at least 80 μV). In contrast, real EEG data contain a variety of artifacts whose properties are unknown. Therefore, real 128-

channel EEG data from 47 subjects was also analysed using the FASTER method, trained individuals, and with SCADS. FASTER was also compared with SCADS on 64- and 32-scalp electrode array subsets of the real data to test the effect of using fewer data points.

## 4.2 Methods for EEG Data collection/simulation

### 4.2.1 Simulated Data

Forty seven sets of simulated data were created. These consisted of 200 epochs of data simulated from P3 dipoles using the BESA Dipole Simulator program[6], which then had artifacts added at random. The procedure for creating artifacts was derived from one of the artifact removal methods implemented in EEGLAB (Delorme et al., 2007). In order to create contaminated channels, white noise was added to a random number of channels (range 0-5). The white noise was of RMS amplitude randomly selected to be 1 - 10 times that of the channel itself. A random number of the 200 epochs (range 0-15) had a high-amplitude (30 - 150μV) low frequency (1 - 3Hz) wave added to all channels to simulate an electrode-shift artifact. The position of all artifacts was recorded and the data were then processed. The pre-artifact data and post-processing data were compared at the position of each artifact to assess the degree of artifact removal.

### 4.2.2 Real Data

Forty-seven datasets from healthy controls from a visual oddball paradigm were analysed (mean age = 37.6 years, 28 male) - see Appendix B for details of this study and application of FASTER to the clinical population. ERP data were recorded in a soundproofed room using the ActiveTwo Biosemi™ electrode system from 134 electrodes (128 scalp electrodes) organized according the 10-5 system digitized at 512 Hz. The vertical and horizontal electro-oculograms were recorded bilaterally from approximately 3 cm below the eye and from the outer canthi respectively. An additional two electrodes were placed on the mastoids bilaterally.

Subjects observed blue circles, separated by an inter-stimulus interval of 2±0.5s seconds (uniformly distributed), presented for 205 trials in a pseudorandom order. Frequent

[6] http://www.besa.de/updates/tools/

non-target (80%) and infrequent target (20%) circles were 2 cm or 4 cm in diameter, respectively. Subjects were instructed to press a button as quickly as possible following a target stimulus. This type of oddball task typically evokes a positive deflection in the ERP with a latency of approximately 300ms. This is called the P3/P300 component. These data were acquired with the understanding and written consent of each subject, the approval of St. Vincent's University Hospital Ethics Committee, and in compliance with national legislation and the Code of Ethical Principles for Medical Research Involving Human Subjects of the World Medical Association (Declaration of Helsinki).

All data were recorded from a Biosemi ActiveTwo 128 channel EEG system at 512Hz. The Biosemi system replaces the ground electrodes used in conventional systems with two separate electrodes: Common Mode Sense (CMS) active electrode and Driven Right Leg (DRL) passive electrode. These two electrodes form a feedback loop, which drives the average potential of the subject (the Common Mode voltage) as close as possible to the analogue-to-digital reference voltage in the AD-box (the analogue-to-digital reference can be considered the virtual ground of the amplifier). The reference signal is the DRL minus the CMS.

## 4.3 Methods for Artifact Detection and Removal

### 4.3.1 General Process

For all methods (FASTER, SCADS and Manual process), the below process was followed, with the respective appropriate artifact detection method applied.

- The datasets were converted to EEGLAB format and then referenced to Fz – this was chosen as it was common to the 128-, 64- and 32-channel datasets.
- The EEG data were filtered offline using equiripple filters between 1 - 95 Hz with a notch filter at 50 Hz (bandwidth 6 Hz) to remove mains interference. All filters used were finite impulse response (FIR) designed using the Parks-McClellan Chebyshev design method. The *firfilt* MATLAB library[7] was used to design these. Filters were applied forwards and backwards to ensure zero phase distortion. The frequency design specifications thus denote -6dB levels. The high-pass filter cut-off frequency was initially chosen for computational reasons –

[7] http://www.uni-leipzig.de/~biocog/content/widmann/eeglab-plugins/

for FIR filters, the number of filter coefficients, and thus the time needed to compute them, greatly increases as the cut-off frequency decreases. This also increases the length and amplitude of the filter artifact which appears at the start and end of the recording. The 1Hz cut-off thus provided an acceptable compromise of retaining frequency content, clean data and computation time. Later, visualisation of the data recorded in Chapters 6 and 7 after filtering with a 0.1Hz high-pass infinite impulse response (IIR) filter revealed high-amplitude low-frequency contributions which dominated the data and appeared to be artifactual; therefore the 1Hz filter was used. The 95Hz cut-off provided protection from the 100Hz harmonic of the 50Hz mains noise, while retaining content in the high-gamma band.

- Channels were analysed for artifacts, and any contaminated channels were interpolated.
- Data were then epoched from -500ms to 1500ms, and baseline corrected from -200ms to 0ms.
- Epochs were analysed for artifacts, and any contaminated epochs were removed from the dataset.
- The data were converted to be in average reference.
- Infomax ICA was then performed on the full dataset including external channels, to give best chance of detecting EOG artifacts, and the resulting ICs were analysed for artifacts.
- Contaminated ICs were subtracted from the dataset, from all channels, including externals.
- Each channel in each epoch was then analysed for artifacts, and if found to be contaminated, was interpolated.
- Finally, the ERP of each dataset was taken, baseline corrected from -200ms to 0ms, and concatenated to make a grand average dataset. Each subjects ERP was analysed for artifacts, and if found to be of poor quality, removed from the average.

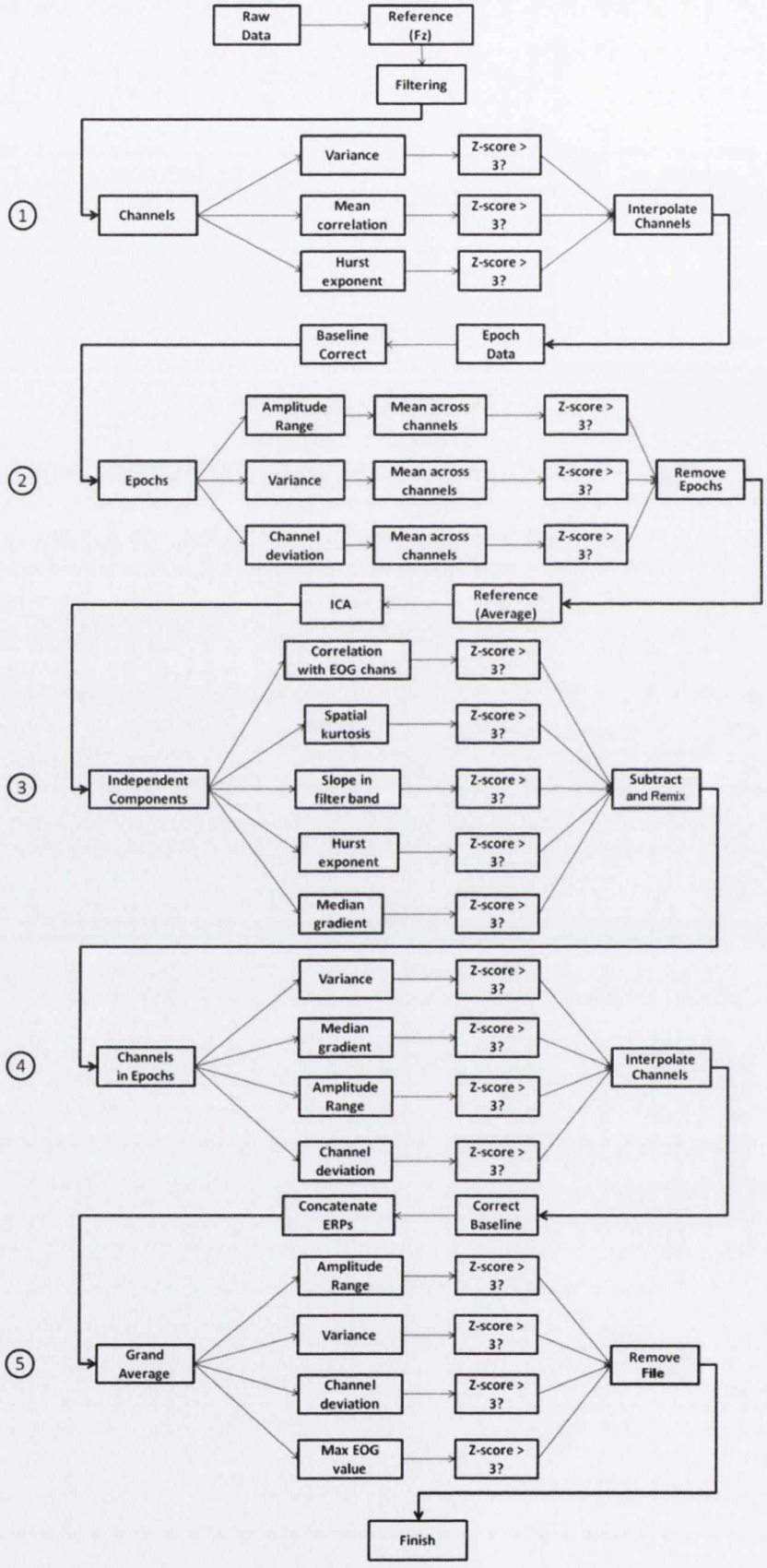


Figure 4.1 Flowchart detailing each step of the FASTER method.

### 4.3.2 FASTER

Data artifacts were detected and corrected in five aspects of the EEG data: channels, epochs, ICs, single-channel single-epochs, and aggregated data (i.e. across subjects). For each aspect, statistical parameters of the data were calculated by computing. The metric that defined contaminated data was a **z-score ≥ ±3** for that parameter - this is a definition of an outlier. This is applied to all parameters. The z-scores are calculated by computing the mean and standard deviation for each parameter across each channel, epoch, IC, single-channel single-epoch or aggregated data, then subtracting the mean from the parameter values and dividing them by the standard deviation. For example, to compute the z-score for the variance of channels, the mean of the variance for all channels would be computed, along with the standard deviation. The mean would be subtracted from all variance values, and they would all be divided by the standard deviation. Any transformed values ≥ 3 or ≤ -3 larger would be deemed to be contaminated. Various other methods for thresholding were considered (and rejected), and are discussed in the supplemental methods section.

For the mathematical descriptions of the properties, the following conventions apply:

$n = 1, 2, ..., N$ - indicates a specific channel ($N$ is the number of channels in the dataset)

$e = 1, 2, ..., E$ - indicates a specific epoch ($E$ is the number of epochs in the dataset)

$c = 1, 2, ..., C$ - indicates a specific IC ($C$ is the number of components in the dataset)

$x_n$ - indicates the data in channel $n$

$x_{n_e}$ - indicates the data in channel $n$ within epoch $e$

$x_{c_t}$ - indicates the temporal data in component $c$

$x_{c_s}$ - indicates the spatial data in component $c$

$s^2{}_x$ - indicates the variance of data

$\langle x \rangle$ - indicates taking the mean of data

$\langle x \rangle_N$ - indicates taking the mean of data across channels

$\langle x \rangle_E$ - indicates taking the mean of data across epochs

$EOG_{1,2,3,4}$ - the EOG electrodes

F(x) - power spectrum (calculated using MATLAB's *pwelch* function)

1. Channel Artifacts.

An electrode or subset of electrodes in an EEG dataset may move during an EEG session, resulting in bad contact with the scalp and therefore a poor quality signal. More rarely, electrodes may also have mechanical faults, for example frayed wiring, which can partially or wholly degrade the signal received. Such electrodes can produce erratic signals. To classify channels as artifactual, three parameters of each channel along with their z-scores were calculated:

- The first parameter was the mean of the channel's correlation coefficients with other channels. Most channels, especially in a high-density system, should correlate highly with neighboring channels. Therefore, a channel with contaminated data will likely have a low correlation with other channels.

  Parameter 1: $\frac{\sum_{m=1}^{N} r_{x_n,x_m}}{N}$, the mean correlation coefficient of channel *n*, where $r_{x_n,x_m}$ is the Pearson correlation coefficient between channels n and m

- Alternatively, a contaminated channel may correlate quite well with other channels, but have a higher variance (due to additive noise) and therefore the second parameter is the variance of the channel.

  Parameter 2: $s^2{}_{x_n}$, the variance of channel *n*

- The third parameter was the *Hurst exponent*. The Hurst exponent is a measure of long-range dependence within a signal. Human phenomena such as EEG have values of H ≈ 0.7, and signals lying outside of this range can be considered artifacts (for more details see Appendix A).

Parameter 3: $H_{x_n}$, the Hurst exponent of channel $n$

The above parameters were corrected for reference offset using the method described in (Junghöfer et al., 2000). Channels identified as contaminated were removed and data at this electrode were reconstructed by interpolating from neighboring electrodes using the EEGLAB 7 spherical spline interpolation function.

2. Epoch Artifacts.

An epoch in an EEG dataset may at times be contaminated with all-channel noise, typically caused by subject movement, and subsequent physical movement of the electrodes. To detect such epochs, 3 parameters were computed for each channel within the epoch, and z-scores calculated.

- The movement of electrodes on the scalp results in a change in impedance between the scalp and the electrodes, which consequently affects the electrode voltage offsets. This offset change contaminates epochs, and can be identified by its high amplitude. To detect this contamination, the first parameter computed was the amplitude range of the epoch.

Parameter 4: $\langle \max(x_{n_e}) - \min(x_{n_e}) \rangle_N$, the mean amplitude range across channels in epoch $e$

- Shifting electrodes may also produce less extreme movements that may not have sufficient amplitude range to exceed the threshold of a z-score equal to 3, but still contaminate an epoch. This type of artifact may be reflected in a high deviation of that epoch's average value from the average values across all channels. The second parameter computed was the deviation from each channel's average value.

Parameter 5: $\langle \langle x_{n_e} \rangle - \langle x_n \rangle \rangle_N$, the mean deviation across channels from the channel average in epoch $e$

- Subject movement also produces EMG interference. A high variance will reflect such activity, and so the third parameter calculated was the variance.

Parameter 6: $\langle s^2{}_{x_{ne}} \rangle_N$, the mean variance across channels in epoch $e$

3. IC Artifacts.

The *Infomax* (Bell and Sejnowski, 1995) algorithm was employed to perform the ICA decomposition. The number of data points needed to find C stable components from ICA is typically $kC^2$ for each data channel, where $k$ is a multiplier. The $k$ value was set to 25, as recommended in (Onton et al., 2006). For example, our real data were of length 512*205 = 104960 points, and with 128 scalp channels, 4 EOG channels and 2 mastoid channels, the maximum possible number of ICs would be 134. However, this would not have met the k = 25 criterion, which would necessitate 25 * $(134)^2$ = 448900 data points. Therefore, the value of C was reduced to $C_{pca}$ by performing Principal Component Analysis (PCA) on the EEG data and keeping only the first $C_{pca}$ principal components (Shlens, 2005). $C_{pca}$ was calculated as:

$C_{pca} = floor\left(\sqrt{\frac{L}{k}}\right)$, where L is the length of the EEG dataset (in samples), and floor indicates rounding down to the nearest integer.

This reduces the rank of the data and so a smaller number of ICs are computed. Interpolation of channels also reduces the rank of the data, and so $C_{pca}$ was corrected to account for this:

$C_{pca} = \min(floor\left(\sqrt{\frac{L}{k}}\right), N - N_{interpolated})$, where N was the original number of channels and $N_{interpolated}$ was the number of channels interpolated in the channel interpolation step.

ICA often produces ICs which consist entirely of artifactual data. These can then be subtracted from the dataset, leaving EEG data without the artifact. To classify ICs, five parameters were computed, and z-scores calculated.

- To identify artifacts caused by eye blinks (vertical EOG, VEOG) or saccades (horizontal EOG, HEOG) , the correlation coefficients of each IC time series with the four recorded EOG (two VEOG and two HEOG) data channels were calculated, and the maximum absolute value was taken as the first parameter. The absolute was taken to account for possible differences in polarity between the EOG channel data and the IC time series.

  Parameter 7: $\max\left(\left|r_{x_{c_t},x_{EOG_{1,2,3,4}}}\right|\right)$, the maximum of the absolute correlation coefficient between component $c$ time-course and EOG channels

- Another common type of artifact singled out by ICA is a short, high-amplitude, single-electrode offset, often termed a "pop-off". An IC consisting of a pop-off has spatial data which shows activity in a single channel and none otherwise. This is reflected in a high kurtosis value in the spatial data, as kurtosis measures the peakedness of data. The second parameter computed was the kurtosis of the spatial data.

  Parameter 8: $\frac{\mu_4}{{\mu_2}^2} - 3$, where $\mu_i$ gives the i-th central moment of the spatial data, is the equation for kurtosis of the spatial information in Component $c$

- There is typically white noise in the acquired data due to hardware properties. White noise has a close-to-flat frequency power spectrum, as opposed to EEG components which have a $\frac{1}{f}$ power spectrum distribution. Residual white noise may remain after filtering, albeit with a very low contribution. Independent components consisting of white noise were identified by calculating the slope of the spectrum over the low-pass filter band as the third parameter.

  Parameter 9: $\left\langle\frac{dF(x_{c_t})}{df}\right\rangle\Big|\ f_{LP1} < f < f_{LP2}$, the mean slope of the power spectrum of the component $c$ time-course, between the band edges of the low-pass filter band

- The fourth parameter estimated was the Hurst exponent (see Appendix A).

  Parameter 10: $H_{x_{c_t}}$, the Hurst exponent of component $c$ time-course

- The fifth parameter was the median gradient value, which is above threshold if the IC contains considerable high-frequency content, was also calculated for each IC time series.

  Parameter 11: $median\left(\frac{d(x_{c_t})}{dt}\right)$, the median slope of the component $c$ time-course

4. Single-Channel, Single-Epoch Artifacts.

Following the previous three steps, a high percentage of artifacts will have been removed. Some small transient artifacts may remain on single channels, within single epochs – for example, short bursts of white noise due to transient electrical faults, or electrodes that lost contact during a recording and were not sufficiently noisy to be detected as bad channels. Such artifacts were corrected by interpolating single channels within single epochs, using spherical splines. To detect the artifacts, four parameters were computed for each channel within each epoch, and z-scores calculated.

- The first parameter was the variance, to detect single channels in single epochs with additive noise.

  Parameter 12: $s^2{}_{x_{n_e}}$, the variance of channel $n$ in epoch $e$

- The second was the median gradient, to detect other high-frequency activity.

  Parameter 13: $median\left(\frac{d(x_{n_e})}{dt}\right)$, the median slope of the channel $n$ in epoch $e$

- The third was the amplitude range of the channel, to detect pop-offs.

  Parameter 14: $\max(x_{n_e}) - \min(x_{n_e})$, the amplitude range of channel $n$ in epoch $e$

- Fourth, in order to detect electrical drift, the deviation of the mean amplitude in the epoch for each channel from the whole-channel mean amplitude was calculated.

  Parameter 15: $\langle x_{n_e} \rangle - \langle x_n \rangle$, the deviation from the channel average of channel $n$ in epoch $e$

5. Contaminated datasets.

After each file had been processed, a grand average dataset was created (i.e.,. all subjects' data were aggregated) so that each epoch was the ERP of a processed file. In a typical EEG study there are often subjects whose data are contaminated by artifacts to the extent that their data are not a true reflection of neural processes, and therefore distort the grand average data. These subjects' data are often removed entirely from the grand average. In order to identify these subjects, the epoch artifact detection method was repeated for the grand average:

- Property 16: $\langle \max(x_{n_e}) - \min(x_{n_e}) \rangle_N$, the amplitude range in epoch $e$
- Property 17: $\langle {s^2}_{x_{n_e}} \rangle_N$, the variance in epoch $e$
- Property 18: $\langle \langle x_{n_e} \rangle - \langle x_n \rangle \rangle_N$, the deviation from the channel average in epoch $e$
- An additional parameter - the maximum absolute value of the EOG channels in the ERP - was computed for each epoch in order to determine whether EOG artifacts remained, as after EOG component subtraction the maximum value in the EOG channels should be small.

Property 19: $\max\left(\mathrm{x}_{\mathrm{EOG}_{1,2,3,4_e}}\right)$, the maximum value in the EOG channels in epoch e

Thresholds were calculated for each parameter, and any epoch (i.e., subject) that surpassed that threshold was considered contaminated and removed from the grand average file.

### 4.3.3 SCADS

The SCADS method was implemented following the description in (Junghöfer et al., 2000): data were converted to a single reference (Fz, as this was the reference chosen for data using the FASTER method). Editing matrices were composed, consisting of the maximum, standard deviation, and maximum gradient of each channel in each epoch. Limits were computed using the nonparametric formula to detect contaminated channels and channels in epochs. Contaminated channels were interpolated using spherical splines. Data were converted to average reference. Editing matrices were recomposed. At this stage, Junghöfer recommends visual identification of remaining artifacts in channels within epochs. To make this a fully automated process and thus a valid comparison with the FASTER method, this

visual identification was substituted with the 3 z-score threshold used by the FASTER method. Epochs with 10 or more contaminated channels were deemed bad, as suggested by Junghöfer. They were removed from the dataset. Remaining contaminated channels in epochs were interpolated using spherical splines.

### 4.3.4 Supervised, expert artifact identification

Contaminated epochs, contaminated channels and artifactual ICs were identified by seven trained individuals, all of whom had extensive EEG processing experience and who were currently engaged in high-density EEG research. The raw data were filtered and epoched, and the participants were then instructed to list the epochs and channels they believed were artifact-contaminated. This was done by visual identification, using EEGLAB software, which allows users to scroll through EEG data. They were also instructed to list any datasets they believed to be contaminated to the extent that artifact removal would not improve the quality of the data. Such datasets were not used to calculate the average. In the remaining datasets, the listed artifacts were removed, and ICA was performed on the data. Participants were then instructed to list any ICs which they believe were artifact-contaminated, which were subtracted from the data. Each participant analyzed between 4 - 9 datasets each.

### 4.3.5 Artifact removal quantification

In order to quantify the performance of the artifact removal method on real data, a metric for measuring artifact contribution to EEG was defined as the variance in the 500ms baseline prior to the stimulus presentation (Handy et al., 2003). This variance should be zero in a "perfect" dataset (for a task inducing no pre-stimulus effect, such as the P3). This metric has the advantage of making no assumptions about the signal content, other than a lack of pre-stimulus activity. The disadvantage is that a signal with zero amplitude has zero variance, and so any method that removed all data would have perfect performance. Therefore, there is a need to ensure the EEG signal is not being attenuated, and consequently P3 amplitude and latency were also taken as measures of signal quality. The peak of the P3 was found by fitting a parametric function to the ERP from 200ms - 1000ms using a Gaussian profile and determining the delay at the peak amplitude (Gerson et al., 2005). The percentage of epochs

removed was also recorded, as a measure of data retention. These measures were compared for each processing method.

In order to compare the two methods, FASTER vs. SCADS, a factorial ANOVA was conducted with method and number of channels as factors. A Greenhouse-Geisser correction was used to correct for non-sphericity. Type 1 error probability was set at .05, $p_{corrected}$ was set using Bonferroni correction for multiple comparisons adjusted for correlation among dependent variables (see Appendix A), Including all channels when comparing the effect of number of channels may result in differing variances because the higher-density arrays will have more channels further away from the reference. Therefore, the baseline variance at channel Pz (P3 amplitude is typically maximal over Pz) was chosen as this channel was common to all datasets. The simulated data results were calculated from 47 files. Sensitivity and specificity for artifact detection was calculated using the following formulae: sensitivity = detected artifacts / total contaminated data; specificity = 1 - (detected false artifacts / total uncontaminated data).

## 4.4 Results

### 4.4.1 Simulated data

| Method | No. Chans | Percentage of Artifacts Removed | | | | | | |
|---|---|---|---|---|---|---|---|---|
| | | Channels Sensitivity/ Specificity (%) | Epochs Sensitivity/ Specificity (%) | EOG (%) | EMG (%) | Discontinuities (%) | Linear Trends (%) | White Noise (%) |
| **FASTER** | 128 | 94.47/ 98.96 | 60.24/ 97.53 | 98.99 | 99.91 | 82.97 | 93.04 | 92.93 |
| | 64 | 97.02/ 98.48 | 61.83/ 97.54 | 99.07 | 99.19 | 94.68 | 97.02 | 95.30 |
| | 32 | 5.88/ 96.81 | 58.64/ 97.49 | 97.64 | 94.17 | 93.61 | 95.59 | 91.29 |
| **SCADS** | 128 | 100/ 96.42 | 0.15/ 99.99 | 11.69 | 99.73 | 79.43 | 91.19 | 98.13 |
| | 64 | 100/ 94.10 | 0.15/ 99.99 | 14.03 | 98.27 | 87.43 | 93.00 | 96.59 |
| | 32 | 5.88/ 84.50 | 0.15/ 99.99 | 18.31 | 95.36 | 83.33 | 93.22 | 96.53 |

**Table 4.1. Results from the simulated data.**

Due to the non-normal distribution of the detection rates, Wilcoxon Signed Ranks tests were conducted.

*Channel artifacts.* Wilcoxon signed rank tests showed that there was a significant higher channel detection sensitivity for the SCADS method compared to FASTER using 128 channels ($Z = 2.701$, $p < 0.01$). This was not significant using 64 or 32 channels. Analysis of the channel detection specificity of each method, shows that FASTER had a significantly higher specificity than SCADS using 128-, 64- and 32- channel datasets ($Z = 5.375$, $Z = 5.517$, $Z = 5.907$ respectively, $p < 0.001$).

*Epoch artifacts.* Wilcoxon signed rank tests showed that there was a significant improvement in the performance of the FASTER method over SCADS for epoch detection sensitivity using 128-, 64- and 32- channels ($Z = 5.381$, $Z = 5.408$, $Z = 5.315$ respectively, $p < 0.001$. FASTER had a significantly lower specificity than SCADS using 128-, 64- and 32-channel datasets ($Z = 5.304$, $Z = 5.304$, $Z = 5.304$ respectively, $p < 0.001$).

*EOG and EMG artifacts.* A Wilcoxon signed rank test showed significant improvement in EOG removal percentage using the FASTER method compared with the SCADS methods for datasets of 128, 64 and 32 channels ($Z = 5.905$, $Z = 5.841$, $Z = 5.754$ respectively, $p<0.001$). Bonferroni correction for 3 comparisons was used. A Wilcoxon signed rank test showed no significant difference in removal percentage between FASTER and SCADS methods for simulated EMG artifacts.

*Single-channel, single-epoch artifacts.* For linear trends, a Wilcoxon signed rank test showed a significant improvement in removal percentage using the FASTER method compared with the SCADS methods for the 64-channel array only ($Z = 3.330$, $p < 0.005$). For white noise, a Wilcoxon signed rank test showed a significantly lower removal percentage using the FASTER method compared with the SCADS method for datasets of 128 and 32 channels ($Z=2.691$, $p<0.05$, $Z=3.02$, $p<0.01$ respectively). For discontinuities, a Wilcoxon signed rank test showed no significant difference in removal percentage between FASTER and SCADS methods.

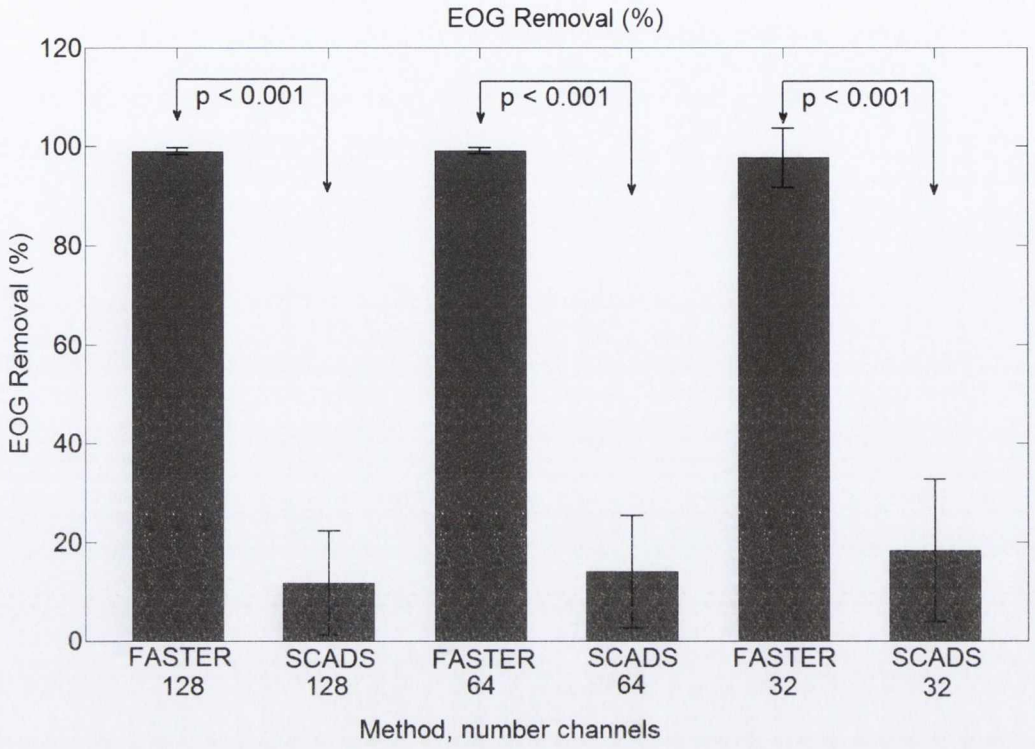


Figure 4.2. Comparing EOG removal percentages between FASTER and SCADS.

### 4.4.2 Real Data

| Method | No. Chans | Baseline Variance (μV) | P3 Amplitude (μV) | P3 Latency (ms) | Peak Width (ms) | Epochs Removed (%) |
|---|---|---|---|---|---|---|
| **FASTER** | 128 | 0.2222 | 7.417 | 372.42 | 49.29 | 3.2 |
| | 64 | 0.2279 | 7.746 | 378.19 | 49.22 | 3.1 |
| | 32 | 0.2204 | 8.387 | 377.59 | 49.95 | 3.3 |
| **SCADS** | 128 | 0.2672 | 6.990 | 361.05 | 48.34 | 2.6 |
| | 64 | 0.2525 | 6.931 | 362.38 | 47.98 | 2.4 |
| | 32 | 0.2334 | 7.732 | 359.83 | 47.30 | 2.4 |
| **Supervised** | 128 | 0.4120 | 6.885 | 400.09 | 46.38 | 3.3 |
| **Raw** | 128 | 0.7580 | 14.943 | 449.48 | 45.33 | - |
| | 64 | 0.7536 | 26.481 | 449.54 | 45.03 | - |
| | 32 | 0.9230 | 12.263 | 449.48 | 45.33 | - |

Table 4.2. Results from the real data.

Baseline variance: The one-way ANOVA comparing baseline variances of FASTER, SCADS and supervised was significant ($F(1.074,41.885) = 5.036$). Follow-up t-tests (refer to Appendix A for multiple comparison correction procedure) showed significantly lower baseline variance for FASTER compared to manual and SCADS methods ($t(39) = 2.531$, $t(42) = 2.708$ respectively, $p_{corrected}<0.0264$). There was no significant difference between manual and SCADS methods. Raw data ERPs were marred by artifacts. Figure 4.3 displays a graphical representation of these results.

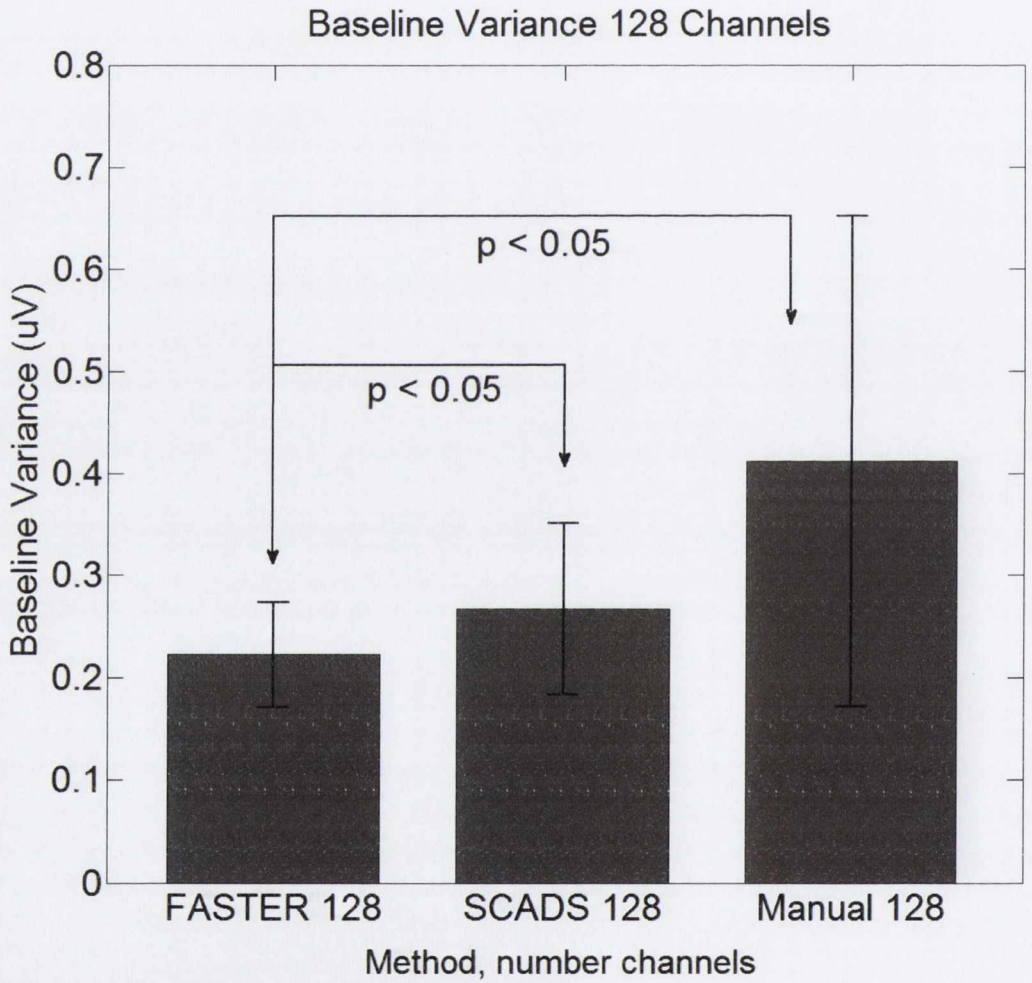


Figure 4.3. Comparing the baseline variance of 128-channel datasets across methods. Bars are mean±standard deviation.

In order to compare FASTER to SCADS for different EEG array densities (128, 64, and 32 channels) series of paired t tests were conducted for each array size. Alpha was set at 0.05, with $p_{corrected}$ = .045 (see Appendix A). FASTER had a significantly lower baseline variance than the SCADS method when using 128 channels (t(42) = 2.708, $p_{corrected}$ < .045) and approached significance using 64 channels (t(42) = 2.039, $p_{corrected}$ = 0.048). There was no significant difference between methods when using 32 channels.

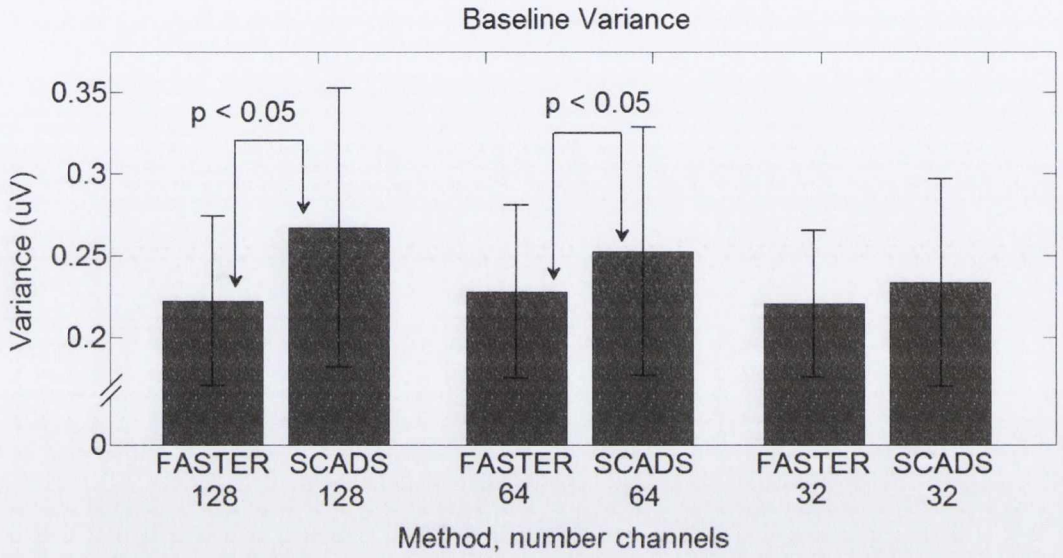


**Figure 4.4. Comparing the baseline variance of different array sizes between FASTER and SCADS. Bars are mean±standard deviation.**

In order to compare the effect of array size within methods, we compared baseline variances of the common channels for each array size. Alpha was set at $p_{corrected}$ = .0418. The FASTER method showed no significant differences in baseline variances depending on the number of channels processed. The SCADS method had a lower baseline variance using 32 channels vs. 128 channels (t(46)=3.212, p<.0418), using 64 channels vs. 128 channels (t(46)=2.267, p<.0418) and using 32 channels vs. 64 channels (t(46)=3.359, p<.0418).

P3 latency and amplitude: The one-way ANOVA comparing P3 latency after FASTER, SCADS and supervised processing methods on datasets with 128 channels was significant (F(1.281,48.689)=5.032, p<0.05). Follow-up t-tests, with alpha set at $p_{corrected}$=0.0284, showed that SCADS processing resulted in significantly shorter latency than FASTER and manual processing (t(42)=2.803, t(40)=2.759 respectively, $p_{corrected}$<0.0284). There was no significant difference in latency between supervised and FASTER processing. FASTER

produced a P3 with a significantly higher amplitude compared to supervised processing, with alpha set at $p_{corrected}$=0.0446 (t(38)=2.201, $p_{corrected}$<0.0446)

Paired t-tests (alpha set at $p_{corrected}$ = 0.0411) showed a significantly higher P3 amplitude for FASTER vs. SCADS using 64 electrodes (t(42)=2.773, $p_{corrected}$<0.0411), and significantly higher P3 latencies (alpha set at $p_{corrected}$ = 0.0371) for FASTER for 128, 64 and 32 electrodes (t(42)=2.803, t(42)=2.642, t(43)=3.684 respectively, $p_{corrected}$<.0371).

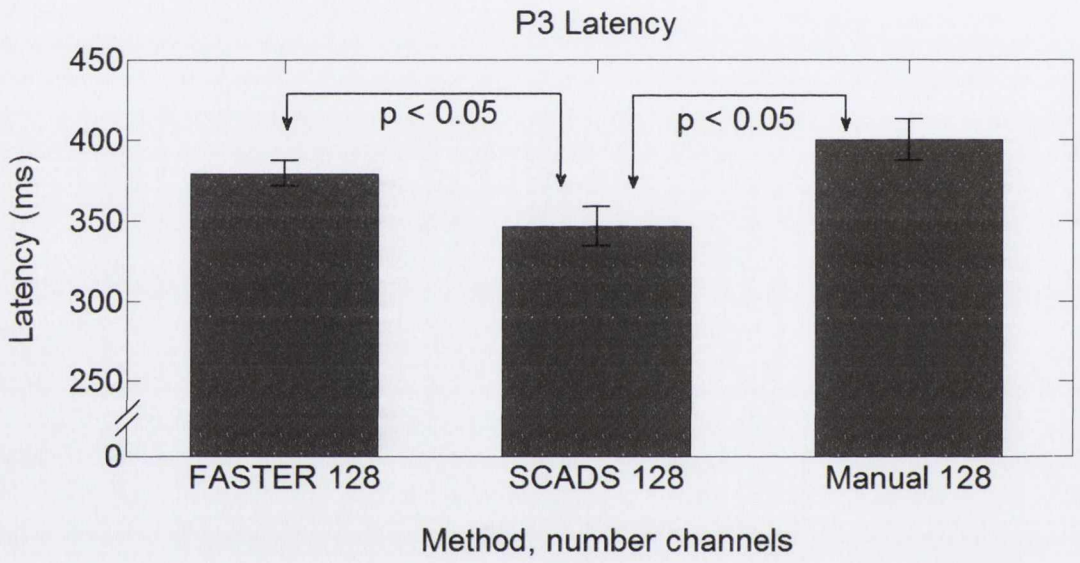


Figure 4.5. Comparison of the latency of the P3 component after processing with different methods.

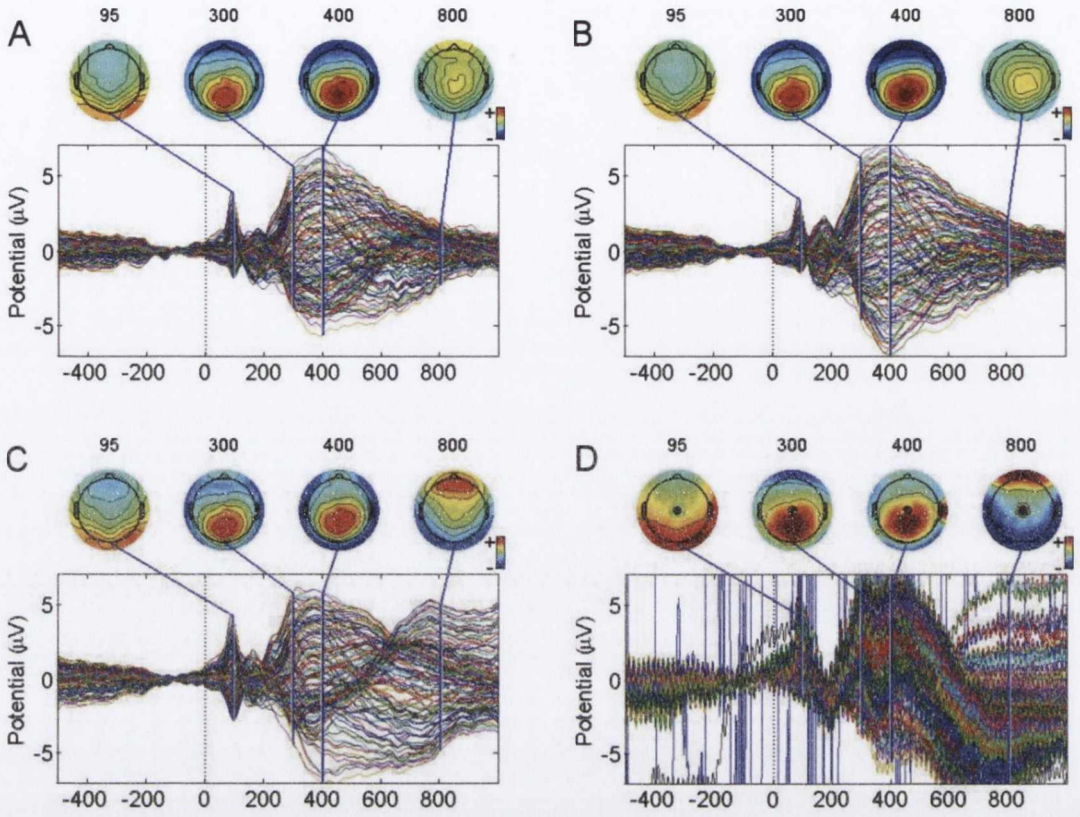


Figure 4.6. Butterfly plot of grand average ERPs after various processing methods. A - supervised processing. B - FASTER processing. C - SCADS processing. D - Filter only. The late frontal component present in C is due to uncorrected EOG artifacts. A 30Hz low-pass filter was applied for display purposes only.

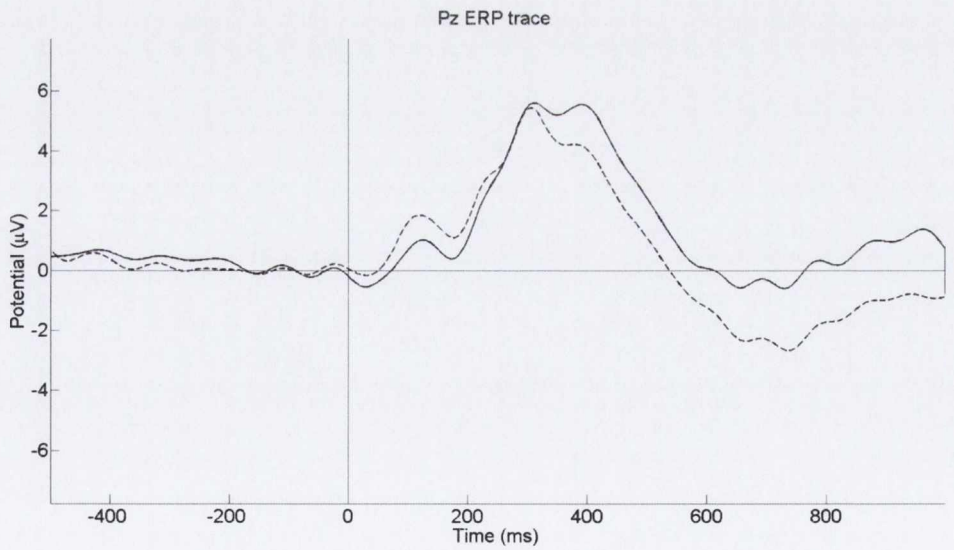


Figure 4.7. ERP at Pz. Solid line is after FASTER processing, dashed line is after SCADS processing. The SCADS method has a narrower peak, which leads to a shorter latency using Gaussian peak picking. A 15Hz low-pass filter was applied for display only.

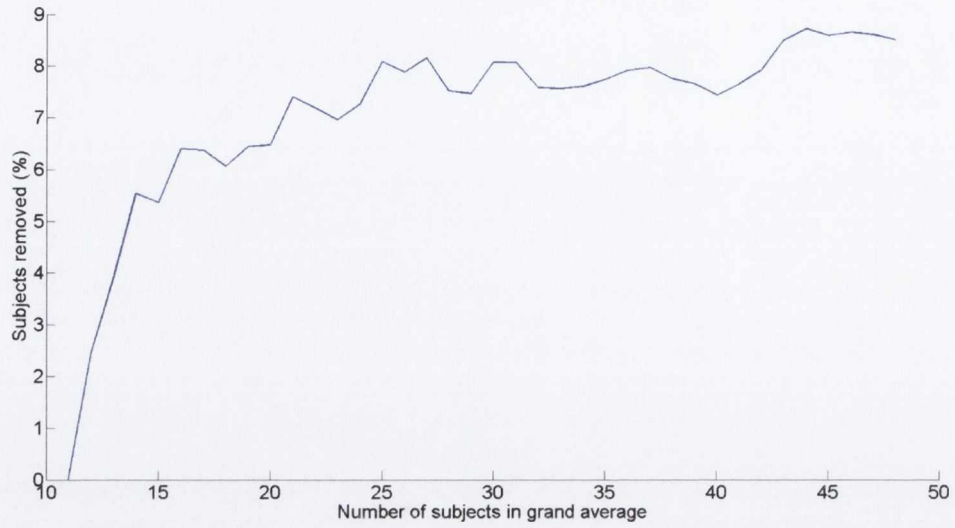


**Figure 4.8. Number of subjects removed as a function of number of subjects present.**

Contaminated subject removal: From a total of 47 subjects, FASTER identified 4 subjects as contaminated in the 128-channel dataset, 4 in the 64-channel dataset, and 2 in the 32 channel dataset. In order to test the effect of identifying contaminated subjects in smaller sample sizes, sub-sets of the data (ranging from 10-47 subjects, with random inclusion of subjects) were generated. The composition of each sub-set was shuffled 100 times and the number of contaminated subjects was recorded for each sample size. Figure 4.8 displays these data.

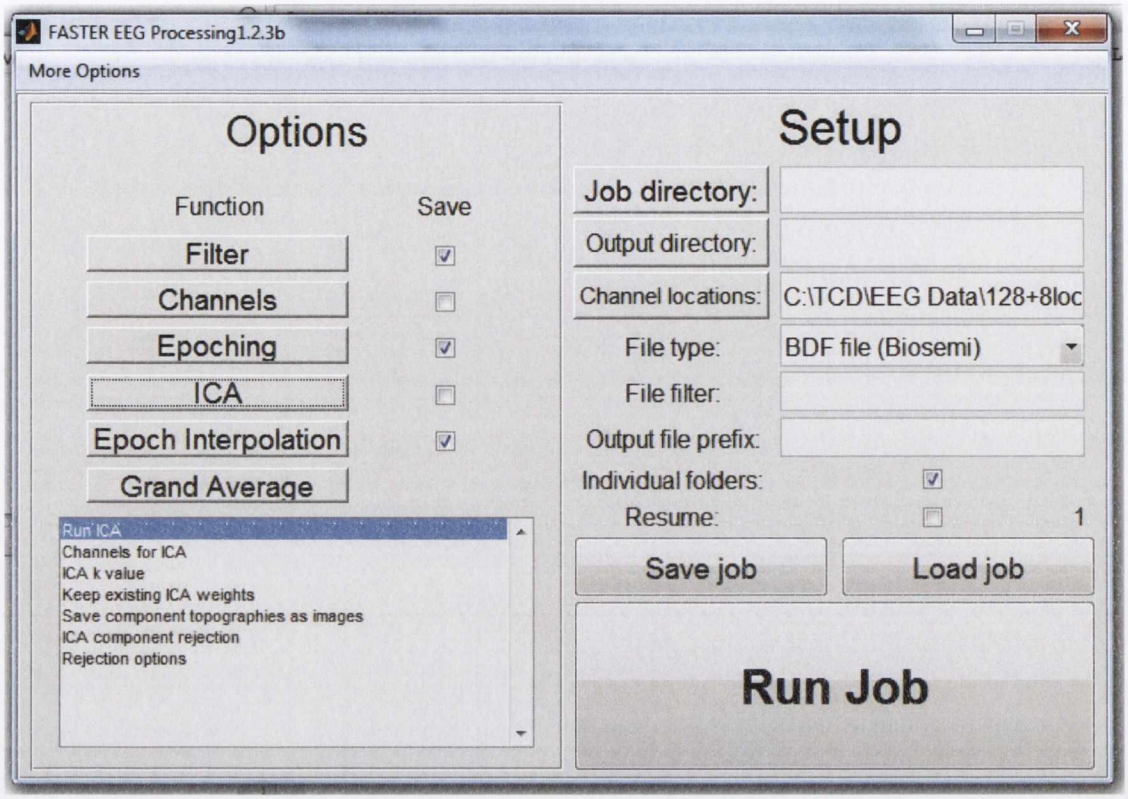


Figure 4.9. The software written to run the FASTER process on a file or group of files. This software was made freely available, and is integrated work with EEGLAB. It has been downloaded over 2000 times as of October 2013.

Figure 4.9 shows the main interface of the FASTER software, written to allow users without a background in signal processing to produce high-quality EEG data with artifacts removed. Default settings are those detailed in Section 4.3; however, as this validation is only based on P3 data, some settings can be varied if users wish to experiment for better performance for their particular data. For example, if the epoching functions are disabled, FASTER can then be applied to continuous EEG data.

## 4.5 Discussion

This chapter details the FASTER processing method and the quality of its output. In order to quantify the performance of FASTER simulated data were analyzed using FASTER and a variant of SCADS. Furthermore, real data were analyzed using FASTER, SCADS, and by supervised detection. FASTER was also tested across different numbers of scalp electrodes (128, 64 and 32). The results of the analysis of the simulated data showed that FASTER had generally high sensitivity and specificity for detection of artifacts. FASTER had

> 90% sensitivity and specificity in simulated datasets for detection of contaminated channels, EOG and EMG artifacts, linear trends and white noise. SCADS had a significantly higher sensitivity to channel artifacts than FASTER using 128 channels. However, specificity was significantly higher for FASTER vs. SCADS across all array sizes. FASTER generally had > 60% sensitivity and specificity for detection of contaminated epochs, versus 0.15% for SCADS. This is a large difference in performance, and may indicate SCADS was designed for use on larger-amplitude epoch artifacts than those simulated here. The variance in the ERP baseline was significantly lower for FASTER, than either the supervised or SCADS methods. ERP amplitude was significantly high for FASTER versus the supervised approach. FASTER was effective in attenuating artifacts in 128-, 64-, and 32-scalp electrode arrays.

One assumption of FASTER is that uncontaminated EEG parameter distributions should be distributed normally, or approximately normally. This assumption may be violated if low numbers of data points are employed, or in elderly or clinical populations where datasets are often noisier or more variable. The results from the real and simulated datasets show that FASTER worked effectively on datasets with 128, 64 and 32 scalp electrodes. However, the sensitivity for contaminated channels decreased dramatically, from 94.47% for 128 scalp electrodes and 97.02% for 64 scalp electrodes to 5.88% for 32 scalp electrodes. This may be a result of using simulated data (where the artifact distribution is normal), as the number of contaminated channels was lower in the 32-electrode datasets, and a result of using statistical thresholding, as the threshold calculation was based on a smaller sample size and consequently variance among channels was increased. Use of different statistical methods, such as nonparametric measures or bootstrapping, may prove useful. This issue also occurred with the SCADS method. The performance on the detection of other artifacts, such as EOG and EMG artifacts, was largely unaffected by the number of channels. The SCADS method had 100% sensitivity to channel artifacts for 128- and 64-electrode datasets, but its specificity dropped as the number of channels decreased, from 96.42% for 128 scalp electrodes to 84.91% for 32 scalp electrodes. This resulted in an average of 4 uncontaminated channels being interpolated for 32-electrode sets.

FASTER was not tested on datasets with fewer than 32 channels. The number of components returned from an ICA decomposition is equal to or less than the number of channels used: hence, component independence may decrease as the number of electrodes decreases. It is possible that FASTER may be effective at removing artifacts at lower

electrode densities, but if so used, consideration must be taken that components may also contain both artifact and true EEG data, and so some EEG data may be lost.

A novel feature of FASTER is that subjects with consistently poor data are rejected from the grand average on objective criteria. This method may be optimal for studies with large numbers of subjects (as outliers are more easily identified). However, FASTER can detect contaminated subjects in samples with 12 or more subjects.

FASTER generally outperformed SCADS on the test data, both real and simulated. SCADS was used in order to provide a comparison between statistical thresholding methods. It should be noted, however, that SCADS was not designed with unsupervised full automation as a goal. It is likely that SCADS would have performed better had some element of supervision been involved. However, its lack of sensitivity to epoch artifacts and the fact that its approach is to remove all data at temporal locations containing artifacts, rather than use methods such as ICA to subtract the artifact only, means that the resultant files have more remaining artifact as well as less valid data for averaging, resulting in low quality ERPs. A key feature of FASTER was the application of a statistical thresholding method to ICA data, and the use of ICA to subtract the EOG contribution to the EEG data. The combination of statistical thresholding and ICA results appears to be an effective method for artifact detection. This may confer a disadvantage to SCADS in the results, however no other readily available automated methods for ICA component removal were found for comparison.

The present set of benchmarking tests was conducted with data from healthy subjects on an oddball task (designed to evoke a P3 ERP), from which manually processed data was available for comparison. Initial data also suggested that FASTER can effectively analyze mismatch negativity data from patients with Parkinson's Disease. The application to the experimental data recorded in Chapter 6 and 7 was a true test of its efficacy; the results in these chapters can be seen to be sensible in scalp, time, spectral and source analysis. Furthermore, its successful and continuing use by researchers in peer-reviewed studies shows that its applicability is generalizable.

The computational requirements of the FASTER method are generally low, with the exception of the ICA decomposition, which can take some time. In this study, the Infomax ICA algorithm was used, processed under 64-bit MATLAB, and the entire processing protocol took up to an hour per 6 minute 128-channel dataset at 512Hz on a 64-bit dual-

core machine running Linux Ubuntu, of which approximately 40 minutes was the ICA decomposition time. Using a different ICA algorithm, for example the FastICA algorithm, and/or a compiled binary implementation of the method would increase the speed.

A key benefit of FASTER is that its use does not require the user to have any knowledge of signal processing. The user can simply select the folder containing the raw data and FASTER will output a grand-averaged dataset. Alternatively, researchers who prefer to process EEG data using their favored approach may choose to use FASTER to conduct a first pass of their data. Furthermore, given the diversity of signal-processing methods applied to EEG data (e.g., different criteria for artifact rejection), the use of FASTER may help standardize the approach to EEG analysis. It is worth noting that the baseline variance of manually processed data was itself quite variable (nearly twice as high as FASTER), indicating that even researchers experienced in EEG analysis can vary in their degree of artifact rejection. FASTER has been integrated into EEGLAB as a plugin, and as a standalone GUI (Delorme and Makeig, 2004), as depicted in Figure 4.9. Since its release in late 2010, it has been downloaded over 2000 times with 34 citations (as of October 2013).

The aim of this study was to demonstrate a fully automated, unsupervised method for EEG artifact detection and rejection. The results show that FASTER can reliably detect artifacts commonly found in EEG data and may even be superior to supervised detection for some metrics. The development of this method to automatically process EEG data facilitated the analysis of the EEG data recorded during the vestibular EEG experiments described in Chapters 6 and 7. Applying the FASTER method to the data recorded required approximately 2 days of processing per experiment, without any manual intervention. To process the data by hand would have taken considerably longer, and moreover would have required human attention for this duration. Thus this automated method allowed for faster turnaround of the data and so gives more time for analysis and interpretation of results, and also enables untrained users to gather and prepare data.

Further applications and extensions of the FASTER methodology are briefly detailed in Appendices B, C and D.

## 4.6 Appendix A - Additional Methods

- The Hurst exponent is a measure of long-range dependence within a signal, with a range of 0 - 1. It can be thought of as the tendency of a signal to promote trends or not. Discussions of its estimation can be found in (Bardet et al., 2003) and (Mielniczuk and Wojdy, 2007). Human phenomena such as EEG have values of H ≈ 0.7, and so it can be used as a measure for detecting non-biological EEG data (Bian et al., 2006; Vorobyov and Cichocki, 2002). To detect channels with a large amount of non-biological noise, Hurst exponents were estimated using MATLAB's *wfmbesti* function (the discrete second order derivative estimate was used).

- The equation used for Bonferroni correction with correlated dependent variables was:

$$\alpha_{new} = \alpha_{old}\left(\bar{r} + \frac{1-\bar{r}}{N}\right)$$

where

$\alpha_{new}$ was the new effective significance value

$\alpha_{old}$ was the original significance value (e.g. 0.05)

$\bar{r}$ was the mean Pearson correlation coefficient among all dependent variables

N was the number of comparisons made

## 4.7 Appendix B - Multiple Sclerosis Studies

The most useful test for any automated method is to run it over a large portion of data. A 4-year longitudinal ERP study on multiple sclerosis (MS) provided an opportunity to test the algorithm over large pools of data which would otherwise be very time-consuming to process by hand. As part of the initial development and vetting process, FASTER's performance at picking artifact features was compared with that of a number of researchers experienced in EEG processing. This was performed using a subset of this longitudinal dataset. The FASTER method is currently being used to greatly reduce the amount of time taken to prepare the EEG data in the study. With over 100 subjects involved including

patients and controls, and 4 datasets per subject, the amount of data is vast. Using FASTER, the amount of manual time spent processing the data is kept to a minimum - manual overviewing of the output is performed as the method is never perfect, but this takes a fraction of the time otherwise necessary.

This study determines and tracks changes in P3 ERPs recorded during auditory and visual oddball paradigms in controls and patients with MS, over a 4-year period. Patients with MS exhibit changes in amplitude, latency and topographic distribution in the P3a and P3b. The disruption of neural transmission that occurs during MS can produce cognitive impairment; one gold standard for this is the paced auditory serial addition test (PASAT). This test unfortunately has a high practise effect, and low repeatability rate. However, during analysis of the P3 data, it was seen that the latency of the auditory P3b correlates highly with the PASAT scores taken during the session (Kiiski et al., 2009; Kiiski et al., 2011b; Kiiski et al., 2010; Whelan et al., 2010a; Whelan et al., 2010c); thus the P3, which does not exhibit such practise effect, may be a good candidate to replace the PASAT as a measure of cognitive impairment.

## 4.8 Appendix C - EEG-fMRI

This study was an extension of the statistical artifact detection methods applied in FASTER, and if fully validated could be integrated as an option into the FASTER software. The integration of fMRI and EEG data is an endeavour which hopes to merge the high spatial resolution possible using fMRI with the high temporal resolution possible using EEG to provide enhanced neuroimaging results. The technology involved in such integrated systems is improving continuously, and state of the art systems may include up to 256 channels[8]. This approach seems, in theory, to be an ideal combination of modalities; however as the EEG electrodes record small electromagnetic signals, there is a large artifact introduced by the MRI scanning procedure (Bénar et al., 2003). This artifact is commonly known as the gradient artifact, referring to the magnetic gradient induced by the MRI scanner. A number of methods are available for removing this artifact, with considerable success (Allen et al., 2000; Negishi et al., 2004; Niazy et al., 2005).

[8] http://www.egi.com/research-division-research-products/eeg-systems/191-ges300mr

A further artifact, the ballistocardiogram (BCG) artifact, is also present in fMRI-EEG data. It arises due to the cardiac-induced movement of the body, which is more variable than the gradient artifact and thus more difficult to remove. A number of methods have been proposed (Bonmassar et al., 2002; Ellingson et al., 2004; Kosma et al., 2009), including some based upon ICA which have shown good results (Huiskamp, 2005; Srivastava et al., 2005). FASTER uses ICA as a method for detecting and removing artifacts whose properties are unusual, and thus the BCG artifact was a candidate to examine the versatility of the algorithm.

An opportunity to apply the algorithm to EEG-fMRI data arose in collaboration with the Trinity College Institute of Neuroscience. A study using joint EEG-fMRI had been performed, and a large amount of data had been collected. The study was investigating age-related changes in resting connectivity. The gradient artifact was removed from the EEG recordings using the Optimal Basis Set approach (Niazy et al., 2005). The EEG data was then processed using FASTER to remove BCG and any remaining additive artifacts. The results were improved based on visual inspection, but not excellent. In response to this, a further wavelet-based rescaling method was developed which implemented statistical adaptive filtering to remove artifacts on a per-scale basis and retain maximal information.

Both the scalp-space and IC-space time-series data were decomposed with an 8-level discrete wavelet transform, using the discrete approximation of the Meyer wavelet family. To reduce BCG and other large artifacts, adaptive filtering was achieved by dividing the IC wavelet coefficients $w_{IC}(x)$ by a rescaling function:

$$w_{IC}(x) = \frac{w_{IC}(x)}{1 + (|L(x)|^k)(T(x))}$$

L(x) was the mean of the upper and lower envelopes (a.k.a. local mean, as used in empirical mode decomposition (Huang et al., 1998)) of the IC wavelet coefficients. |L(x)| indicates the absolute value of L(x).

k was a constant used to increase the rescaling of the large amplitude artifacts. This was selected empirically as 4.

T(x) was a binary function = $|Z(s_x(w_{CH}(x)))|>2$, which evaluates to one when the absolute Z-score transformed value of the GFP of the channel wavelet decomposition was >

2, and zero otherwise. This ensured that only points at which large whole-channel amplitude shifts (i.e. BCG, EOG or EMG artifacts) occurred were rescaled.

This rescaling was performed at each decomposition level, then the IC time-course was recomposed from the rescaled wavelet coefficients, and the scalp-space data recomputed using the IC inverse mixing matrix. This can be applied in conjunction with IC-removal methods such as those used in FASTER.

The difficulty of applying pure IC removal without resorting to further signal processing lies in the varied results of applying ICA. Given infinite data and processing time, the ICA approach will give perfect decompositions of additive signals. In real application, signal separation is not optimal, and it can be seen that in the output from ICA, neural signals are often mixed with artifact signals, or known signals not separated from each other. The Infomax ICA algorithm (Bell and Sejnowski, 1995) used seems well-suited for general purpose use with EEG; however, its ability to decompose using low electrode densities is limited. In this study, 31 electrodes were available. As seen in this chapter, the FASTER algorithm shows good results using 64 and 128 electrode sets. The tests performed using 32 electrodes showed considerably worse performance, as decompositions were incomplete – the ICA algorithm needs more data input to perform well. Here, the use of 31 channels was insufficient to decompose artifacts smoothly, and so the BCG and other artifacts were not easily removable. The classification schemes such as FASTER need to take into account this imperfect separation, and a trade-off between maximal artifacts removed and maximal neural data kept is sought for. For EEG-fMRI solutions, systems are now available with up to 256 electrodes. These would allow for better ICA decompositions and thus better recovered signal. Alternatively, use of different algorithms such as FastICA (Hyvarinen, 1999) or the newly developed AMICA (Palmer et al., 2008) may yield improved results.

The experimental method used in this study shows very good promise based on the results and in tests performed on various different datasets. It has not yet undergone extensive numerical evaluation and performance testing such as those quantifying the FASTER method, but this initial result displays its potential and invites further experimentation. Numerous modifications to the algorithm are possible to adapt, enhance and expand its utility, for example adaptively changing the Z-threshold in T(x) based upon the data distribution, using nonparametric transforms instead of Z-transforms, or statistically determining values of k.

## 4.9 Appendix D - Electrophysiological Comparison of Vasovagal Syncope in Young and Old Adults

The underlying pathophysiology of Vasovagal Syncope (VVS) - commonly known as fainting - has never been completely understood. The role of a cortical focus or trigger has been suggested as a potential contributor to the pathophysiology of VVS. An opportunity to apply the FASTER methodology to data recorded to investigate this hypothesis arose in collaboration with St. James' Hospital.

Fifty six subjects participated in the study (mean age= 47±20 years, range 17-85), 23 male and 33 female. A head up tilt table (HUT) test was performed, tilting subjects to 70° for up the 35 minutes, with an XLTEK EEG system recording EEG data. The international 10-20 system was used for electrode placement. EEG data were filtered between 1Hz and 40Hz, with a band-pass filter at 50Hz to remove any remaining mains interference. The ICA methods from FASTER were adapted and used to remove gross ocular artefacts. Data was analysed in the longitudinal bipolar reference montage, which is a standard clinical referencing system, as well as average reference for comparison.

A number of time-frames were identified for investigative analysis. These were five minutes, one minute and 30 seconds prior to symptom onset along with 30 seconds post symptom onset. The minimum value was chosen as the EEG data was marked manually, introducing some unknown variability between the marked value and the syncope onset; thus 30s was chosen to ensure the syncope period was included. It was initially hoped that some markers of vestibular processing such as the onset potentials discussed in Chapter 7 could also be studied during the tilt-up or tilt-down; however, due to the manual marking, exact onset times were not determinable.

For analysis of EEG defined time-frames, the power spectrum was computed using Welch's method as implemented in MATLAB (Welch, 1967) and the mean power in the delta (1-3 Hz), theta (4-7 Hz), alpha (8-12 Hz), beta (13-25 Hz) and gamma (26-40 Hz) bands was calculated. To normalise these on a per-subject basis, these values were divided by the respective band values of the power spectrum calculated during the 10-minute rest period. Thus the values were interpreted as the change in band power from rest in each of the time intervals of interest. These values were compared between subjects < 60 years of age and subjects > 60 years of age using 2-sample t-tests - which were performed in each

frequency band, at each electrode, for each time interval, on the log10-transformed power values. Post-hoc correction for multiple comparisons was performed using the False Discovery Rate (FDR) method across channels (Benjamini and Hochberg, 1995). The topographic distribution of the p-values were also taken into account when interpreting significance, such that spatially clustered significant electrodes were considered more likely to present true effects than single electrodes.

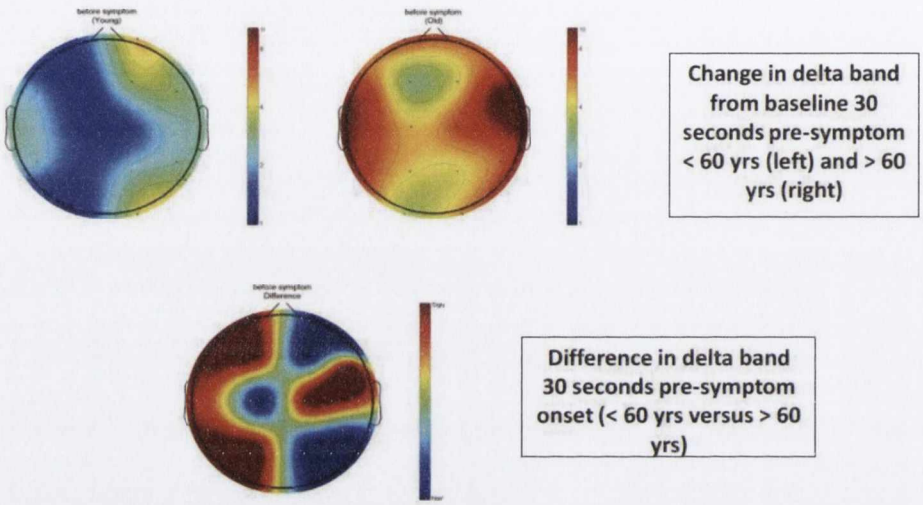


| 30 secs pre-symptom vs rest | <60 years | >60 years | P value |
|---|---|---|---|
| Δ ↓SBP (mmHg) | 30.64 ± 19.37 | 49.56 ± 25.66 | 0.09 |
| Δ ↓DBP (mmHg) | 10.00 ± 11.75 | 16.25 ± 15.04 | 0.332 |
| Δ ↑ HR (BPM) | 15.00 ± 18.27 | 17.38 ± 14.75 | 0.743 |
| Nadir symptom SBP (mmHg) | 94.14 ± 18.03 | 93.88 ± 32.23 | 0.98 |

Figure 4.12. Delta band activity change (red significant increase) and corresponding haemodynamic change 30 seconds pre symptom onset (mmHg = millimetres of mercury; bpm = beats per minute).

Some evidence for a lateralised increase in delta band activity in elderly as compared to younger subjects was found, but the results were highly dependent on the number of datasets included and so cannot be considered robust. These are interesting as they occur before the onset of any VVS symptoms, so if further validated, could be useful as a predictor of VVS.

This study demonstrates the use of aspects of FASTER for added benefit of quantitative EEG to supplement qualitative EEG measures which are commonly used when interpreting cortical changes during VVS. Its use in future research could focus on better characterising individuals, particularly older adults who may be vulnerable and at risk of falls

and injury secondary to VVS. This provides further evidence for the robustness of FASTER across multiple recording systems and data types.

Interestingly, this study lead to convergence with other studies and aspects of this thesis. There is a growing body of knowledge on the vestibulosympathetic reflex (VSyR) – a reflex circuit by which vestibular information, specifically otolith information, affects cardiovascular activity via the sympathetic nervous system (Ray, 2000; Ray and Monahan, 2002b). This reflex helps in mediating blood pressure in response to movement, e.g. to increase blood pressure during standing to counter gravity's effect (Ray and Monahan, 2002b). As vestibular deterioration happens in ageing, along with differences in the manifestation of syncope, there is a possibility that modulation of this reflex due to sensory deterioration and/or changes in vestibular processing contributes to falls in ageing (Ray and Monahan, 2002a). Certainly it is seen that the VSyR is active during orthostatic challenge in ageing (Monahan and Ray, 2002), which is associated with orthostatic syncope (Sarasin et al., 2002). This demonstrates that divisions between multiple causes of dizziness and falls are not clear-cut.

# Chapter 5

# Acquisition of EEG Data on a Stewart Platform

## 5.1 Introduction

Neuroimaging studies of vestibular motion perception and processing in humans have thus far been limited to motion approximation using caloric or galvanic vestibular stimulation, or use of rotational motion. Linear motion stimuli are largely unstudied due to methodological constraints. However, as EEG technology has improved and become portable, the use of EEG recording on a Stewart motion platform (Stewart, 1966) provides an appropriate method of recording neuroimaging data during true self-motion stimuli in a laboratory environment. There are, however, a number of potential drawbacks using a Stewart motion platform in conjunction with EEG recording equipment. For example, noise could be introduced into the EEG signal from the motion of the actuators, the electrical noise of the platform power source, or from muscular activity of the subject as they compensate for the acceleration at the start and finish of the motion. Two studies – (Chen et al., 2009) and (Lin et al., 2007) – have been conducted using EEG on Stewart platforms; however, these high-level studies attempted to record novel findings and did not demonstrate any preliminary validation of the quality of the EEG data. This chapter describes an experiment designed to investigate the validity of using a Stewart platform during EEG recording and its effect on the resultant ERP waveforms during differing amplitudes of motion.

This was assessed by running a standard EEG task – a visual oddball paradigm - with four different motion conditions to address each of these potential issues. The four different levels of motion were termed *static*, *idle*, *slow* and *fast*. The static condition served as a control as there was no interference from the experimental setup and participant motion. In the idle condition the motors raised the platform to its neutral position – this is a centralized position that allows a full range of movement in all directions. The motors require power to maintain this position, and so this condition allows investigation into the influence of electrical noise of the motors on the EEG signal. In the slow and fast conditions, participants experienced sinusoidal acceleration forwards and backwards at a frequency of 0.5Hz. These conditions are of most interest as there may be interference from the setup and use of the electrical motors, but also from the motion of the participant.

## 5.2 Methods

### 5.2.1 Participants

Six male participants with normal or corrected-to-normal vision completed the experiment for payment. The average age was 25 years (range 18-31). Participants gave their informed consent before taking part in the experiment, which was performed in accordance with the ethical standards laid down in the 1964 Declaration of Helsinki.

### 5.2.2 Apparatus

EEG data were recorded using the BrainAmp MRplus™ [9] electrode system from 8 scalp electrodes along the scalp midline and one EOG channel, digitized at 5000Hz. This experiment was later replicated using a Biosemi ActiveTwo™ 128 channel EEG system for one subject. This was important because the Biosemi, unlike the MRplus, is an unshielded system. It was possible, therefore, that electrical noise from the Stewart platform would interfere with the data from the unshielded system. Furthermore, the Biosemi has 128 electrodes, which allows for much better spatial resolution and ERP topographical representation. For this experiment only, the data acquired with the Biosemi were digitized at 2048Hz, with a -3dB bandwidth of 0Hz to 400Hz. They were downsampled to 256Hz. The data from the Pz channel was epoched from 500ms pre-stimulus to 2000ms post-stimulus, baseline-corrected from -500ms to stimulus onset, and then filtered between 2 and 45Hz. For both EEG systems, poor quality epochs were identified and rejected, using a preliminary implementation of the FASTER algorithm, which is described in Chapter 4. The full FASTER process had not been developed, and would not have been suitable applicable to the 8-channel data based on results in Chapter 4.

Following this step, specifically for the Biosemi data, a preliminary version of the ICA analysis from FASTER was performed, removing noisy and artifactual components using statistical methods based on a component's temporal standard deviation, correlation with the EOG channels, spectral power and spectral slope. ICA was not feasible for the BrainAmp data due to the low number of channels, which would not allow for a good approximation of statistical independence.

[9] http://www.brainproducts.com

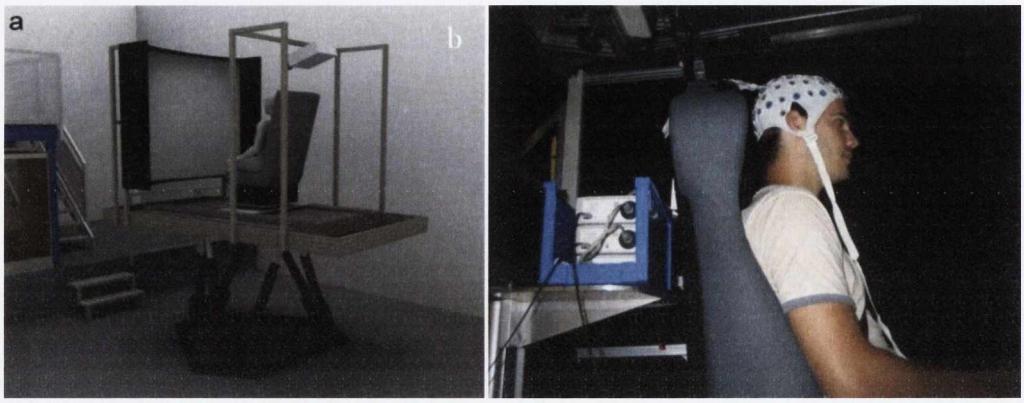


Figure 5.1. Setup and stimuli. (a) Graphical representation of the Stewart motion platform. (b) Experimental setup.

### 5.2.3 Visual oddball paradigm

The visual oddball paradigm consisted of different sized circles presented for 60ms on the screen, separated by an inter-stimulus interval of 2000ms±250ms (uniform distribution), for 205 trials in a pseudorandom order. Frequent standard (80%) and infrequent target (20%) circles differed in size and subtended 2 degrees and 6 degrees, respectively. Subjects were instructed to press a button as quickly as possible following a target (large) circle. The visuals were displayed using Presentation™ software by Neurobehavioural Systems[10].

### 5.2.4 Motion Stimuli

There were four different motion stimuli: static, idle, slow and fast. In the static condition the platform was turned off. In the idle condition the platform was raised to its neutral position then remained idle in this position. In the slow and fast conditions the platform was moved with a sinusoidal acceleration profile in a fore-aft motion at a frequency of 0.5 Hz for 230 cycles at different maximum accelerations of 0.1mG and 0.5mG, respectively. The motions were controlled by Virtools™ [11].

[10] http://www.neurobs.com
[11] http://www.virtools.com

### 5.2.5 Experiment procedure

Participants performed the visual oddball task during all four motion conditions (static, idle, slow and fast). In the idle, slow and fast conditions the motion platform was raised to the neutral position and motion was started before the beginning of the oddball paradigm. The timing of the onset of the visual stimulus was pseudorandom to ensure it was not locked to motion stimulus.

## 5.3 Results

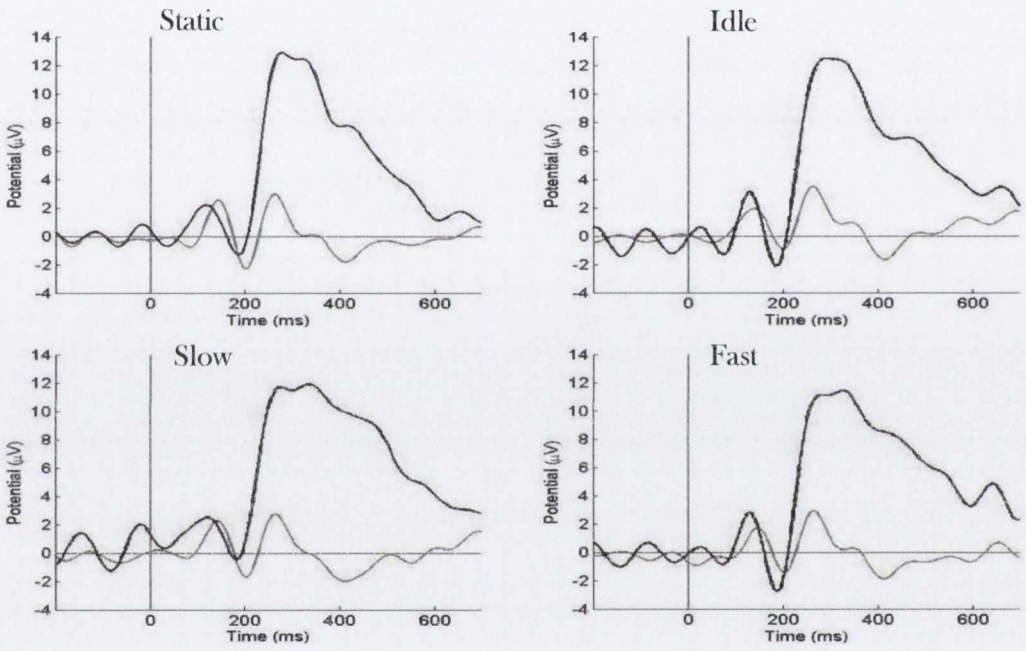


Figure 5.2. Grand average ERP data (n=5) recorded under all motion conditions from Pz acquired using BrainAmp MRplus. Both target (black) and standard (grey) averages are shown.

| | Idle | Slow | Fast |
|---|---|---|---|
| **Static** | 0.9766 | 0.9394 | 0.9682 |
| **Idle** | | 0.9326 | 0.9687 |
| **Slow** | | | 0.9488 |

Table 5.1. P3 correlation coefficients between motion conditions

Figure 5.2 shows the average ERP data (n=5) for each motion condition. A robust and characteristic peak around 300ms can be seen in all the target (grey) ERPs. Table 5.1

shows the correlation coefficients during the interval -100ms to 600ms of the ERPs' time courses, which can all be seen to be above 0.93. For display purposes only, the ERP data in all figures have been subjected to a 13Hz low-pass filter.

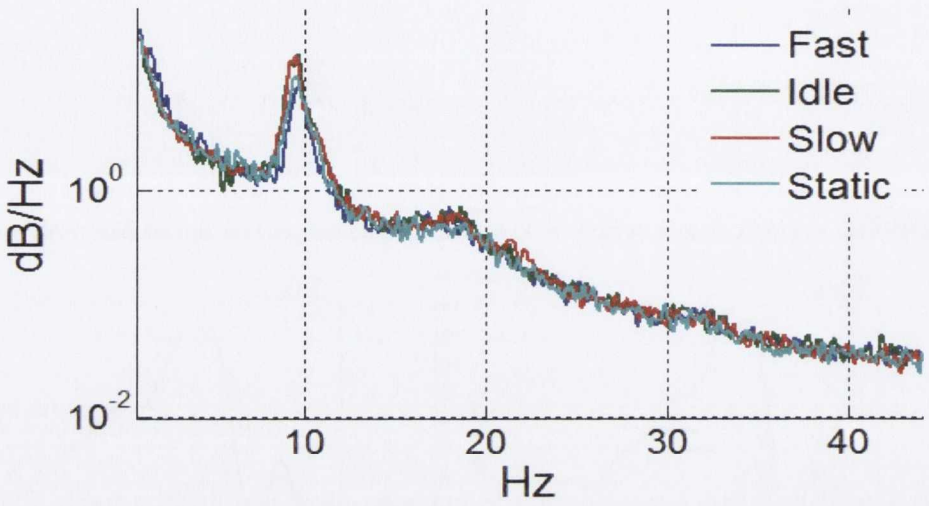


Figure 5.3. Spectra of each motion condition for Subject 2.

Figure 5.3 shows the spectra of ongoing EEG for each of the motion conditions for a representative subject (Subject 2). The spectra were subject to a 20-point moving average smoothing filter for display purposes only. These spectra produce a covariance matrix between spectra with mean±SD of 5.98±0.52 μV.

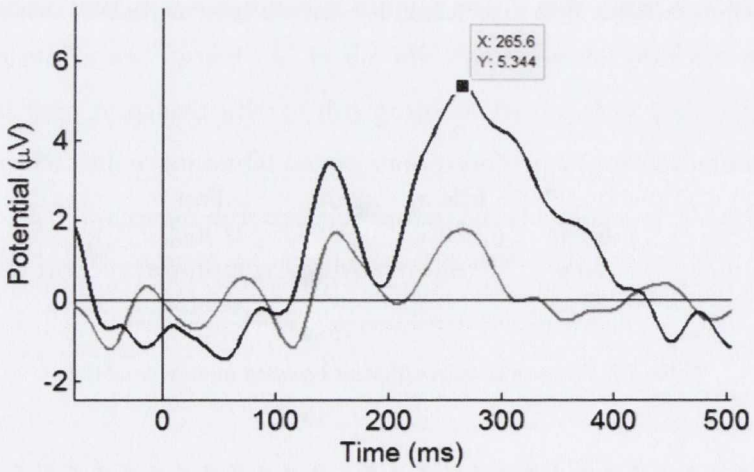

Figure 5.4. ERP data (n=1) recorded using the Biosemi ActiveTwo system during the Idle condition. The target (black) and standard (grey) are shown.

Figure 5.4 shows a P3 recorded with the Biosemi system.

On inspecting epochs, we found there was no rejection required for the BrainAmp data. The automated rejection tool selected 5 out of 5536 epochs from the static, slow and fast dataset for the Biosemi data.

## 5.4 Discussion

It was found that there was minimal detectable interference to the EEG signal during motion of the participants on the platform, using either the shielded MRplus system or the unshielded Biosemi system. A robust and reliable P3 ERP was evoked in all conditions (Katayama and Polich, 1996), as demonstrated by the peak around 300ms in the target ERP (black), which was not present in the standard ERP (grey). Furthermore, as Table 5.1 shows, the correlation between the static (motors-off) condition and the other 3 conditions is similar to the correlation between the motors-on conditions, indicating that the recorded data are unaffected by the platform's state. This is also reflected on examination of the rejected epochs, which show no electromagnetic artifacts caused by the Stewart platform, and negligible difference in rejection rates across different motion conditions.

More evidence can be seen upon inspection of Figure 5.3, which shows the spectra of each of Subject 2's sessions, overlaid. There are no large deviations from the overall trend, as can be seen by visual inspection, and shown in the small standard deviation in the covariance matrix between the spectra - there is little variation between spectra regardless of conditions. This is common in all subjects' recordings.

These results validate the experimental paradigm of using an EEG system in conjunction with a Stewart platform, as they show there is no appreciable distortion of the EEG data recorded as a result of the Stewart platform motion or other interference sources such as e.g. muscle movement. This result was somewhat surprising, as it was expected that there would be some interference to deal with in the unshielded Biosemi system. However, as the Biosemi amplifier has a high common mode rejection ratio (CMRR), and the electrodes are close together relative to their distance from the platform motors, the system is able to remove any interference through differential amplification. Their active electrode

system also contributes to this, as discussed on the website[12]. This result thus provided a basis for the design of experiments to investigate the perception of linear self-motion.

Since this experiment was performed, EEG methods have been further demonstrated to have application in self-motion perception studies using different paradigms. Most notably, a number of studies have begun to investigate the possibility of ambulatory EEG on treadmill systems. These studies have shown that standard ERP responses such as visual evoked potentials can be computed, aided by the use of some signal processing methods such as ICA and clustering (Gramann et al., 2010; Gwin et al., 2010). Furthermore, the first step towards investigation of active motion perception and generation was performed in a study by Presacco (Presacco et al., 2011) which used EEG recordings on a treadmill to infer joint angles and kinematics with a high degree of accuracy. These studies demonstrate the promise for future work in the field of electrophysiology and motion perception.

[12] http://www.biosemi.com/faq/shielding%20vs%20active%20electrodes.htm

# Chapter 6

# Vestibular P3

## 6.1 Introduction

In Chapter 5, it was shown that EEG recordings made during translation on a Stewart platform produced ERPs without noticeable interference. The stimuli driving these ERPs were designed so that their time-course was not related to that of the translatory movement. These results provided a positive step towards recording the neural correlates of translatory movement. In this chapter, the P3 ERP component is used to record a true response to a motion stimulus, confirm that the response is cortical in origin, and investigate the cortical processing of vestibular stimuli.

The P3 is an ERP component that occurs in response to an unusual or novel stimulus presentation. This manifests as a topographically centro-parietal peak in the ERP approximately 300 - 400ms after stimulus presentation, depending on stimulus modality (Polich, 1993). There are two sub-divisions, the P3a and P3b, which reflect processing of target stimuli which require a response (P3b), and distractor stimuli which do not (P3a) (Katayama and Polich, 1996). The P3a is associated with stimulus-driven attentional orienting and the P3b has been associated with memory processing (e.g. Polich, 2007). The common experimental paradigm to elicit the P3b is the oddball paradigm - two similar stimuli are selected, and presented in a random fashion with uneven probability so that one stimulus is frequent and the other infrequent. A common ratio is 80%-20%. The infrequent stimulus is the target to be responded to or noted. ERPs from the frequent and infrequent stimuli can then be compared to reveal the additional P3 component in the target wave. The P3a is targeted by extending this paradigm and presenting more rare stimuli (e.g. 10% probability) that must be ignored. In this chapter, the P3b is used to probe ERP responses to true motion.

The P3b is seen to be generated via a range of stimuli from different modalities, and even multimodal paradigms (Comerchero and Polich, 1999; Giard and Peronnet, 1999; Ito et al., 1995; Morgan et al., 1999). This lead to the hypothesis that the P3b is a cognitive potential, which is generated during updating of the internal representation of the environment (Polich, 2007). It has a similar spatial profile across all modalities, and so is a

useful tool to probe the cognitive processing of novel modalities. In particular, this chapter investigates whether the vestibular information provided by true motion stimuli are processed in a similar manner to other sensory stimuli. As vestibular cortical representation is seen to be highly multisensory, and is often considered not to be explicitly perceived, the manner in which the sensory information is processed cognitively is not necessarily straightforward.

As discussed in the Chapter 2, the use of heading as a window into motion perception is a useful investigative paradigm. Here the heading angle is varied to create two heading stimuli, which are presented in an oddball paradigm. In Chapter 5, it was seen that the use of EEG on a Stewart platform is a viable means of recording neuroimaging data during true self-motion without noticeable electromagnetic, EOG or EMG interference. However, the responses recorded are not in response to the motion itself. In this chapter, the P3b in response to motion stimuli is recorded. The two main purposes of this are to validate the cortical nature of ERPs recorded in response to motion stimuli, and to investigate the cognitive processing of vestibular stimuli. A secondary consideration was evaluating this paradigm as an easily deployable measure of vestibular integrity and the perception of self-motion with support from P3 literature. Such cognitive aspects of vestibular processing have not previously been investigated with neuroimaging, but are highly relevant in motion perception, self-orientation and even in the creation of body schema (Lopez et al., 2008; Siegler et al., 2000; Yen Pik Sang et al., 2006).

## 6.2 Methods

### 6.2.1 Participants

Sixteen neurologically typical participants with normal or corrected-to-normal vision, per self-report, participated in this experiment. The age range was 22 - 35 (mean 28.1 ± standard deviation 3.9). Participants gave their written consent before taking part in the experiment, which was performed in accordance with the ethical standards laid down in the 1964 Declaration of Helsinki. One participant was subsequently removed from the study due to excessively noisy data.

### 6.2.2 Apparatus

The Stewart platform and EEG system used are described in Chapter 3.

**Figure 6.1. (A) The outside of the Stewart platform. (B) During this study, a cloth sheet covered the platform to mask visual motion cues, and a Biosemi ActiveTwo EEG system was installed to record EEG data. (C) Top down view of the experiment. Example of the Vestibular heading oddball task, using a motion platform, participants were translated forward along two possible linear heading directions θ=±45°, left and right, which were alternatively the standard (p=0.8) and target (p=0.2) stimuli.**

### 6.2.3 Vestibular Oddball Heading Paradigm

The classical oddball paradigm, consisting of two stimuli in which an infrequent target is identified in a sequence of frequent standard stimuli (Katayama and Polich, 1999), was adapted for heading stimuli. The stimuli used were the standard 1s motion profile s(t) described in Chapter 3, with angle $\theta = \pm 45°$. Participants completed a total of 8 blocks. Each block lasted 5 minutes and consisted of 50 heading trials, 40 standard (p=0.8) and 10 target (p=0.2) stimuli. For each block, $\theta = +45°$ and $\theta = -45°$ were assigned as standard and target so that each subject received 4 blocks of +45° target and 4 blocks of -45° target. This yielded a total of 320 standards and 80 targets per participant. The start of each trial was indicated by an auditory 10ms beep, followed by the onset of motion after 1.5s-2s (uniform distribution). Following each motion the platform returned to the start position via a sub-threshold motion lasting approximately 5 seconds, thus ensuring that the participant had no indirect feedback about the previous motion. The standard and target were presented in a pseudo-random fashion, ensuring that at least three standard stimuli were presented between target stimuli. All participants were given two breaks lasting 5-10 minutes after the second and fifth block.

Participants were seated upon the motion platform while EEG data was acquired. Participants were instructed to fixate on a cross displayed on the platform's screen during stimulus delivery. Verbal instructions were given before each block as to which directions were the target and standard direction. Participants only responded to targets and the response-hand was counterbalanced across blocks. The standard and target stimulus were linear forward motions with a leftward or rightward heading of ±45° (Figure 6.1C), which were counterbalanced, such that each participant completed four leftward and four rightward target blocks, consisting of two blocks in which they responded with their left-hand and two blocks with their right-hand. The standard and target were chosen such that they were perpendicular from each other and were well above the threshold of detection of non-visual heading reported in the literature (Butler et al., 2010; de Winkel et al., 2010; Fetsch et al., 2009; Telford et al., 1995).

### 6.2.4 Data Processing

EEG data were processed as described in Chapter 3. During recording for one subject, the button-response system malfunctioned. For this subject all target epochs were included rather than only those with a correct response, as the overall false response rates were very low. Data from this subject were also not included in the calculation of the response rates in Table 6.1.

### 6.2.5 EEG Analysis

Epoched data were separated into two groups, standard stimulus and target stimulus, to detect the P3 waveform. These groups were further separated into left- and right-going motions, in order to test for the effect of directionality. Event-related potentials (ERPs) were computed for each group. To test for the presence of the P3, mean amplitude measurements were obtained in a 100ms window centred at the group-mean peak latency for the largest component. From the literature, frontal (Fz), central (Cz) and parietal (Pz) midline electrodes were identified as regions of interest for initial investigation.

After the initial investigation, the full 128-channel high-density recording was used to identify with good spatial accuracy the spatio-temporal extent of the P3 distribution on the scalp, to perform source localization using sLORETA on the P3 waveform, investigate time-

frequency properties, and to demonstrate the P3 feature's validity on the single-participant level.

To achieve this, statistic parametric maps as described in Chapter 3 were first created across the entire scalp and across time in order to test for topographical differences in ERP amplitude between the standard and target conditions (as seen in Garrido et al., 2008), and also between left- and right-ward target conditions, and left- and right-hand button-press conditions. Based on visual assessment of the ERP, a temporal epoch of interest of 300-950ms was applied for the SPM analysis of the P3.

sLORETA was used to map the cortical sources of the P3 ERP component using the difference wave. The difference wave was computed by subtracting the standard ERP from the target ERP. sLORETA maps of the 100ms mean around the P3 peak were created, and SnPM statistics were performed on this peak vs. baseline.

As the stimulus profile is novel, time-frequency spectrograms were created for the standard and target conditions using the short-time Fourier transform as described in Chapter 3, with FDR and "running t-test" correction applied.

Statistical analysis was also performed on ERPs at a single participant level. A bootstrapped t-test ($N_{boot}$ = 2000 t-tests) between standard and target epochs was applied to the 100ms, 5-electrode average value centered on the parietal central site (Pz) around the individual average peak values. This was selected as the maximum value in the individual participant's average target ERP from 300 - 950ms. For one subject (S11 in Figure 6.6) the detected peak was not the P3 peak - the later P3 peak was visually identified - and this was corrected manually. For each t-test, a subset of target and standard epochs were randomly selected from all of the participant's available target and standard epochs, respectively. The number of standard target epochs selected in the bootstrapping process was increased in steps of 10 targets and 40 standards to correspond with the 20%-80% target-standard probabilities (Rosenblad, 2009). The number of epochs for significance was chosen as the number at which ≥ 95% of bootstrapped t-tests between the standard and target epochs were significant ($p<0.05$). This ensured statistical significance on an individual level, and also enabled the computation of the minimum number of epochs necessary for the detection of a difference between the target and standard epochs.

## 6.3 Results

### 6.3.1 Behavioural Results

Mean and standard deviations of reaction times and hit rates in response to targets were computed for each motion direction, see Table 6.1.

| Measure | Value (mean ± SD) | Intra-participant SD |
|---|---|---|
| **Reaction time, overall (ms)** | 876 ± 214 | 57 ± 24 |
| **Reaction time, right (ms)** | 872 ± 223 | 67 ± 34 |
| **Reaction time, left (ms)** | 886 ± 221 | 61 ± 51 |
| **Hit rate, right (%)** | 95.14 ± 5.60 | - |
| **Hit rate, left (%)** | 93.91 ± 9.36 | - |
| **False positive, right (%)** | 0.44 ± 1.12 | - |
| **False positive, left (%)** | 0.70 ± 1.90 | - |

Table 6.1. The group average and standard deviation of the reaction times and hit rate for the target.

To ensure that there was no difference between target directions, the left and right target reaction times, true positives and false positives were submitted to paired t-tests. The tests revealed no significant difference, $t_{13}$=-1.836, p=0.0893, $t_{13}$=-0.3340, p=0.744, and $t_{13}$=-0.582, p=0.572, respectively. These tests were performed on 14 of 15 subjects, as the response button malfunctioned for one subject. There may be a trend towards a small difference in left and right reaction times.

### 6.3.2 EEG Results

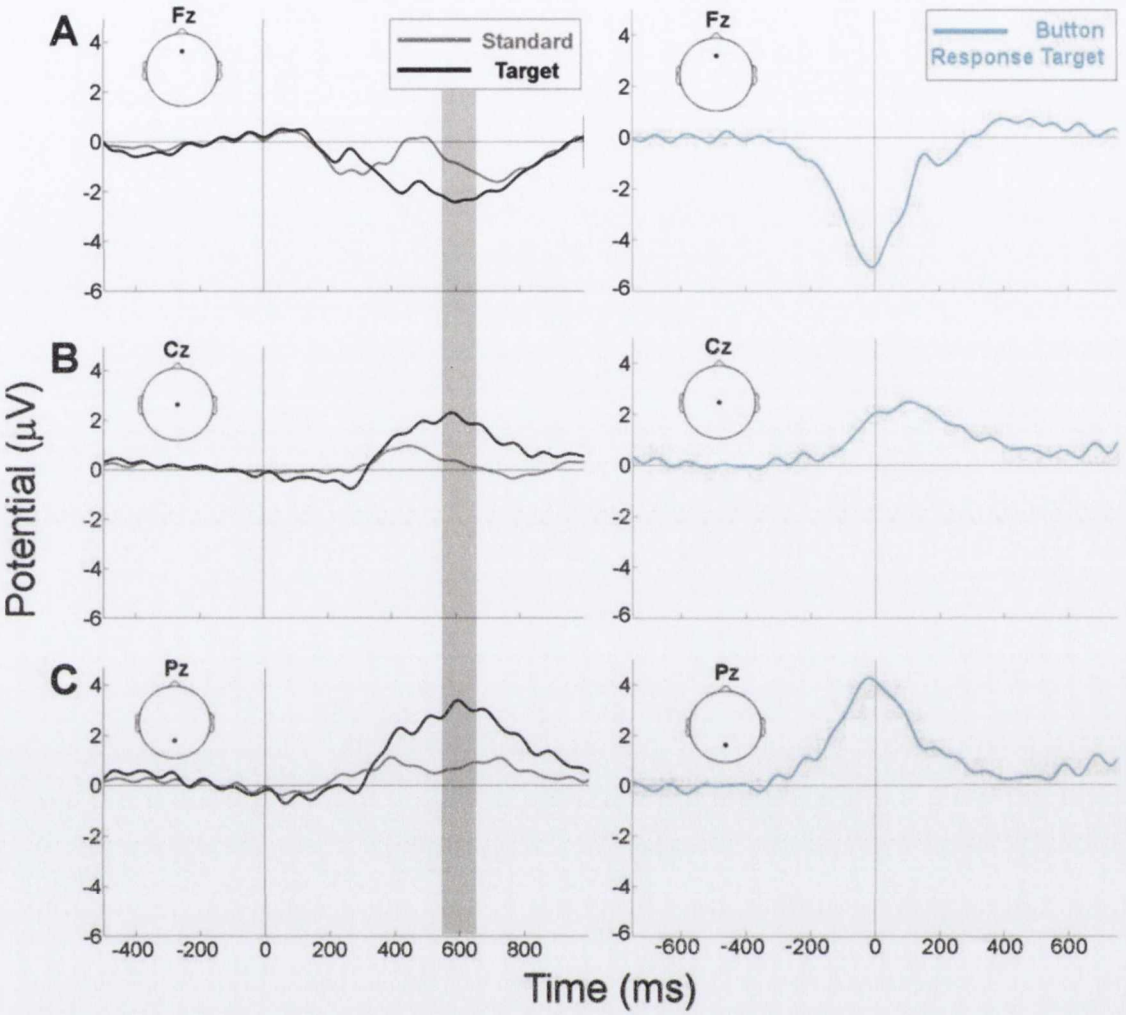


Figure 6.2. Left: Group average standard (black) and target (grey) ERPs calculated from Fz (A), Cz (B) and Pz (C), after epoching relative to the motion onset. The highlighted section indicates the temporal region of interest for peak analysis. Right: Group average target from Fz (A), Cz (B) and Pz (C), after epoching relative to the motion onset.

Figure 6.2 depicts the ERPs for standard (black) and target (grey) conditions along the midline electrodes. The waveforms are seen to be maximally different at 600ms, with highest target amplitude at Pz - this is the P3 peak. A 100ms window (±50ms) around this peak was chosen for preliminary analysis on these electrodes, and is denoted by the highlighted section on the left in Figure 6.2. On the right, in blue, is the target ERP after averaging relative to the response button press for each target. This response-time corrected averaging method is intended to correct for differences in cognitive performance - the behavioural results in Table 6.1 implies a wide spread of response-times - and so the resulting main peak is not as wide as in the left-hand ERP (Gibbons and Stahl, 2007).

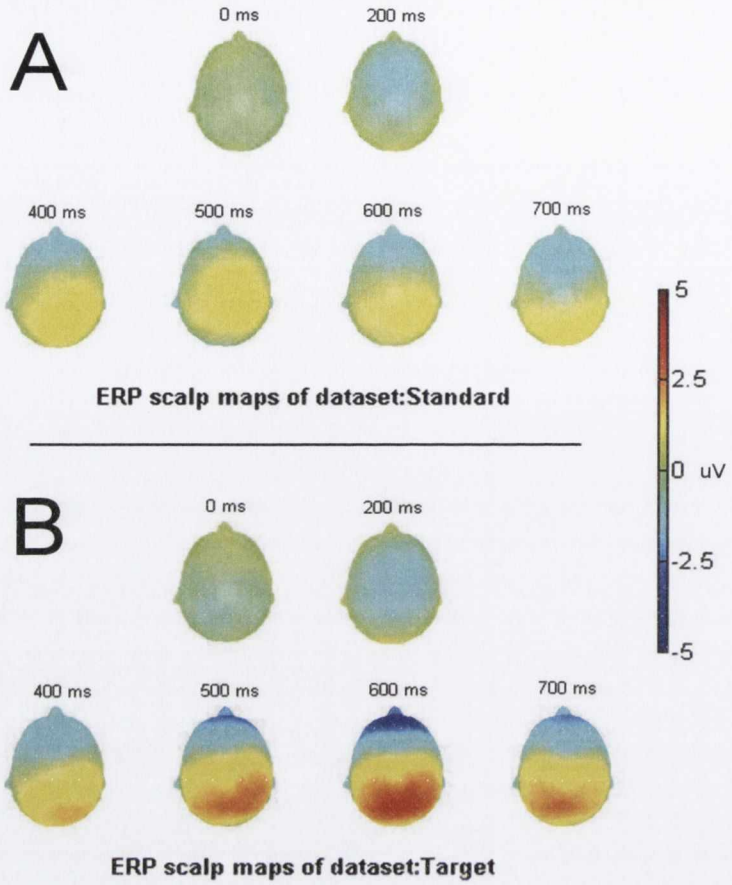


Figure 6.3. Topographic representations of (A) the standard ERP and (B) the target grand average ERP.

Figure 6.3 displays topographical plots of the group average standard (A) and target (B). From these topographies we can see the target ERP's divergence at 400ms from the standard ERP, and the parieto-central peak, which starts at 500ms, is maximum at 600ms and wanes at 700ms.

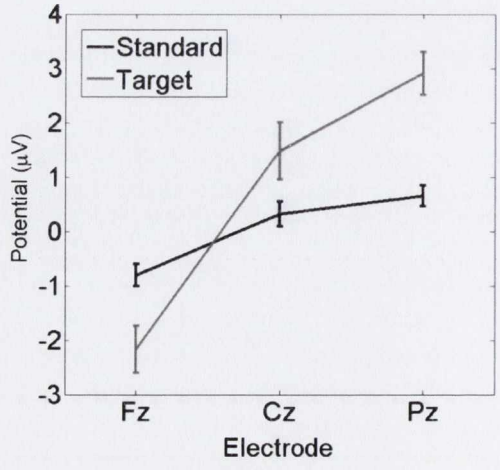


Figure 6.4. Mean amplitudes of the P3 peak at midline electrodes; error bars represent standard error of the mean.

Preliminary statistical analysis was performed on this peak (100ms average from 550ms to 650ms) along the midline electrodes Fz, Cz and Pz. A two-way ANOVA showed main effects of both Standard vs. Target ($F_{1,86}$=7.2, p=0.0087) and electrode ($F_{2,86}$=39.67, p<0.0001). Figure 6.4 depicts the means, with standard error bars, of the 600ms peak at these midline electrodes.

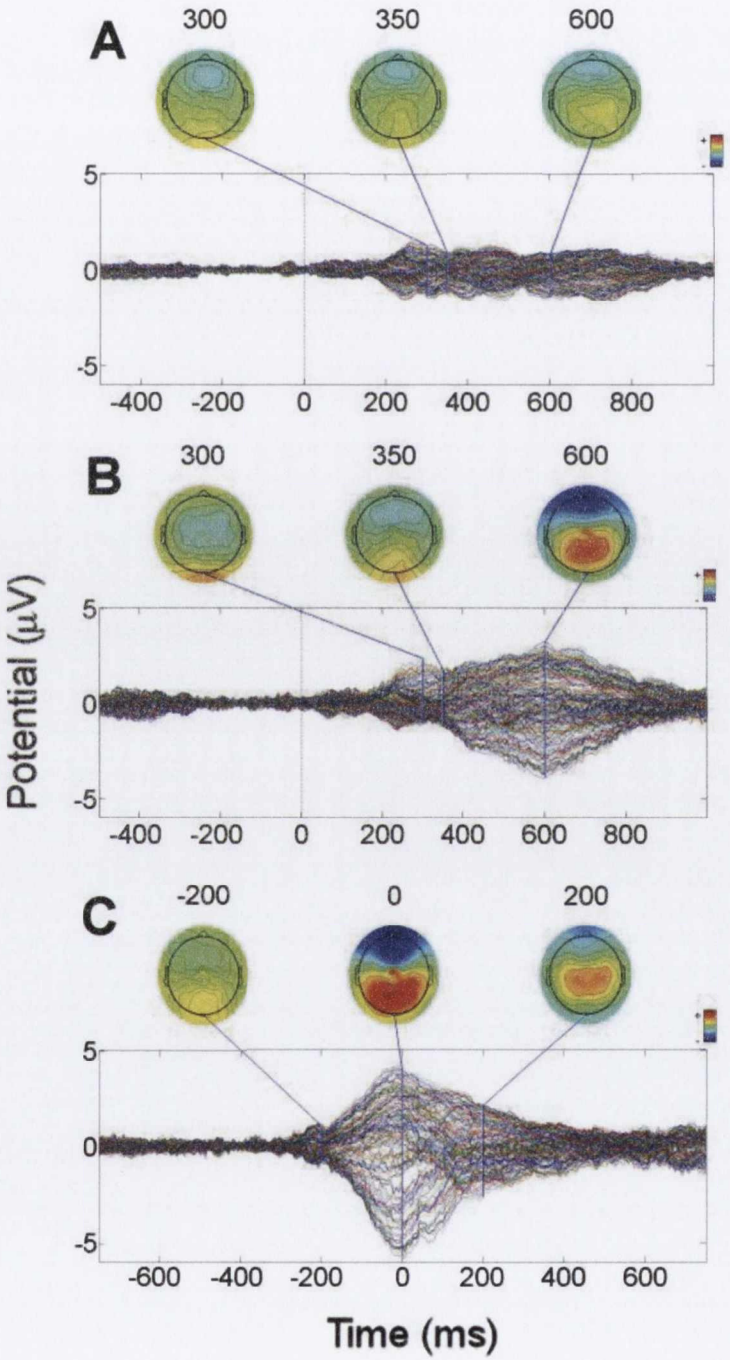


Figure 6.5. Butterfly plots of (A) the standard, (B) the target and (C) the response-time corrected target ERPs.

Figure 6.5 displays butterfly plots of the full 128 channels, with the peak at 600ms topography displaying spatial similarity to the P3 peaks of literature. The response-time corrected target has a higher amplitude and smaller peak width.

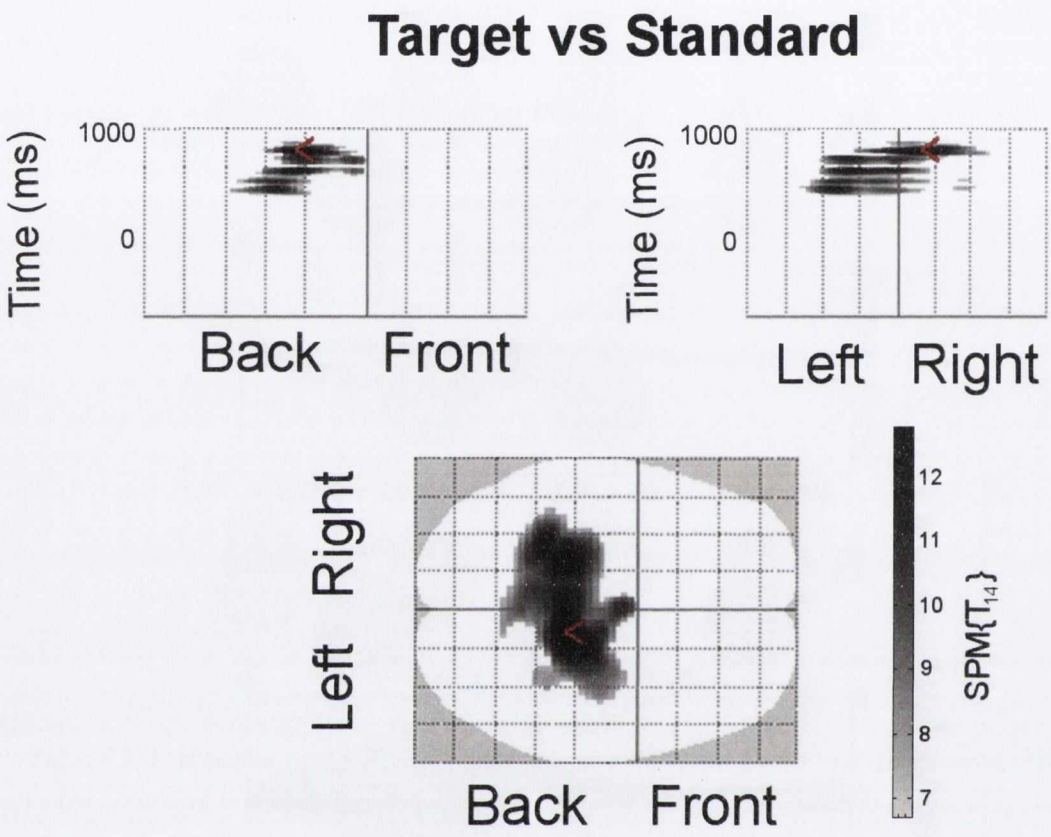


**Figure 6.6. SPM output showing temporal and topographical differences between the standard and target conditions. The red arrow indicates the maximum T-value. Each plot is an isometric view of a 3D space x space x time volume.**

To gain a deeper understanding of the spatiotemporal properties of the P3 waveform we conducted further analysis using a paired t-test design in SPM. Figure 6.6 shows the results of the spatio-temporal SPM analysis. This plot displays the areas of significant difference in the ERP, on the scalp and across time. The non-white areas shown in Figure 6.6 are those with significant differences between target and standard conditions (target > standard) after FWE correction at $p < 0.05$. Significant cutoff after FWE correction was $t_{14} \geq 6.68$.

Further SPM analyses showed no significant difference between left- and right-going target ERPs ($p \geq 0.05$), or between left- and right-handed button press target ERPs ($p \geq 0.05$).

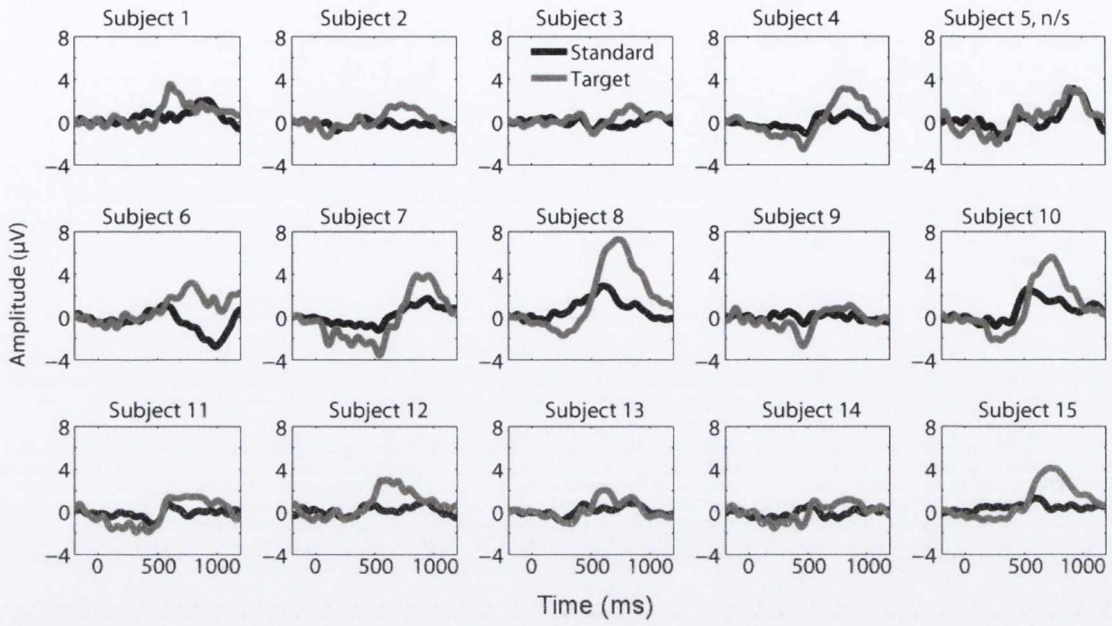


**Figure 6.7. Individual participants' average standard (black) and target (grey) ERPs at the 5-channel average around the parietal central site (Pz). 14 of the 15 subjects exhibit significant difference between standard and target at their individual target peaks, with the non-significant subject marked "n/s". A 20Hz low-pass filter was applied for display only.**

The differences in the P3 peak can be seen to be present at the single participant level, as illustrated in Figure 6.7 for all participants. Individual participant bootstrap analysis revealed that 14 of 15 participants exhibited significantly different values between standard and target ERPs at the individual P3 peak. Furthermore, the critical number of target epochs necessary to detect this difference was found to be within the 95% confidence interval of 43.78-70.07 epochs. A conservative estimate of 80 targets, which was used here, would be suitable. Thus the vestibular P3 is seen to be a measure which can be applied on a single-participant basis, and the approximate minimum number of trials necessary for implementation on a single-participant level has been determined.

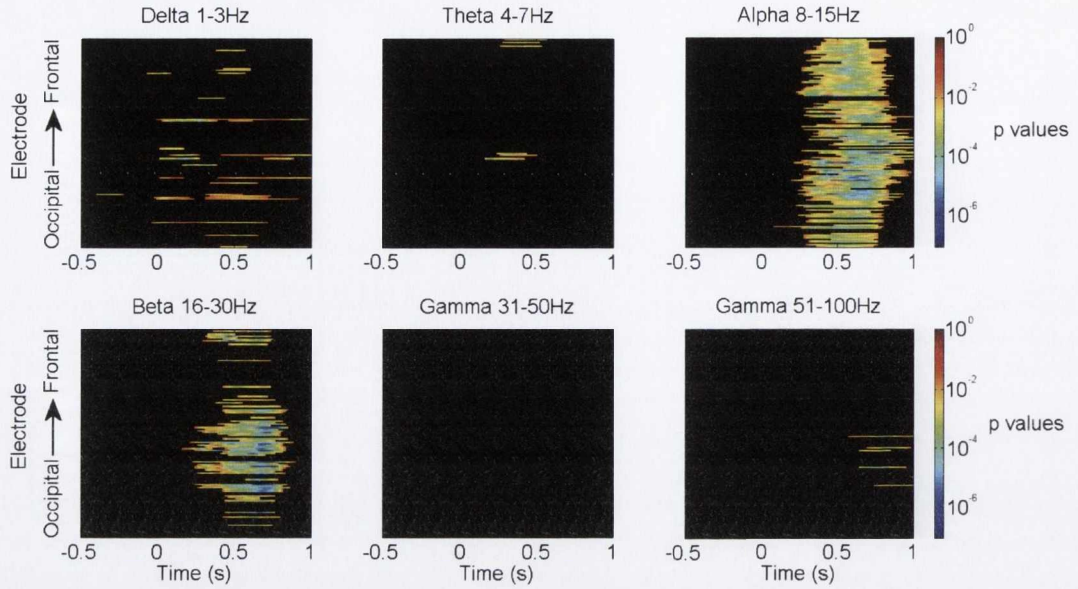


**Figure 6.8. Spectral power analysis of the Target versus Standard ERPs. Depicted are running t-tests of each frequency band, depicting temporal regions where the power in the bands significantly differ. Note that all scales are log scales.**

Figure 6.8 depicts the results of a time-frequency analysis of the differences between the standard and target ERPs. This analysis reveals statistically significant activity in the alpha and beta band across >50% of electrodes from 400ms to 800ms, which is consistent with the time period shown in the analysis of the broad band ERP. Patchy activity in the delta band is more difficult to interpret. The lack of a large amount of difference in the gamma band is encouraging as it implies a lack of EMG contribution to the P3.

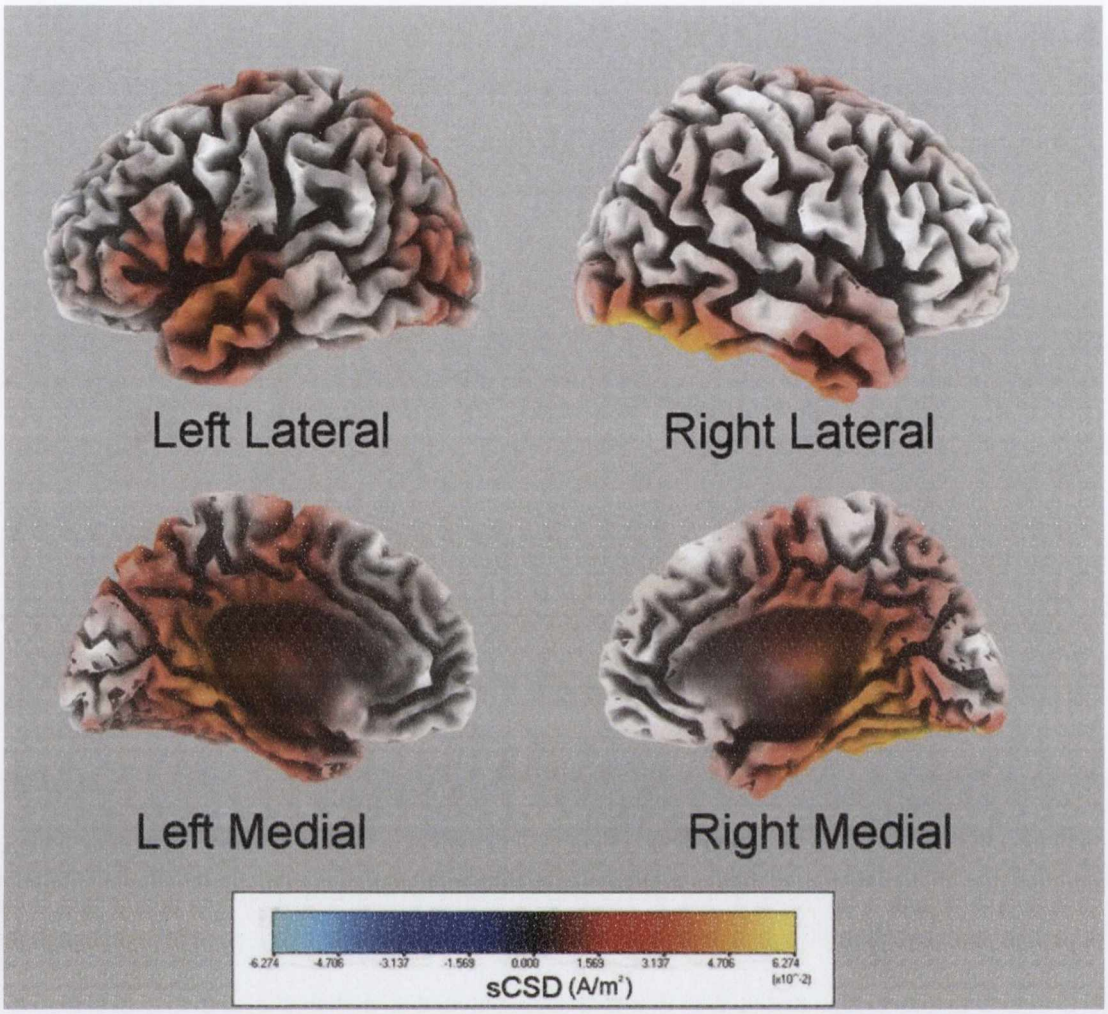


Figure 6.9. sLORETA output from grand average data showing cortical regions where the P3 component was active. Units are standardised current source density.

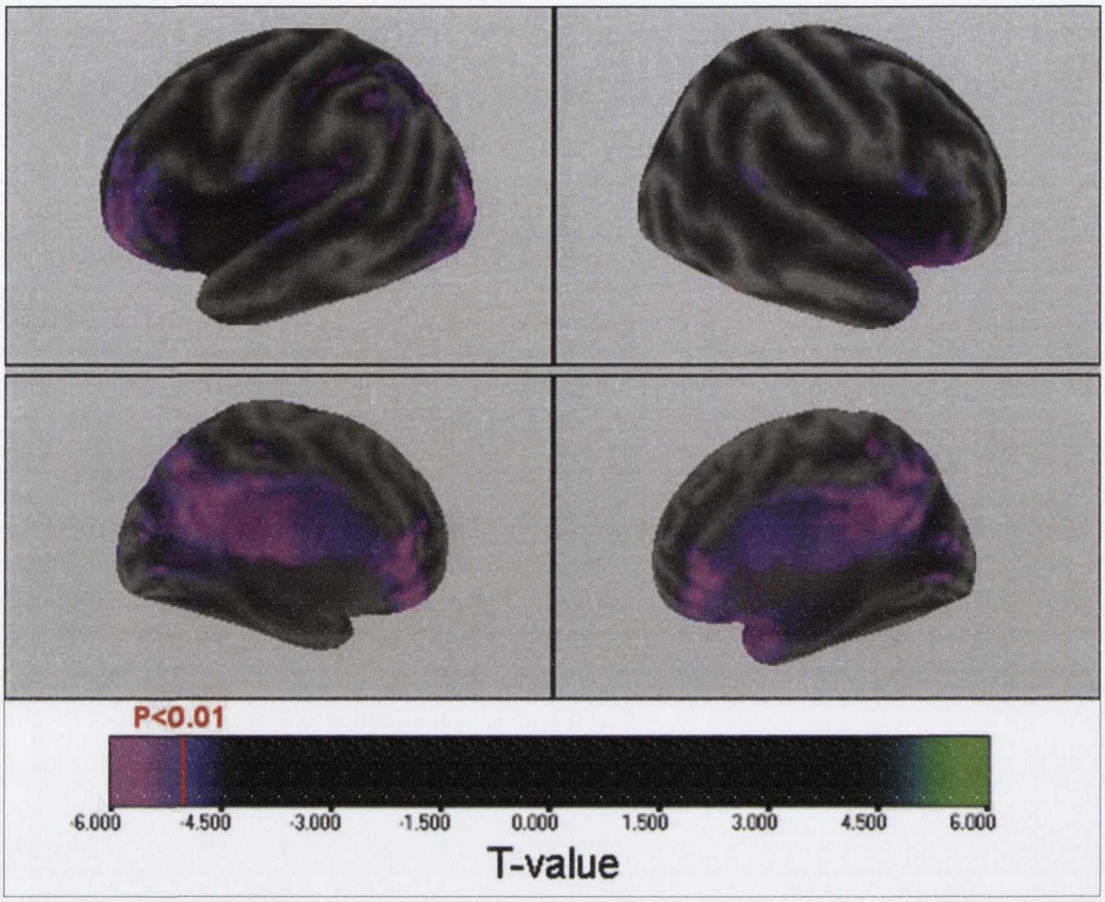


Figure 6.10. sLORETA statistical output showing cortical regions where the P3 component was active. This shows the areas where the averaged baseline values are statistically smaller than the 100ms average value around the P3 peak. Units are T-values. Bootstrapped significant p threshold is noted on the scale axis. These p values were: $p<0.01$, $|T|>5.285$, $p<0.05$, $|T|>4.253$, $p<0.1$, $|T|>3.876$.

Figures 6.9 and 6.10 present standardised current source density (sCSD) maps of the P3 peak (average of 550-650ms), calculated using standardized low resolution tomography (sLORETA). While the spatial resolution is low, the areas of activation can be viewed in light of previous studies which have identified P3 generators using fMRI and invasive recordings. Activity can be seen to be high in the temporal lobe, spanning areas such as the fusiform gyrus and the medial temporal gyrus, and extending through the parahippocampal gyrus to the parietal lobule and frontal gyrus (Brázdil et al., 2005; Clark et al., 2000; Halgren et al., 1995; Knight et al., 1989; Stevens et al., 2000; Yoshiura et al., 1999). Further activity is seen around the insula, Sylvian fissure and superior temporal gyrus (Horn et al., 2003; Linden et al., 1999). For further reading, Brázdil et al., (2005) extensively review the anatomical correlates of P3 tasks. This anatomical concordance of our results with the literature emphasizes the normal nature of the P3 waveform. In Figure 6.9, the large extent

of the cortical activation reflects the low spatial resolution of EEG source imaging methods, along with the arbitrary scaling of the sLORETA software – this scale was chosen as the areas depicted are all known to be involved in P3 generation.

In Figure 6.10, statistical comparison of the peak to baseline isolates areas which are statistically different from baseline. This includes a number of the areas mentioned above, along with extreme frontal and occipital areas.

## 6.4 Discussion

In this study the electrophysiological correlates of the detection of a vestibular heading oddball stimulus were investigated. The results reveal a waveform with a parieto-central distribution and latency of 600ms – see Figures 6.5 and 6.6. This has a typical P3 topography (see Polich and Heine, 1996), which indicates that vestibular oddball stimuli are processed in a similar fashion as other sensory modalities. This lends weight to the argument that vestibular signals are treated and processed in the brain in a similar fashion to other sensory signals, as the P3 is known to be representative of cognitive processes (Polich, 1993) and hence reflects the cognitive processing of sensory information. The 2-stimulus oddball paradigm used here evokes a P3b response, which is associated with updating of the internal representation of the environmental context (Polich, 2007). The P3b is known to have a parieto-central topographic distribution, consistent with the results seen here.

The temporal features of the P3 are unusual in comparison with what is generally seen in the literature. The main difference in this study is that the sinusoidal acceleration motion stimulus used here is quite different from the discrete stimuli used in auditory and visual experiments, which tend to have stimulus lengths less than 50ms. A 1.25s stimulus results in a response more like continuous EEG than a standard ERP. Furthermore due to the ramp-up period, some of the initial portion of the stimulus is underneath the detection threshold, and therefore the discrimination between the target and standard is not instantaneous, leading to delay. This delay can be quantified as the time to the initial ERP response, which is approximately 150ms (Figure 6.5 and 6.6). Taking this as a start-point, the P3 component arises approximately 450ms after the stimulus is initially detected, which is closer to normal values. The peak is also wide, with statistical analysis showing differences between standard and target for over 300ms. As the response times are highly variable, this may be due to inter-individual differences. The variability of response times between subjects is

considerably higher than the variability within subjects. The P3 peak is also wide, but decreases in width when the data is aligned based on the response (Figure 6.1); thus the P3 also has a variable onset and dictates the response time. This variable onset then most likely relates to a variable motion detection threshold, as the sinusoidal stimulus ramps sufficiently slowly to see the inter-subject differences. After initial detection of motion, the stimulus may not be strong enough to detect heading direction, which may also add to the longer latency. A decrease in alpha power also corresponds to the P3 peak; this is known to correlate with attention and excitation (Klimesch et al., 2007; Wolfgang, 1999), so this may be a further factor to investigate individual vestibular perception. This may also imply an activation of the visual cortex, due to an expectation of vestibular-visual interaction during motion.

This latency of the P3 can be contrasted with the reflexive responses initiated by the vestibular system. The VOR and VCR, for example, have latencies in the order of milliseconds to tens of milliseconds (Séverac Cauquil et al., 2003). As the P3 latency is at approximately 600ms, and the button response latency is 876ms, it appears that cognitive processing of motion stimuli is slow, especially compared to the autonomic responses that are resultant of motion. This has been noted previously (Baxter and Travis, 1938), and it has also been seen behaviourally that responses to rotational and translational (Barnett-Cowan and Harris, 2009; Barnett-Cowan et al., 2010) vestibular motion stimuli are slower than responses to visual and auditory stimuli. Future experiments are required to investigate the nature of this delay as it could give insight into the time course of the perception of vestibular cues.

The issue of interference from EMG and EOG signals was important to consider. EMG contamination is seen to be a broadband phenomenon, with amplitude at high frequencies compared to EEG. It can also peak in the beta band, as seen in the contamination study by (Goncharova et al., 2003), but this is still associated with gamma band increase; as EEG power in the gamma band is low, this makes it easy to isolate EMG. Time-frequency analysis of the ERP data revealed that there were significant differences in the beta band, but very little significant low or high gamma (30-100Hz) activity. Furthermore, the parieto-central topographic peak of the ERPs does not exhibit the strong activity at the edges of the scalp that are typical of EMG activity. From this analysis we conclude that there is minimal contribution from EMG to the recorded response. With regard to EOG activity, the parieto-central topographic distribution again is not in concordance with the unipolar frontal topographies obtained from EOG activity. The use of sLORETA to map ERPs acquired to brain structures shows considerable overlap with literature in P3 and vestibular regions; this

is dealt with thoroughly in Chapter 7, but the sensible results shown here are promising. Here, one notable observation is that there is considerable overlap in the areas seen during vestibular processing, and those seen during P3 generation. As the spatial resolution is not sufficient to differentiate between these areas, this limits the utility of source analysis in this case. One potential solution to this would be to perform a P3 task in a separate modality and use a conjunction analysis to find the common areas. This would identify the areas common to the P3 generator only. This may also identify whether increased activity in vestibular areas occurs to a new stimulus – habituation to constant vestibular stimulation is known to happen over time (Cohen et al., 1992).

While the result of a P3 might seem like an intuitive result, it is not entirely obvious. There is still an on-going debate within the self-motion behavioural literature about the utility of vestibular signals in human self-motion perception. A number of studies have shown that the introduction of non-visual self-motion cues signals does not always benefit self-motion perception (de Winkel et al., 2010; Ohmi, 1996; Telford et al., 1995), and hence the vestibular cues might not be processed in a similar fashion to other sensory modalities. On the other hand, recent studies have shown an optimal benefit to the introduction of vestibular signals in the discrimination of heading (Butler et al., 2010; Fetsch et al., 2010; Fetsch et al., 2009), which is more in line with the nature of the vestibular P3 presented here.

The visual, auditory and olfactory P3 have been used to shed light on functional differences between controls and patients with a variety of diseases, including Multiple Sclerosis (MS) and Alzheimer's disease (Juckel et al., 2008; Morgan and Murphy, 2002; Polich, 1998; Whelan et al., 2010b). Features of the visual P3 component have been shown to be a reliable biomarker; for example, Whelan et al., (2010) show that P3 peak amplitude and latency abnormalities have a high correlation with cognitive impairment in patients with MS. Thus the vestibular P3 may have potential use for investigating changes in vestibular perception with age.

It has been seen recently (Setti et al., 2011) that audio-visual multisensory integration is less efficient in older subjects who fall compared to older non-fallers. The perception of temporally distinct stimuli as concurrent was seen to happen for considerably longer temporal intervals, manifesting as the inappropriate multisensory integration of stimuli separated by 270ms. At this extended time scale, this could indicate a top-down problem in modulating the cognitive processing of sensory information, rather than a problem of sensory decline, and so the phenomenon may not be specific to audio-visual sensory modalities. As discussed in Chapter 2.6, central and cortical components also need to be

considered when investigating falls in the elderly. As the P3 is also a measurement of the central processing of peripheral sensory information, it has the potential to be to be useful as an investigative biomarker.

To this end it was shown, using a bootstrapping procedure, that 93.33% of participants exhibit a P3 component; furthermore we identified a conservative minimum number of target trials required for individual statistical analysis of the P3. This enables the possibility of using the motion-based P3 for testing of vestibular stimulus processing in individual participants. It should be noted that a 1Hz high-pass filter was used; this has been shown to reduce P3 amplitude (Kappenman and Luck, 2010), however initial visualisation of the ERPs with a high-pass filter at 0.1Hz revealed a low-frequency component which dominated a number of subjects' ERPs and appeared to be an artifact due to its very large amplitude. Furthermore, it has been shown that using button-responses also reduces the amplitude of the P3 (Salisbury et al., 2001); for the purposes of this study, button-response was practical and allowed psychophysical measurements of reaction times and correct identification, and the P3 response was robust enough to be detected even at the single subject-level regardless of these attenuations. It may, however, be possible to reduce trial number requirements by addressing some of these factors using e.g. silent counting instead of button pressing.

The use of a Stewart platform and a high density electrode grid were important to establish the vestibular P3 using precise and controlled stimuli, and to confirm that the topographical distribution was similar to that of other modalities. This validation enables the use of an inexpensive arrangement with, for example, three electrodes and a unidirectional motion track. Such practical arrangements have greater clinical application. Future experiments could also extend the scope of this cognitive motion processing paradigm by investigating whether a 3-stimulus paradigm evokes a topographically distinguishable P3a waveform, as is seen in literature (Polich, 2007).

In summary, this study has demonstrated that a motion oddball stimulus evokes a vestibular-based P3 ERP, which is similar in its morphology to the P3 in other modalities. The validation of this methodology provides a strong grounding on which to investigate the processing of vestibular cues and could be a useful tool in understanding vestibular disorders. However, the P3 is a very particular type of processing, the processing of novel stimuli. While this experiment shows the vestibular stimuli can elicit such a cortical response, these responses recorded do not specifically target areas of the brain responsible for processing vestibular stimuli or perceiving motion. To further our understanding of what is involved in these processes, and thus enable further investigation into changes in vestibular

processing associated with age, it would be highly beneficial to investigate brain areas and responses associated with perception of motion. Therefore in Chapter 7, such an experiment is performed.

# Chapter 7

# True Motion Vestibular Evoked Potentials

## 7.1 Introduction

In Chapter 6 it was seen that the P3 task successfully elicited a P3 ERP which is a cognitive response to a change in vestibular stimulus, using true motion stimuli in an oddball paradigm. This chapter details an experiment in which the evoked potential responses to motion are recorded - no task was performed, and the ERPs recorded depict only the neural activity related to true motion perception itself. Motion is a fundamental part of everyday life. The perception and accurate representation of motion, in particular the self-motion, is a key factor in maintaining mobility. Compromised or degraded perception of motion can be debilitating or dangerous, as discussed in Chapter 2.

The sense of self-motion is a multisensory phenomenon, with contributions from the visual and vestibular systems (Berger and Bülthoff, 2009; Butler et al., 2010; Harris et al., 2000), as well as the somatosensory and proprioceptive systems (Frissen et al., 2011; Mergner and Rosemeier, 1998). Numerous studies have investigated the neural correlates of self-motion from visual cues alone. These studies have used the phenomenon of vection, which is the sensation of motion induced using optic flow; these studies have primarily used constant velocity profiles to maintain a sense of self-movement (Kovacs et al., 2008). However as vestibular information is a key factor in motion perception, vestibular contributions to motion perception must be investigated.

The literature of human vestibular neuroimaging has thus far been conducted using fMRI and PET. While, these imaging methodologies provide good spatial resolution, their temporal resolution is in the order of seconds. Furthermore, due to their fixed nature they are limited in the type of vestibular cues that can be provided - galvanic or caloric stimulation are the only options (Dieterich and Brandt, 2008; Fasold et al., 2002; Lobel et al., 1998), which have the disadvantage of only non-selectively stimulating both SCCs and otoliths, and both are generally experienced as rotational acceleration. This experiment thus builds on the validity of the responses seen in Chapters 5 and 6 to introduce true motion

EEG as a viable method for neuroimaging vestibular function, with the benefits of ecological true motion stimuli.

There have been a small number of EEG studies of vestibular function outside of this thesis. Vestibular evoked potentials have been recorded to rotational stimuli with step profiles, and their temporal profile shows a response which spans a small number of milliseconds (Hofferberth, 1995; Molinari and Mingrino, 1974; Rodionov et al., 1996; Schneider et al., 1996). These studies used a small number of electrodes, without attempting to remove any ocular artifact, and did not plot topographic maps or attempt to localise the sources of the recorded response. Responses to linear motion have rarely been studied. Furthermore, the step stimuli used are not representative of common situations - people do not often experience high-amplitude accelerations without ramp-up or ramp-down.

The current knowledge of the neural processing of vestibular self-motion cues in humans remains primarily in the description of reflex circuits and central processing as discussed in Chapter 2, rather than cortical components such as those examined in Chapter 6. The perception of self-motion and the integration of this information into the cognitive state happens at a cortical level, and studies into this aspect of vestibular processing in humans are sparse (for review see Lopez and Blanke, 2011).

In this experiment, high-density EEG was recorded while participants were translated forwards and backward with a sinusoidal acceleration profile on a Stewart platform in the manner described in Chapter 3. The data were analysed using time-series, frequency-domain and source-space analyses, to extract the maximum amount of information from the results, and to best separate true cortical responses from motion-related artifacts. The results could then be related to self-motion studies which employed fMRI and PET, such that the vestibular evoked potential to true linear motion in humans could be investigated. This experiment represents a novel venture into vestibular electrophysiology; the recorded responses are quite different to other EEG experiments discussed in Chapter 2, and represent electrical activity as opposed to haemodynamic changes of fMRI or PET. The results obtained are exploratory and allow investigation into how EEG data may manifest in response to a true motion stimulus.

## 7.2 Methods

### 7.2.1 Motion Stimulus Presentation

Two motion stimuli using the motion profile described in Chapter 3 were used, one forwards (F, $\theta$=0°) and one backwards (B, $\theta$=180°). These were presented sequentially, with a randomized gap of 1.5s - 2s between them. Subjects repeated 50 F and 50 B trials in a row, and were given a small rest. Two larger breaks out of the simulator with drinks of water were also provided, to alleviate tiredness. In total, 6 sets of 50 translations were performed, yielding 300 F and 300 B trials per subject.

### 7.2.2 EEG Data Acquisition

EEG data was recorded using a Biosemi 128-channel ActiveTwo amplifier as described in Chapter 3.

### 7.2.3 EEG Data Processing

The EEG data from each run was processed using the FASTER method as described in Chapter 4 and separated into 2s epochs (including a 300ms baseline, with the average subtracted for each trial) for B and F stimuli.

Event-related potentials (ERPs) were then calculated for the F and B conditions. Temporal ROIs were chosen visually as a 100ms window around the peaks at 700ms and 1200ms, which were close to the peaks of the acceleration profile (Figures 7.1 and 7.2, and compared to Figures 3.1 and 3.2). To compare the peaks of the F and B conditions, t-tests were performed at each electrode over the temporal ROIs, and false discovery rate (FDR) post-correction (Benjamini and Hochberg, 1995) for multiple comparisons was applied. These were plotted topographically on scalp maps (Figure 7.3). To investigate differences across time, pointwise t-tests were performed comparing the F and B ERPs, with FDR correction applied across electrodes and time, and a "running t-test" correction was applied for each time-point - any points which were not significant for at least 10 consecutive time-points were marked insignificant. Global field power (GFP) - defined as the standard deviation across electrodes of the time-domain signal, which shows a reference-free measure

of overall spread of cortical activity (Lehmann and Skrandies, 1980) - was calculated for the ERPs to show overall measures of spread and correspondence with the acceleration profile.

Two composite waveforms were also created, the sum and difference waveforms, created by pointwise adding F + B and subtracting F - B respectively. These waveforms were derived from observation of the F and B waveforms which lead to the hypothesis that the 1s stimulus was eliciting both transient onset responses and steady-state responses to the acceleration stimulus; commonly, ERP studies looking at only transient responses use short profiles of tens of milliseconds, e.g. (Aminoff and Goodin, 1994; Chiappa, 1997). As the F and B acceleration profiles are 180° out of phase they sum to zero, therefore by summing the F and B waveforms, steady-state EEG responses proportional to acceleration would sum to zero, and any common components of the F and B ERPs would be doubled. Conversely, by subtracting B from F, any steady state responses will be doubled, and common components subtract to zero. The signal to noise ratio of these ERPs is also higher than either F or B alone, by a factor of $\sqrt{2}$.

To test for latent contamination by EOG artifacts, the cross-correlation between the difference wave ERP and the mean of the EOG channel averages was computed for each subject. The lag at which the maximum absolute correlation was found, and t-tests were performed for this lag value at each channel to determine whether it was a non-zero value. FDR correction was applied to the p-values, and the results were plotted topographically on a scalp map (Figure 7.5). SPM was also performed between F and B waveforms, but no significant results arose.

### 7.2.4 Source Modelling

Source modelling was performed using sLORETA (Pascual-Marqui, 2002) on each subject's ERP to localise the cortical generators at the peak ROIs. This was performed on the F, B, difference and sum ERPs. Statistical analysis in sLORETA was performed on temporal ROIs versus 300ms baseline average. Statistical output from the analysis depicts T-values in voxels projected onto a standardized cortex and MRI scan, after SnPM correction for multiple comparisons (Nichols and Holmes, 2002). This method uses bootstrapping (N=5000) to compute robust critical thresholds (Figures 7.6, 7.7, 7.8).

### 7.2.5 Time-frequency Analysis

Time-frequency plots were created using both FFT spectrograms and wavelet methods, as detailed in Chapter 3. A full-band ERSP (1-256Hz at 1Hz intervals) was also created using the wavelet method for F and B conditions for the neck electrode channel, to further understand EMG interference (Figure 7.11).

### 7.2.6 Time-series Integrals

The EOG channel ERPs were investigated using simple cumulative trapezoidal numerical integration across time, as their temporal profile visually resembled that of the temporal derivative of the acceleration profile, a.k.a. the jerk profile (Figure 7.13). This was then performed on the EEG channels, for comparison (Figure 7.14). This was for visual comparison only, and no statistics were performed.

## 7.3 Results

To best investigate the cortical electrophysiology of the vestibular system, the recorded data were analysed in a number of ways. Initially, traditional ERP measures were explored.

### 7.3.1 Time-domain ERPs

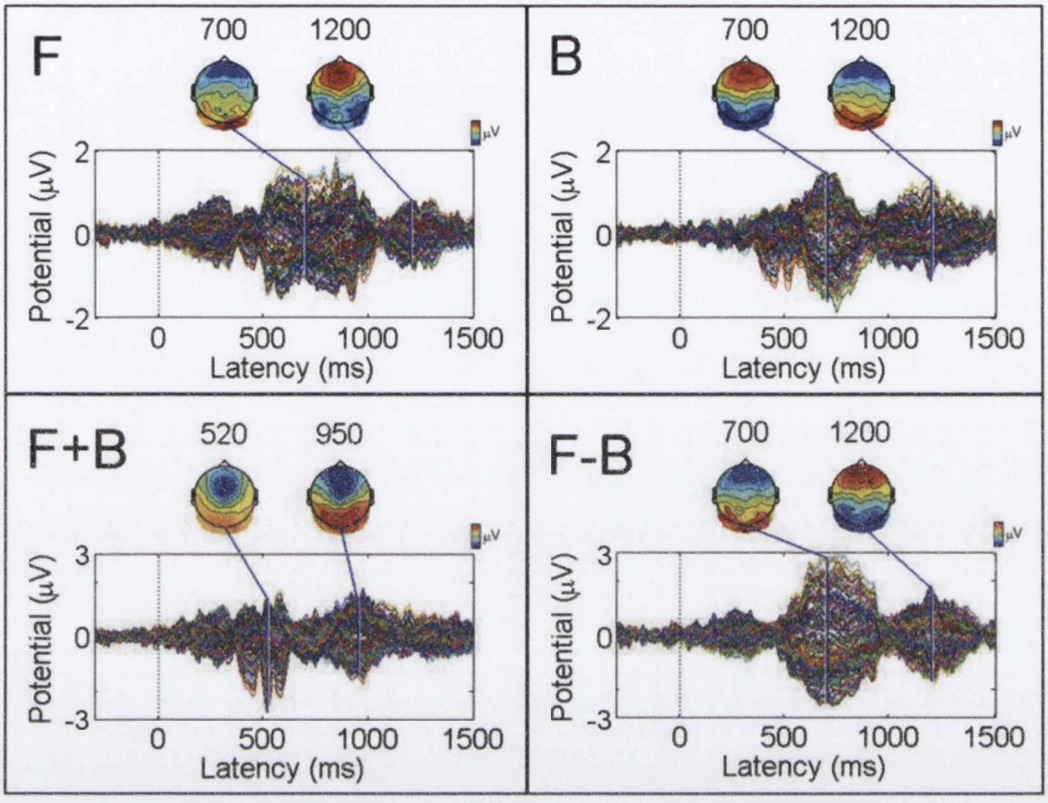


Figure 7.1. Butterfly plots of all electrodes and topographic plot at acceleration peaks in F, B, F+B and F-B conditions. These images depict the ERPs generated at each electrode overlaid, with corresponding topographic plots at temporal regions of interest to show the scalp distribution of the EEG activity.

Figure 7.1 depicts butterfly plots of the forwards, backwards, sum and difference ERPs. These show the ERPs from each channel overlaid, with topographic maps at temporal points of interest shown. Note the scale difference between the compound (sum and difference) ERPs and the stimulus-only ERPs.

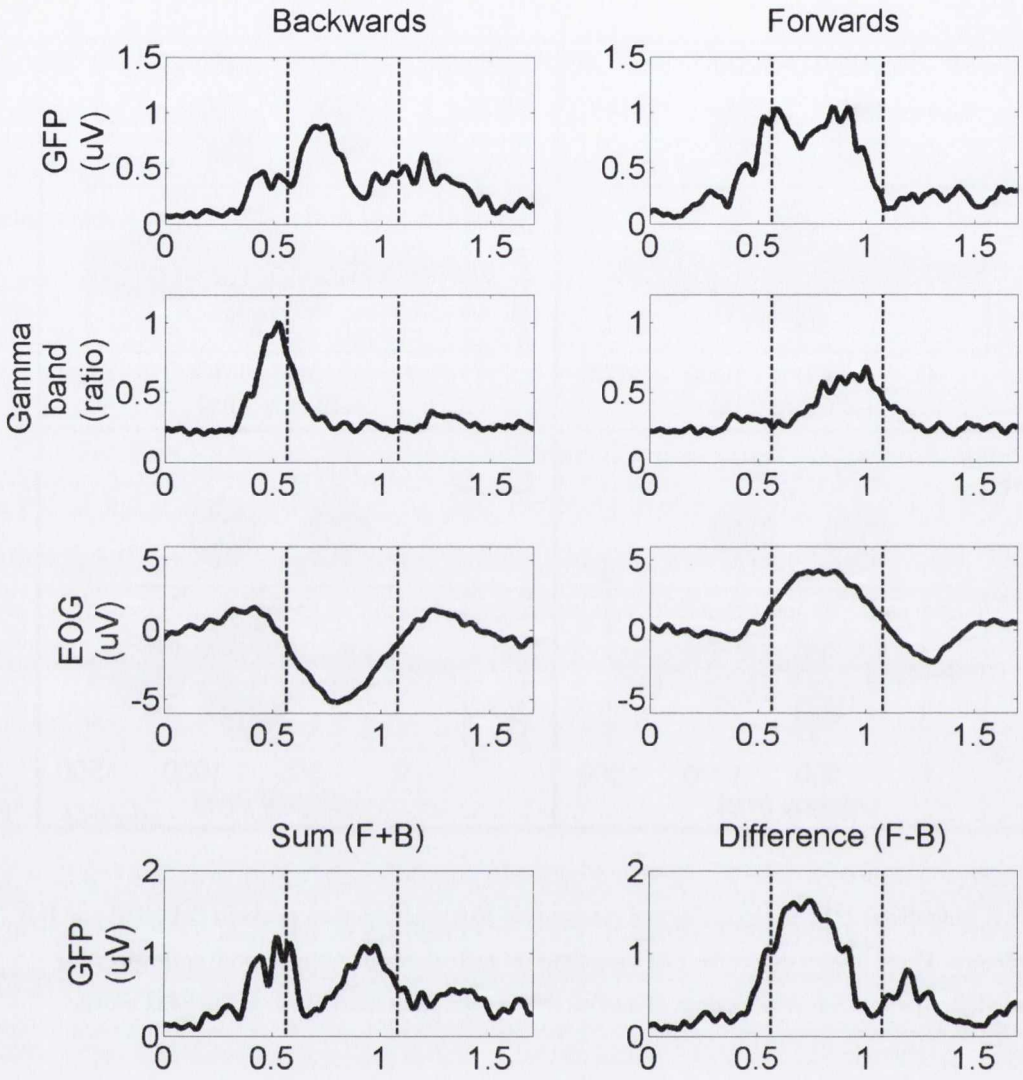


**Figure 7.2. Global field power plots depicting the overall spread of activity across all EEG electrodes in the grand average ERPs. Depicted are the ERPs in response to F and B and the ERSP of the gamma band in response to F and B. The averages from the EOG channels are also displayed, along with the F-B and F+B waves. A 20Hz low-pass display filter applied. The dashed line denotes the peaks of the acceleration profile.**

Figure 7.2 displays the GFP of the ERPs of the F, B, sum and difference conditions, along with that of the gamma band ERSPs. The EOG averages are also displayed for reference, and the peaks of the acceleration profile are shown to indicate how these relate temporally to the motion profile. These plots allow visual comparison of the time-course and peak times of the ERPs with those of EOG profile and EMG profile, as represented by the gamma band.

### 7.3.2 Peak statistics

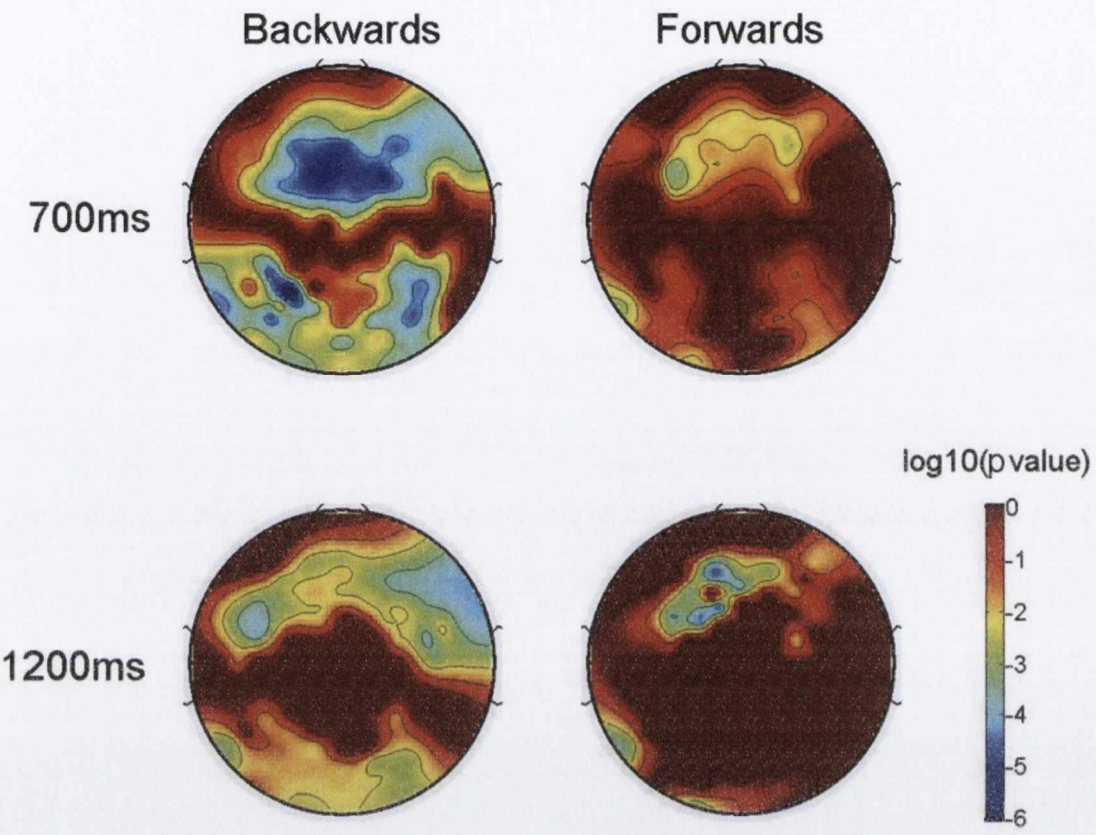


**Figure 7.3. Topographic maps of t-tests of a 100ms average of the 700ms and 1200ms peak ROIs against baseline for each electrode, after FDR correction for multiple comparisons. Color maps represent log-transformed p values, with any non-significant values set to 0.**

Figure 7.3 shows a topographic map of t-test results comparing ERP peak activity to baseline. A 100ms window was taken around the group average peak value, to allow for individual variability. Non-significant-values were set to 0, leaving any areas of significant change from baseline. The 700ms peak has a higher level of significant activity, corresponding with the group average ERP topographies from Figure 7.1, although with less activity at edge electrodes.

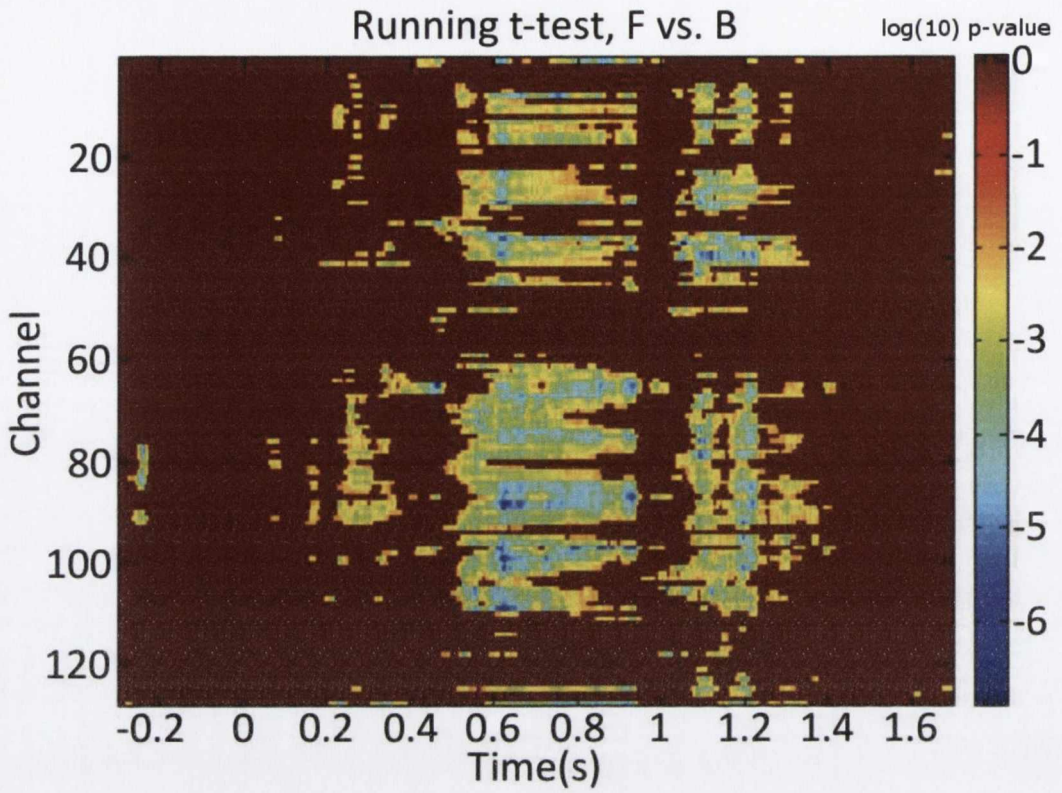


Figure 7.4. Running t-test showing time-points of significant difference between the F and B ERPs. False discovery rate was used to correct for multiple comparisons, and then any points which were not significant for at least 10 consecutive time-points were marked insignificant. Values are log-transformed p values, with any non-significant values set to 0. Electrodes range from occipital to frontal, increasing in number.

Figure 7.4 depicts areas of significant differences between the F and B ERPs. This identifies the time windows within each channel where the ERPs differ. This can be contrasted with source analysis and SPM, which do not show any differences between the ERPs – the sources appear similar despite differences in time-domain activity. This may also be due to increased variability due to the source reconstruction methods, although the method uses linear recombination of the channel data so variability is unlikely to be increased overall.

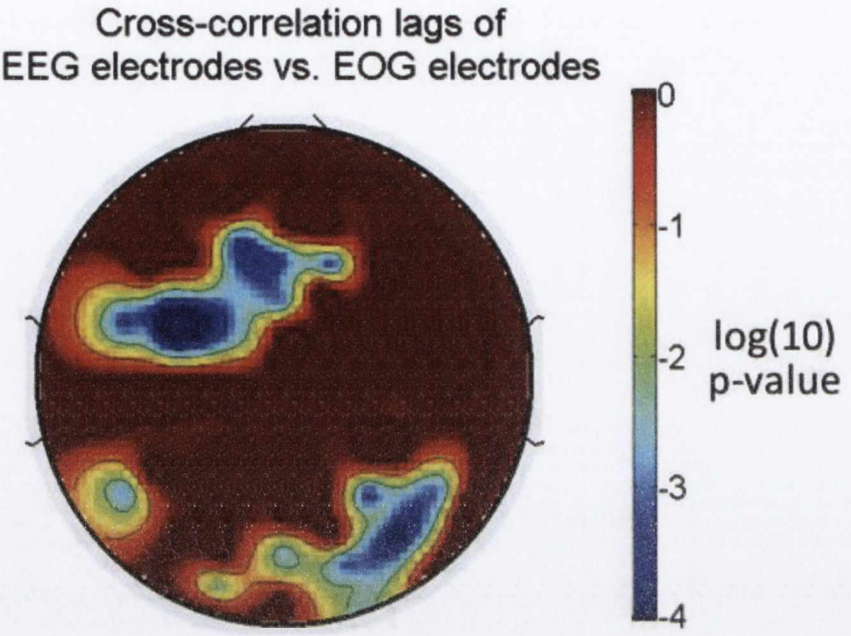


Figure 7.5. Topographic map of t-tests depicting where the peaks of the EOG are significantly lagging the peaks of the EEG in the difference wave. Values shown are log-transformed p-values.

Figure 7.5 displays a statistical topographic scalp plot where the time point of maximum cross correlation value of the time-domain ERP at each electrode and the EOG average is significantly less than 0ms, indicating that the ERP peaks at these electrodes show a significant lead of the EOG activity. This indicates that the ERP peaks may come before the EOG activity and thus are not contemporaneous to them, and can be considered to be separately generated or even generative of the EOG activity. The values shown are $\log_{10}(p)$. After FDR correction, the appropriate p-value for $\alpha=0.05$ was $p<0.0137$. All non-significant electrodes had their log p-value set to 0. All significant values correspond to EEG electrodes leading the EOG signal. No EEG electrode was seen to lag the EOG electrode.

### 7.3.3 Source Modelling

The peak source distribution compared to baseline was calculated for the Sum and Difference ERPs in Figures 7.6 and 7.7. The difference in source activity between F and B stimuli was investigated at the largest peak's latency, and this is illustrated in Figure 7.8. The SnPM correction method for multiple comparisons gives a specific critical value for each comparison made; therefore each figure has a different critical t-value for $\alpha=0.05$, 0.01. Scales were chosen to show any statistically significant results while keeping the scale bar

intelligible. All units in sLORETA plots are T-values. The overlaid numbers relate the source activity to areas identified in previous vestibular imaging studies, which are compiled in Table 7.1.

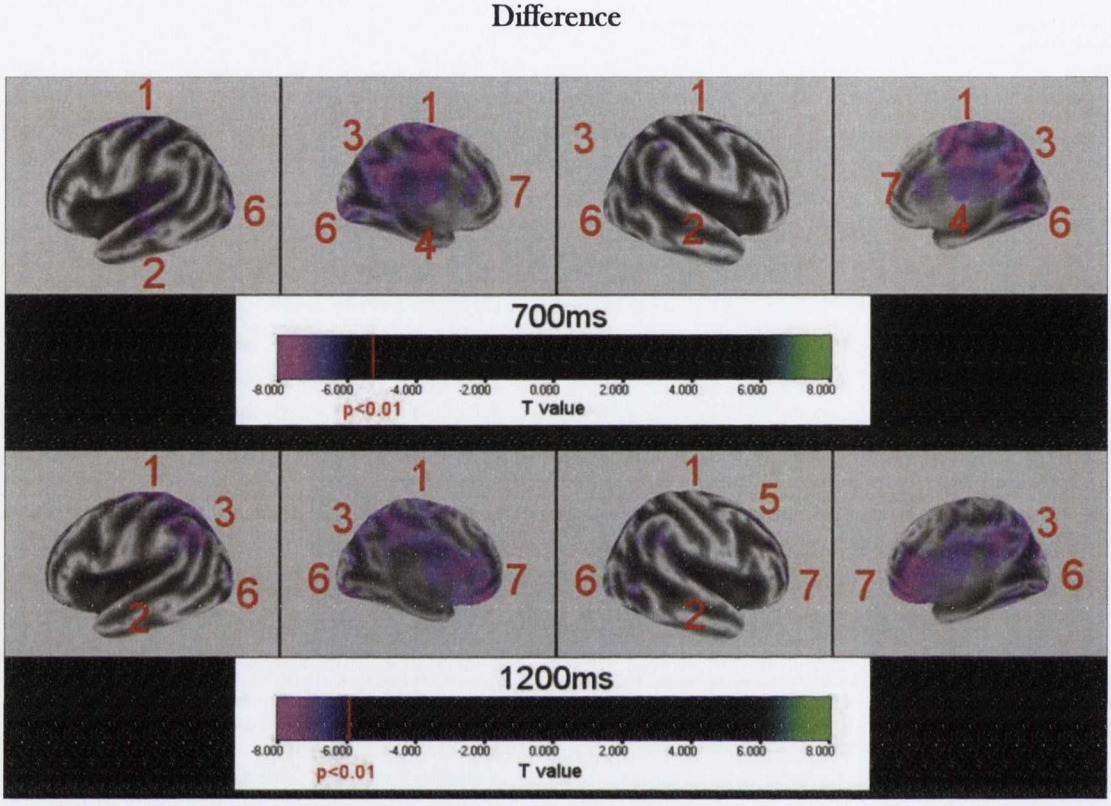


Figure 7.6. sLORETA statistical differences in the F-B condition. The top set of images is a comparison of the peak at 700ms vs. baseline, and the bottom set of images is a comparison of the peak at 1200ms vs. baseline. Negative T values imply peak activation was significantly higher than baseline in the given areas. Statistical thresholds following SnPM correction are: 700ms peak, ($p<0.01$, $|T|>5.385$), ($p<0.05$, $|T|>4.238$), ($p<0.1$, $|T|>3.698$). 1200ms peak, ($p<0.01$, $|T|>5.942$), ($p<0.05$, $|T|>4.593$), ($p<0.1$, $|T|>4.030$). Areas of difference depicted are all highly significant.

Sum

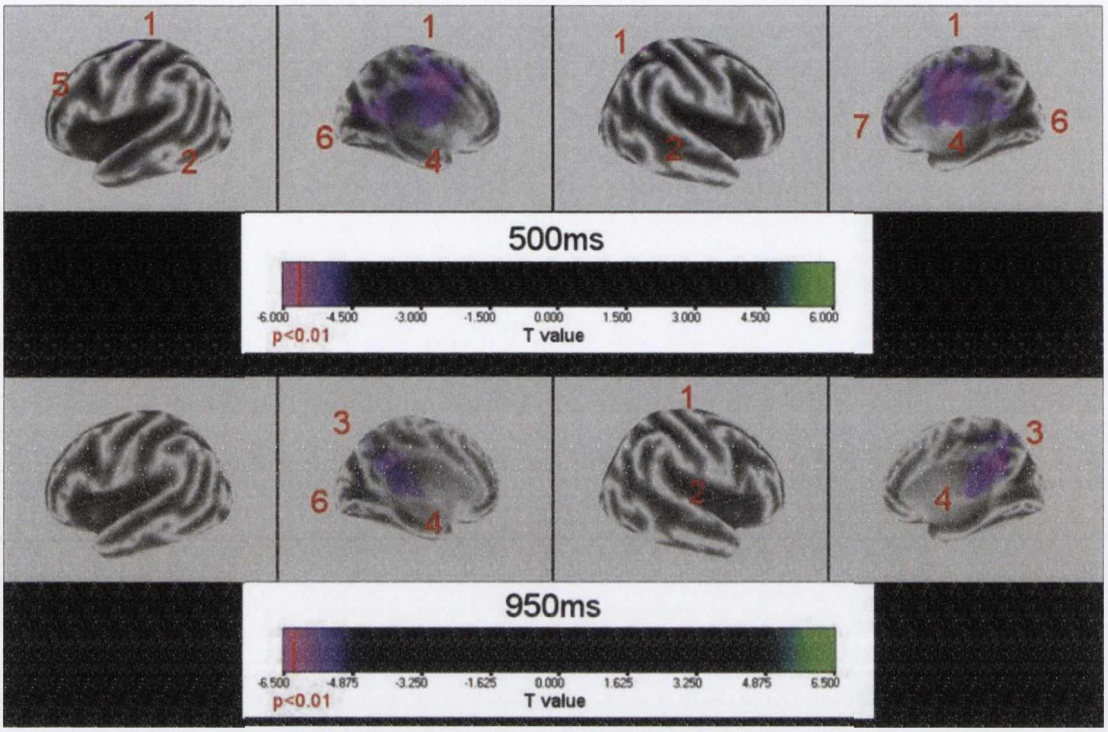


Figure 7.7. sLORETA statistical differences in the F+B condition. The top set of images is a comparison of the peak at 500ms vs. baseline, and the bottom set of images is a comparison of the peak at 950ms vs. baseline. Negative T values imply peak activation was significantly higher than baseline in the given areas. Statistical thresholds following SnPM correction are: 500ms peak, ($p<0.01$, $|T|> 5.685$), ($p<0.05$, $|T|>4.772$), ($p<0.1$, $|T|>4.392$). 950ms peak, ($p<0.01$, $|T|>6.356$), ($p<0.05$, $|T|>5.311$), ($p<0.1$, $|T|>4.891$). Areas of difference depicted at the 500ms and 950ms peaks are marginally significant.

Forward vs. Backward

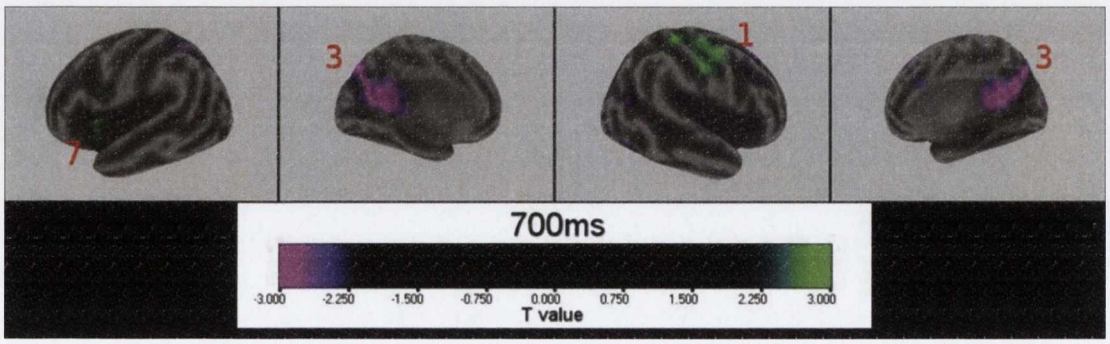


Figure 7.8. sLORETA statistical analysis comparing F > B at the 700ms peak. No voxels met the SnPM corrected $p<0.05$ T-value of 5.7.

**sLORETA Marked Regions**

| Area Number | Name | Literature Reference for Vestibular Involvement |
|---|---|---|
| 1 | Superior/inferior parietal cortex (S/IPL), ventral-intra parietal (VIP), pre- and post-central gyrus | (Bense et al., 2001; Blanke et al., 2000; Bottini et al., 1994; Brandt and Dieterich, 1999; Dieterich et al., 2003; Fasold et al., 2002; Naito et al., 2003; Schlindwein et al., 2008; Stephan et al., 2005; Suzuki et al., 2001) |
| 2 | Parieto-temporal insular junction | (Bense et al., 2001; Bottini et al., 1994; Brandt et al., 1998; Cardin and Smith, 2009; Chen et al., 2010; Dieterich et al., 2005; Dieterich et al., 2003; Eickhoff et al., 2006; Fasold et al., 2002; Lobel et al., 1998; Lopez et al., 2012; Schlindwein et al., 2008; Stephan et al., 2005; Suzuki et al., 2001) |
| 3 | Parieto-occipital cortex, cuneus | (Bense et al., 2001; Brandt et al., 1998; Cardin and Smith, 2009; Dieterich et al., 2003; Fasold et al., 2002; Kovacs et al., 2007; Naito et al., 2003; Schlindwein et al., 2008) |
| 4 | Hippocampal gyrus and midcingulate gyrus | (Bense et al., 2001; Bottini et al., 1994; Naito et al., 2003; Smith et al., 2011; Stephan et al., 2005; Suzuki et al., 2001; Vitte et al., 1996) |
| 5 | Frontal cortex | (Bense et al., 2001; Dieterich et al., 2003; Fasold et al., 2002; Israel et al., 1995; Kluge et al., 2000; Lobel et al., 1998; Naito et al., 2003) |
| 6 | Extreme occipital cortex | Activation in this area is confounded with EMG artifact |
| 7 | Extreme frontal cortex | Activation in this area is confounded with EOG artifact |

**Table 7.1. List of areas identified in the sLORETA plots, with literature references implicating their involvement in vestibular processing.**

### 7.3.4 Time-frequency Analysis

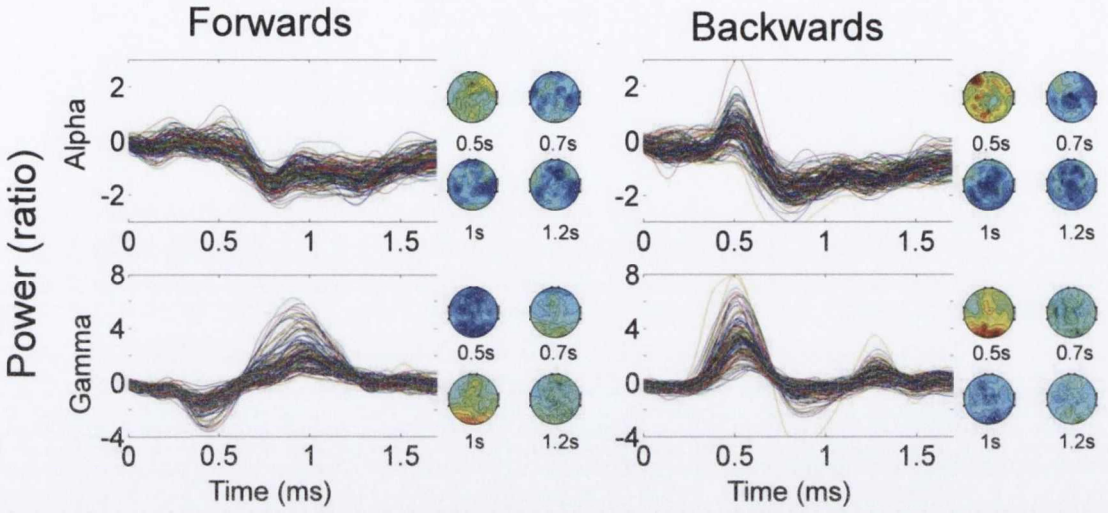


**Figure 7.9. Time-frequency decomposition of the responses to forwards and backwards conditions in the alpha (8 - 12 Hz) and high gamma (>50Hz) bands. Event-related spectral perturbations (ERSPs) depict signal power as a ratio of baseline power, to show increases and decreases from baseline. Topographic maps depict the scalp distribution of these ERSP waves at various temporal regions of interest.**

Time-frequency analysis here enables the separation and visualisation of different components of the ERPs recorded. Wavelet decomposition was used to reduce processing time; FFT spectrogram analysis was initially performed and computation time was considerably higher for a lower effective temporal resolution. In Figure 7.9, the temporal modulation in the time-series of the alpha and gamma frequency bands are depicted. These are the two most relevant bands to this study - the gamma band is well-known to be associated with EMG activity (Freeman et al., 2003; Goncharova et al., 2003), and so from the gamma band time profile it is possible to determine the spatiotemporal dynamics of EMG occurring in response to the motion profile. This relates well to the time-frequency profiles of the neck electrode in Figure 7.11. The alpha band, in contrast, is known to be associated with attention and various cognitive functions (Klimesch et al., 2007; Wolfgang, 1999), and thus can be used to investigate cortical genesis of the ERPs. Of considerable note is the time of the peaks of the EMG activity - 0.5s and 1s, with gamma band activity approaching zero at 0.7s and 1.2s, the times at which the overall ERP amplitude is highest. This is promising and points to a dissociation between overall EEG and EMG responses.

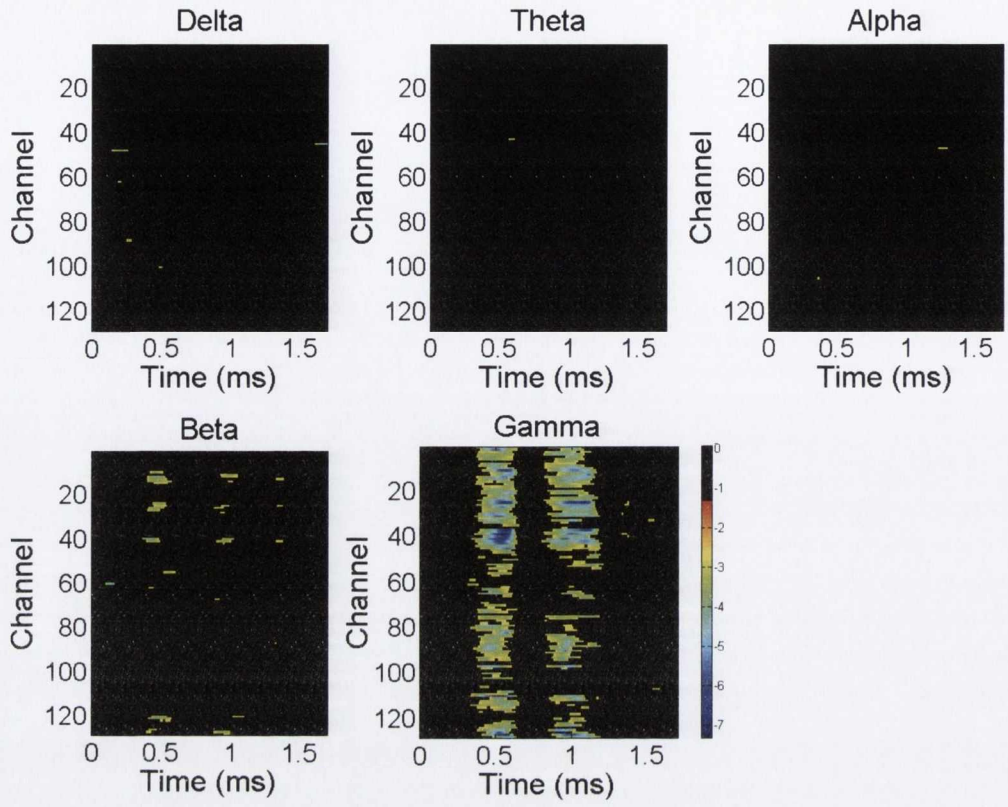


**Figure 7.10. Pointwise t-test detecting differences between backward and forward conditions at each electrode and time-point, in each frequency band. Values are log-transformed p-values. Critical 5% cutoff after FDR correction was ($p<0.0015$). Channel order is occipital (1) to frontal (128).**

Figure 7.10 displays pointwise t-tests showing differences between the F and B time-series at each channel for the five standard EEG frequency bands (Delta: 1-3Hz, Theta 4-7Hz, Alpha: 8-12Hz, Beta: 13-35Hz, Gamma: >35Hz). It can be seen that only the gamma band shows considerable significant differences, with a few channels showing differences in the beta band and a few randomly distributed patches of significance in the delta, theta and alpha bands. This demonstrates that the F and B ERPs differ at high frequencies. The temporal regions of difference at high frequencies are seen to correspond with the peaks seen in Figure 7.9 and Figure 7.11, which are temporally distinct from the peaks of the broadband ERP. The lack of difference at lower frequency bands may indicate similarity within these bands, but may also represent higher variability within each band.

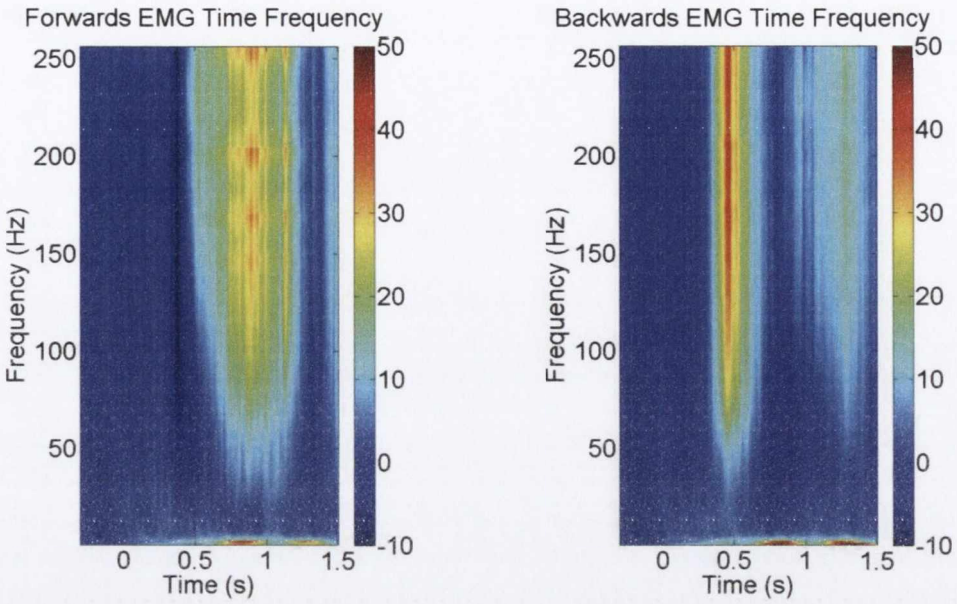


Figure 7.11. Full-band time-frequency plot of EMG channel, with color bars depicting ratio vs. RMS of baseline. The high-frequency activity bands peak at times 0.4s and 0.9s in the F condition, and 0.45s and 1.3s in the B condition. The low-frequency activity peaks at 0.8s, and 1.3s in both.

Figure 7.11 shows the power increases and decreases in the EMG electrode across all frequencies from 1-256Hz. Large increases in high-frequency activity are visible at 0.9s in the F response and at 0.4s in the B response. This response spans the frequency spectrum, as would be expected for an EMG response. There is also a smaller decrease in power at 0.4s in the F condition, and a smaller increase in power at 1.3s in the B condition. Low-frequency activity is also present, peaking at 0.25s, 0.6s and 1.1s in both conditions.

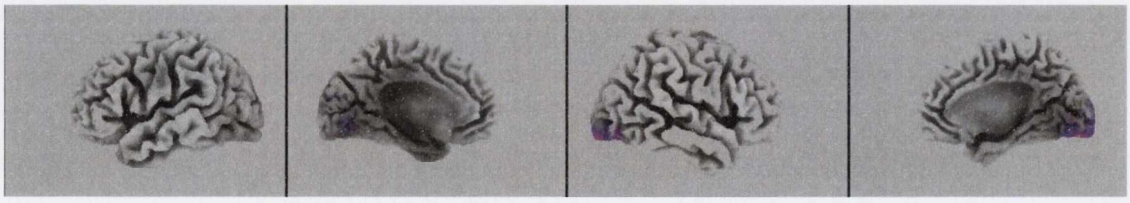

Figure 7.12. sLORETA map of the gamma activity at 500ms in the backwards waveform. Map is not statistical, arbitrary scaling is not shown. The regions showing activity is that previously noted as confounded with artifact.

Figure 7.12 is a sLORETA map of the 500ms peak in the gamma waveform, going backwards. This exhibits a single regional source, on the extreme occipital cortex, probably

due to reflexive activation of the trapezius muscles to stabilise the head. As the gamma band is highly related to EMG contamination, sLORETA activity in this region in the broadband ERP are likely mixed with EMG activity.

### 7.3.5 Signal Integration with Cumulative Trapezoidal Integral

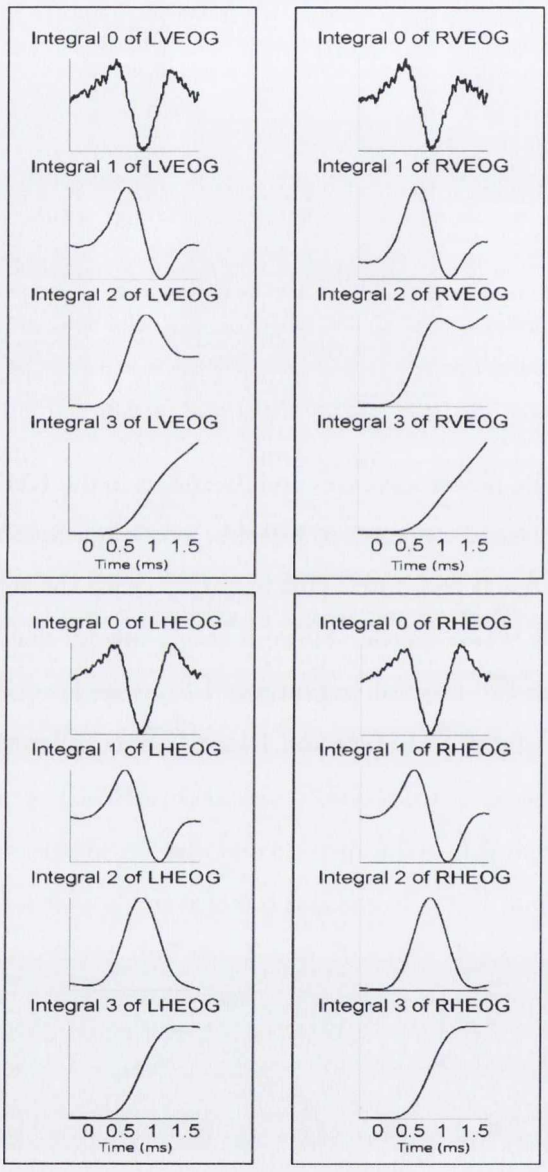


**Figure 7.13. Cumulative trapezoidal numerical integral performed on the ERPs of the EOG channels, for B stimulus. LVEOG, left vertical EOG. LHEOG, left horizontal EOG. RVEOG, right vertival EOG. RHEOG right horizontal EOG. Units are arbitrary on the y axes.**

Figure 7.13 shows the cumulative trapezoidal numerical integral of the EOG channels for the B stimulus. The results show that the horizontal EOG response is a very good match for the jerk response to the motion profile - the first integral closely approximates the acceleration profile, the second the velocity and the third the position. As it is very easy for these responses to become divergent due to the cumulative nature of their summation, it is promising that the result is so clear. The vertical EOG profiles demonstrate some divergence towards the latter half of the second integral, which affects the third integral's shape.

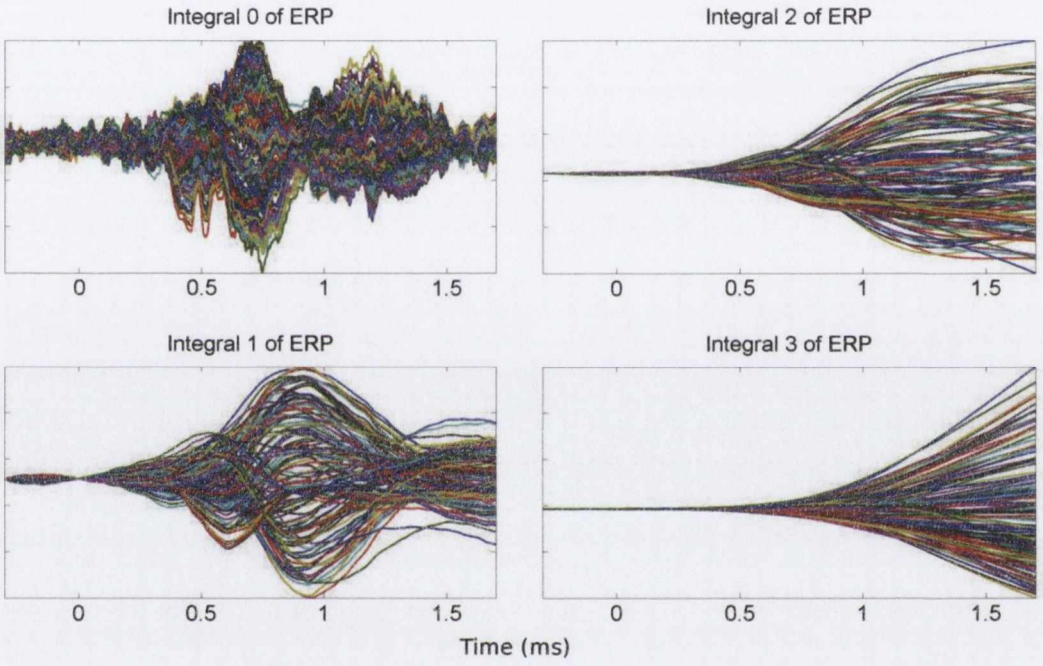


**Figure 7.14. Cumulative sum performed on the scalp channel ERPs, shown in butterfly plot format. Calculated for B stimulus. Units are arbitrary on the y axes.**

Figure 7.14 represents the cumulative trapezoidal numerical integral of the EEG channels of the B ERP. The shape is quite different from that of the EOG channels. A large number of the EEG channels appear to match an acceleration response - the first integral appears similar to the velocity profile, and the second integral appears similar to the displacement profile - which is distinct from the EOG channels' jerk-like appearance.

## 7.4 Discussion

The aim of this study was to investigate the neural correlates of human motion perception during true, non-visual self-motion. High-density EEG recordings were used to study the spatio-temporal neural dynamics of motion processing, while employing a Stewart motion-platform to present self-motion stimuli to subjects. This approach to investigating motion perception was the culmination of the experiments described in Chapters 5 and 6, and was supported by the method described in Chapter 4. Such an approach is a novel and modern method of investigating vestibular function and self-motion perception, with a wide range of information coming from the results, and a number of follow-on studies possible. The experiment is exploratory, as there is no precedent for the type of EEG responses that result from a prolonged natural motion stimulus; much of the discussion focuses on potential interpretations of different aspects of the ERPs recorded.

Visual analysis of the traditional ERP plots shows that the broadband waveforms can be seen to be visually similar to the acceleration profile in their time-course. As the ERPs are representative of vestibular information (as discussed in Chapter 3 and throughout the thesis), this seems sensible. Further to this, the topographic maps are inverted at the 700ms and 1200ms peaks of the F and B conditions (Figure 7.1), where the acceleration profiles are maximally inverse and the waveforms are statistically different from baseline and each other. Before interpreting the recorded responses, it was important to determine whether the information could be classified correctly as cortical in origin, rather than EOG or EMG from the VOR and VCR. As was seen in Chapter 6, it is possible to record true cortically generated EEG data without notable interference; however, the P3 is a differential measure. Any common components of standard and target were subtracted; therefore it is possible that artifact contamination remained in the ERPs, but was subtracted away. Nonetheless this showed that cortical ERPs recorded were not too small to detect over artifact. In the present study, a three step approach was used to determine what ERP data can be classified as cortically generated: 1) investigating the broadband topographies, 2) using frequency analysis to isolate the frequency responses and 3) localising the cortical sources of peak activity.

The topographic distributions of the ERP peaks at the 700ms and 1200ms, those closest to the peaks of the acceleration, are bipolar, with a fronto-central peak that begins to wane at the frontal electrodes (Figure 7.1). In contrast, EOG has a monopolar frontal distribution with sharp fall-off (Croft and Barry, 2000). Figure 7.3 shows topographic regions of statistical difference from baseline - there is no statistical difference at the frontal

electrodes, which are the most affected by ocular artifacts. Figure 7.5 provides further evidence, showing that a number of scalp electrodes lead the EOG electrodes; no scalp electrodes lag the EOG response. Figures 7.13 and 7.14 also show that the horizontal EOG responses almost perfectly match a jerk response, as their first, second and third integrals match the shape of the acceleration, velocity and position profiles. The vertical responses are less exact, but still approach the acceleration profile at the first integral. The ERP responses, in contrast, approach the velocity profile in their first integral, which implies proportionality to acceleration, with some additional lower amplitude activity; thus from this perspective, the EOG and EEG ERPs have quite different properties. This jerk-like property of the horizontal EOG is interesting in its own right; it has been suggested before that jerk is a contributing factor to the linear VOR (Angelaki, 1992; Angelaki et al., 1993; Angelaki and Hess, 1996; Mergner and Glasauer, 1999; Niven et al., 1966), although this was met with disagreement by (Raphan et al., 1996). These facts come together to suggest that the responses recorded on the scalp are not marred by excessive EOG interference. The use of independent component analysis (ICA) and the FASTER method was certainly advantageous in this regard, as EOG activity is easily separated from EEG data using ICA, which can then be detected and removed using FASTER. The EOG signal was retained for analysis for Figure 7.13.

The VCR generates strong contractions in the trapezius muscles, with lesser contributions from the sternocleidomastoids (Ferber-Viart et al., 1997). As the trapezius derives part of its origin from the occipital protuberance, EMG recorded on the scalp would be expected to manifest maximally at the occipital electrodes. In Figure 7.2, we can indeed see this to be the case in the broadband ERP at the peaks of interest at 700ms and 1200ms. However, we can also look at the time-frequency distribution of the ERP in Figure 7.9. EMG has a broadband distribution, with peaks in EEG beta and gamma bands (Goncharova et al., 2003). A full-band frequency analysis of the neck electrode in Figure 7.11 confirms that this is indeed the case - there are strong peaks at high frequencies. Thus we can look to the gamma band ERSP to inform us of the distribution of the EMG interference present in the ERPs. Figure 7.9 portrays the gamma band activity as a tri-phasic waveform, maximal occipitally, but peaking at 450ms, 950ms and 1350ms, and with zero-crossings at the 700ms and 1200ms ERP peaks - therefore the EEG peaks do not appear to be driven by the EMG activity. The sLORETA analysis in Figure 7.12 shows that the cortical map most strongly driving gamma is in the extreme occipital cortex, and so this area should be discounted as

artifactual. As the ERP maps in Figures 7.6 and 7.7 contain only a small activation of this area compared to other regions, this allows us to further see that the influence of EMG is minimal in comparison to activity at other cortical sites.

There is also low frequency activity seen in the neck electrode; EMG is known to span the whole frequency spectrum, and due to the continuous sinusoidal stimulation, this may be continuous low-frequency EMG activity opposing head movement. This peaks at 600 and 1300ms in both F and B. These peaks do not coincide with any ERP peaks, which is promising, but the 800ms peak may be wide enough - particularly in the F condition - to overlap with the 700ms broadband ERP peaks seen in Figure 7.1. The shape does not correspond to these ERPs so it is most likely not the only factor driving the ERPs, but it may be a contributing factor to why the F waveform has a wider peak around 700ms. EMG activity is difficult to remove using ICA, as it has multiple sources, and so there may remain some low-frequency EMG contamination in the ERPs. The topographic maps do at some points extend to the edges of the scalp, and the total inversion seen is not a typical feature of cortically-based ERPs. A dedicated EMG system for proper recording of neck EMG with appropriate electrode choice would enable a much better ability to identify and separate EMG from EEG activity, and would be a recommended outcome of this study. Thus, some of the results and potential interpretations discussed below may be confounded by the persisting presence of low-frequency EMG artifact. However, while the sLORETA mappings do exhibit some contributions from the area identified as a source of EMG, these are small in comparison to the other areas identified. Compiling these observations, there is evidence that ERP can be considered to be dominantly true EEG activity, with the possibility of a relatively small amount of low frequency EMG contamination.

This ERP distribution is unusual with respect to literature, as it is a continuous response to a 1.25s stimulus; most common ERP tasks are elicited using short (sub-100ms) stimuli by convention. One consideration for the stimulus and the ERPs is that continuous stimulation such as this may disallow the phase-reset mechanism of ERP generation. This may be a contributing factor to the relatively low amplitude of all ERPs. From visual appraisal of the ERP, it appeared that there was two components to the ERP - an onset response related to the detection of motion, combined with a continuous response related to on-going processing of the acceleration. The onset response has some correspondence in literature, as discussed above with relation to the EMG signal (Keshner, 2003). As the F and B conditions are responses to inverse acceleration profiles, the difference ERP created by

subtracting these two would double any response responding only to acceleration. Furthermore, any common components of these ERPs will be cancelled. Conversely, adding the two responses would double the common components and cancel the acceleration response. The difference and sum ERPs portrayed in Figures 7.1 and 7.2 show that this is approximately true. While the time-series data appear to be inverse versions of each other, neither the time-frequency nor the source-space analyses show any significant differences between the F and B ERPs in the temporal regions of interest, therefore the results of the difference and sum waves are considered as representative of both F and B activity. The low spatial resolution of EEG and the SnPM correction in sLORETA over 6000 voxels may also play a role in reducing statistical significance in this modality. Such an inversion is often due to a source dipole whose direction changes; thus there is no difference in the source location of the activation. These inversion effects are seen in visual spatial attention tasks, e.g. (Di Russo et al., 2003), but it must be noted that this total inversion is unusual; it is not entirely clear what mechanisms are involved in this or whether this is residual artifact.

The difference ERP has a temporal distribution similar to the acceleration profile, as seen in Chapter 3. This is seen in Figure 7.1 and the peak times in Figure 7.2. This suggests that the difference ERP may represent a neural component involved in the on-going processing of acceleration information. It was discussed by (Dieterich et al., 2003) that the human PIVC has direct connections to and from the vestibular nuclei; therefore it would be reasonable to expect a neural representation of acceleration in the cortex. One noticeable feature of the difference wave, evident in Figure 7.2, is the amplitude attenuation between the first and second peak. This may be related to the information relayed in Figure 7.5, which demonstrates that electrodes at the peak of the ERPs are leading the EOG activity, i.e. leading the VOR. This would imply that the neural data recorded is involving the mediation of the VOR. While the VOR is a short-latency reflex which does not need cortical input to occur, the experimental paradigm required subjects to fix their gaze on a static point during motion, thus requiring suppression of the VOR. Thus we can hypothesize that we may have recorded an EEG manifestation of VOR suppression, which is a top-down task involving a number of cortical structures and the integration of visual-vestibular information. This suppression mechanism may explain the attenuation of the ERP across time, as it is seen in Barnes and Paige, (2004) that suppression of angular VOR using observer-static targets leads to EOG activity which is progressively attenuated over the course of the acceleration, as we see here. The experiment had been designed to be taskless, with fixation included to reduce

the VOR; however, as this was the only requirement, it may be that the ERP is related to the task of fixation.

Another explanation for the amplitude attenuation is that adaptation occurs over the course of the ERP, and so the response is attenuated. Such adaptation is seen in St George and Fitzpatrick, (2011), in response to rotational true motion stimuli. However, the model developed in their study exhibits an adaptation time-constant of 75.9s, and only during constant acceleration; based on such a model, a 1s sinusoidal stimulus would not exhibit such a level of attenuation. The possibility remains that such a model based on linear acceleration or the higher-amplitude sinusoidal acceleration used in this thesis would exhibit different properties, but overall this explanation seems less convincing.

The sum ERP, in comparison, has earlier onset peaks, situated at 500ms and 975ms. These peaks coincide with the EMG peak amplitudes, which may indicate that the sum ERP is related to EMG. However, as can be seen from the time-frequency analyses of the gamma band and neck electrodes in Figures 7.9 and 7.11, the EMG profiles are roughly inverse versions of each other. As the sum ERP keeps what is common to both B and F, it is likely not a proportional response to muscle activity. Confounding this interpretation, however, is the fact that the F and B waves do show statistical differences at the 500ms peak - see Figure 7.4. However, the sum ERP peak occurs before the gamma band ERP does, which would indicate another generator of the sum ERP, at least coinciding. On balance, there is evidence to posit that the sum ERP may, at least partially, represent the response to a change in acceleration - the peak times coincide with the start of the acceleration and deceleration portions of the motion profile. Similar onset ERPs have been reported in literature, e.g. (Pyykkö et al., 1995), in response to high-amplitude vestibular stimulation, and as discussed by Keshner, (2003). To fully understand this response further investigation is required, e.g. the use of a variety of motion profiles.

Figures 7.6 and 7.7 illustrate the sources localised at the major peaks of the difference and sum waves. The F and B conditions showed no statistical differences in source space (See Figure 7.8 for example), so only the difference and sum ERP are presented, to increase the signal-to-noise ratio for the respective peaks. There are a number of regions of statistical significance from baseline demarcated. It must be noted that the extreme frontal (region 7) and occipital regions (region 6) are likely active due to residual EOG and EMG activity respectively, as can be seen for EMG in the sLORETA analysis in

the gamma band in Figure 7.12. While these regions may conceivably also contain true brain activity - region 7, for example, may contain activity in the anterior cingulate cortex, known to be active in self-motion perception (Bottini et al., 1994) - their proximity to possible artifactual projection sites is confounding.

A number of brain areas have been observed to be active during the movement. The parieto-temporal insular junction (area 2 in Figure 7.6) has been identified as a key area in vestibular perception (Lopez et al., 2012; zu Eulenburg et al., 2012), and is often thought to be the human homologue of the monkey parieto-insular vestibular cortex; topologically it is in a similar location and appears to perform similar function receiving a high proportion of vestibular cortical projections. Other areas identified from the analysis of the ERPs are the VIP, IPL, anterior, middle and posterior cingulate cortex, and the parts of the frontal cortex, which have all been identified numerous times as being active during vestibular stimulation (Bense et al., 2001; Bottini et al., 1994; Lobel et al., 1998; Lopez and Blanke, 2011; Schlack et al., 2002; zu Eulenburg et al., 2012). The concordance of our results with literature presents a strong case for the vestibular nature of the response. The highly distributed nature of the results is not surprising as the concept of the "inner vestibular circle" is sometimes used in animal literature to describe the range of sites activated during vestibular stimulation, and is being used in a number of human studies also.

It has been concluded a number of times (Ramat et al., 2005; Roy and Cullen, 1998) that the VOR arc needs to receive context-driven input from cortical areas to function properly. This phenomenon has been studied using PET imaging of suppression of caloric-induced VOR. The cuneus (here, area 3 in Figure 7.6) is seen to be active during suppression; this area is thought to be involved in a visual-vestibular inhibitory process with the PIVC (Brandt et al., 1998), which could be a potential interaction for suppression of a vestibular-based reflex. The IPL (in area 1 in Figure 7.6) and frontal gyrus (area 5 in Figure 7.6) are also seen to be activated during fixation (Naito et al., 2003).

Translational VOR involves more visual integration than the rotational VOR (Angelaki, 2004), and as caloric stimulation targets the semicircular canals (Fetter et al., 1998), the fixation mechanisms and cortical processes will differ with stimulus type. While there have been studies on the VOR using head-fixed targets during rotational motion (Barnes and Paige, 2004), and static targets during translational motion (Paige and Seidman, 1999), the present study is, to the best of the author's knowledge, the first to monitor VOR

during translation motion using a head-fixed target. As this information was initially considered supplementary to the main aims of the experiment, further studies involving an in-depth characterization specifically targeting the VOR would be very informative.

Frequency analysis was also performed on the F and B ERPs. The gamma band has already been discussed - while there may be true EEG information mixed with EMG contribution, we cannot separate them, and it is more likely to be the opposite case. A reasonable assumption is that there is less contribution from EMG to frequency bands other than the gamma and beta bands (Goncharova et al., 2003) and this appears to be the case at the time points of interest; in particular activity in the alpha band at times when the gamma band approaches zero amplitude. The alpha band has been seen to be associated with cognition in general (Wolfgang, 1999), and is hypothesised to reflect the modulation of inhibition (Klimesch et al., 2007). Here we can see in Figure 7.9 that, after an initial peak at 500ms which is confounded with EMG interference, the alpha band has a decrease in power at 700ms. This is continued across the length of the epoch, with some slower trending towards zero. This adds further weight to the argument that the ERP is neurally based, as the alpha band progression is similar in both F and B conditions - in Figure 7.10, there is no difference detected in the alpha band - and is quite unlike the acceleration profile. One compelling interpretation of alpha decrease is that it is associated with the cognitive suppression of the vestibular reflex - as its progression fits the amplitude trend seen in the difference wave, this would fit the responses observed. Disinhibition of cortical areas related to VOR modulation such as the cuneus (Naito et al., 2003), would imply modulatory feedback from the cortex based on the state of the VOR. This alpha decrease could also be the reflexive activation of the visual system, attempting to provide a visual motion cue to supplement the vestibular information incoming. Another potential explanation is that the alpha profile is related to the conscious perception of motion, and that the slow trend to zero is related to stimulus habituation.

Figure 7.8 displays the sLORETA statistical analysis comparing the 700ms peak between the F and B conditions. While these results are not statistically significant after SnPM correction, they point to a potential avenue for research which might prove interesting with more focused further work. The results show that the parieto-occipital cortex shows higher activity in the F conditions, while areas near the somatosensory cortex show higher activity in the B condition. As the parieto-occipital cortex is known to be involved in visual-vestibular processes (Brandt et al., 1998), this might point to a difference between backwards

and forwards sensory processing during self-motion – visual cues are relevant to collision avoidance when going forward, but somatosensory cues would be more informative of collision when going backwards. As collision and looming stimuli are known to alter subjective perception of time (Regan and Vincent, 1995; van Wassenhove et al., 2008), this is an interesting phenomenon which warrants further investigation. It may also explain some of the differences in temporal profiles of the F and B ERPs, particularly the early peak seen in Figure 7.4.

The dynamics of the high-frequency EMG profile are interesting in their own right. Since the VCR is usually seen to be a proportional response to acceleration with up to 100ms lag, it is not immediately obvious how this EMG profile is generated. Such profiles are also seen in a study characterising neck-trunk dynamics during linear acceleration (Keshner, 2003). In this study, it was hypothesised that the early peak is caused by low-latency disynaptic connections from the vestibular nerve to neck muscles, caused either by the initial acceleration, or sound-induced responses. The second and third peaks would then be proportional responses to acceleration; this would give an unusually long latency response however, so is not entirely plausible. (Blouin et al., 2003) also sheds some light on possible mechanisms – in this study, the EMG adaptation to 10 periodic accelerations was measured as a shortening of the response latency. In this experiment, a total of 300 accelerations were used per subject. This allows for a much greater magnitude of adaptation, and therefore another proposal is that as the inter-trial interval (ITI) has only a small amount of randomization (500ms difference between minimum and maximum ITIs), subjects learn to brace in expectation of motion in order to better stabilise the head. The tri-phasic nature is common of EMG activation (Cooke and Brown, 1990), and the occipital manifestation is in line with a trapezoidal origin; therefore this explanation may better fit the observations seen. Yet another explanation is that the EMG profile, like the EOG profile, is related to jerk; while there is precedence in literature for the VOR to be related to jerk, no literature exists on the VCR and its nonlinear relationship to acceleration.

Future directions of this research include further characterisation of the dynamics of motion processing using differing motion profiles and speeds, and neuroimaging using visual and vestibular motion stimuli. The combining motion perception with neuroimaging of active motions is now approaching the realm of experimental possibility. Recording EEG during active motion has been demonstrated in such studies as (Gramann et al., 2010; Gwin et al., 2010), which develop methodologies for isolating true brain activity. The investigation

of the cortical processes underlying co-ordination of motion perception and response co-ordination is a promising direction for future research in aging and rehabilitation. A full and detailed investigation into the amount of EMG contamination would also provide a more solid backing for these results, and allow investigation into the unusual VCR activations seen.

In summary, EEG was successfully used to record human cortical responses during full body translation. The use of time-series, time-frequency and source-space analysis allows the ERP to be segregated into artifactual and true brain activity with relatively little overlap. The results show that the ERP follows the acceleration profile, with an early component which may be an onset detection potential. Source analysis shows that regions involved are in concordance with literature. The ERP can be seen to lead the EOG activity at its peaks, and its morphology is quite similar; this morphology is representative of VOR suppression, which would indicate that cortical processing of vestibular information involves contextual mediation of the VOR. Concurrent power decrease in the alpha band, which is associated with attention and excitation generally, also supports this conclusion. The VOR, in particular in the horizontal direction, reflects a proportional response to jerk. The gamma band portrays information about the VCR, which appears to adapt to lead the acceleration profile in the case of the highly repeated stimulus used.

This is the first time that the neuroimaging of human linear vestibular processing has been documented using true motion; EEG was shown to be a suitable tool for the task. This methodology allows the study of motion-processing using more naturalistic stimuli and environments than previous fMRI and PET studies. Anatomical similarity to these methodologies is preserved, while enhancing temporal resolution and enabling simultaneous imaging of vestibular reflexes during recording. These results bring us closer to the use of neuroimaging for self-motion perception in every-day situations.

# Chapter 8

# Discussion

## 8.1 Thesis Aims

The aims of this thesis were to facilitate further investigation in the use of vestibular neuroimaging. Current practises of fMRI and PET scanning use non-targeted galvanic or caloric vestibular stimulation. Therefore, imaging methods using true motion stimuli were developed to provide more ecologically valid vestibular cues, also allowing selective otolith stimulation using linear acceleration. To enable this, EEG was used to record the neural responses; this also provides an increase in temporal resolution over PET or fMRI. These goals were achieved over the course of three imaging experiments and one methodological development. First, the use of EEG as a method of neuroimaging during true motion was validated by recording the response to visual stimuli while subjects were in motion on a Stewart platform. The results of this experiment are described and reported in Chapter 5. Next, the validity of ERPs recorded in response to true motion was ascertained using an oddball motion paradigm to elicit a P3, which is an ERP component with known spatiotemporal properties, thus demonstrating that ERPs recorded are cortical, rather than artifactual, in origin. Finally, the ERPs in response to forward and backward linear motions were recorded and characterised, showing a number of interesting properties such as variable timing of onset potentials, acceleration-following ERP time-course, and an out of phase EMG response. The data processing involved in these studies was supported by the development of a fully automated toolbox for processing EEG data and removing artifacts, which was made available to the scientific community. This method was also applied in a clinical study of EEG during syncope, which is another determining factor for falls (Kenny, 2003), and may be affected by vestibular decline.

## 8.2 Validity of Vestibular Electrophysiology using EEG

The use of EEG as opposed to fMRI or PET to record neural responses to vestibular stimulation provides a much greater flexibility for experimental design, along with a much higher temporal resolution and the capacity to analyse time-series data on the

millisecond scale, as compared to the second scale involved in e.g. fMRI. This comes with the trade-off of lower spatial resolution - as is seen in the sLORETA output in Chapters 6 and 7, the ability to localise the sources of EEG activity is limited to wide patches of cortex, with no deep-brain activity recording. Nonetheless, the application of EEG source localisation within the context of literature which used more spatially accurate measures provides a wealth of information. Throughout the thesis, it is seen that the use of EEG allows neuroimaging during true motion with comparable source activity to that seen in non-motion based vestibular stimulation, greatly extending the range of experimental designs possible in the future.

The validity of these results is a fundamental requirement for their use to investigate vestibular changes within ageing. The case for the validity of vestibular ERPs recorded on a Stewart platform is incrementally built throughout Chapters 5, 6 and 7. This issue is an important one, as there are many potential factors which could confound the interpretation of these ERPs. The first issue which was dealt with was the issue of platform interference - the possibility that the EEG amplifiers would record the large electromagnetic fields emitting from the platform motors as current was drawn during motion. As is seen in Chapter 5, this was not an issue - there was no interference detectable visually or by frequency analysis in either the raw recordings or the ERPs. This was remarkable, as it was assumed that there would be a need for correction for some amount of artifact, but there was no difference between the ERPs recorded at rest compared to those recorded during slow or fast movements. The differential amplification employed by the Biosemi system has a common-mode rejection ratio (CMRR) of >100dB, and as the channels are relatively close together with respect to their distance from the motors, it is likely that most motor noise was subtracted as common mode noise. The magnitude of the motor noise was evident when using an unshielded USB cable to transport trigger information - spurious triggers arose during platform movement until the cable, situated approximately eight meters from the motors, was replaced with a shielded cable. Thus the use of proper shielding and amplifier systems with a good CMRR is important in such a noise-prone environment. Alternatively, as seen in Chapter 5, a shielded amplifier also provides useable data, although since any EEG system must provide differential amplification, the CMRR may still play a part.

After it had been ascertained that the data was not impacted by the motor noise, the possibility of recording responses to motion itself became possible. This was performed in two stages, comprising two different experiments, as detailed in Chapters 6 and 7. The

vestibular P3 experiment was performed first, as it had a known outcome which could be compared to literature. With respect to validation of the EEG data forthcoming, the vestibular P3 provided a framework for the evaluation of the neural nature of responses recorded directly in response to motion. While the study in Chapter 5 validated the data with respect to non-biological noise, Chapter 6 investigated whether any recorded responses to motion come from the brain or are overpowered by any responses coming from ocular or myogenic vestibular responses which are also generated by motion.

The P3 waveform can be easily extracted by subtracting the standard waveform from the target waveform. While in the P3 paradigm, the standard and target had different heading angles, these were balanced across runs and subjects so that the averaged standard and target waveforms should sum to a heading angle of zero. Therefore, assuming linearly summed responses, any biological signals such as the vestibular reflexes which are proportional to the acceleration and not related to the oddball paradigm should be balanced and sum to zero. If it were the case that there was no signal coming from the cortex, the P3 waveform should therefore be zero, or only noise. However, as was seen in the results of Chapter 6, a parieto-central peak was seen to be highly significant in the difference waveform, and can be considered a P3 response to vestibular motion stimuli (Comerchero and Polich, 1999). This shows that cortical responses can be recorded from motion stimuli, in a differential manner, such that non-cortical biological responses related to the acceleration are cancelled.

Finally, the cortical response to acceleration is recorded in a non-differential manner in Chapter 7. This meant that any biological non-cortical signals were mixed with the true brain signals. The FASTER processing method uses ICA to attempt to separate these signals and classify those non-cortical signals. This is quite effective in the case of eye movement, and so it is useful for removing the VOR. However, as the separation is not perfect, any remaining signal is averaged and will affect the grand average ERP. This can be seen particularly in the sLORETA outputs in Figures 7.6, where a significant activation projecting from the eyes into the cortex is present. This is seen in the topographies in Figure 7.1 as the scalp topography extends to the frontal electrodes. However, as EOG topographies are unipolar with high amplitudes at the extreme frontal electrodes but a sharp gradient (Croft and Barry, 2000), the frontal scalp activation in the ERP extending past Fz towards Cz and inverting after is not likely to be driven by EOG. Further evidence of this comes from the peak correlation topography - at numerous electrodes near Cz, the ERP is significantly

leading the EOG average - therefore the ERP is portraying different information than EOG at least at these electrodes, and given that the correction for multiple comparisons was quite stringent, it is reasonable to deem only the frontal part of the ERP topography as representing EOG residue. This is also represented in source analysis as activity in the frontal extremity of the brain - this can be seen to be present, but stronger activity is seen elsewhere in areas related to vestibular and motion processing. Still further evidence comes when looking at the waveforms; there are similarities, but when viewing the cumulative sum in Figure 7.13 (approximating numeric integration) it can be seen that the EOG integral approaches a sinusoid, while the EEG integral has a different morphology, indicating at least that there is more recorded than EOG, and of comparable or higher amplitude.

Thus, FASTER was effective at reducing the amplitude of artifacts related to the VOR, but not perfect - Infomax ICA (Bell and Sejnowski, 1995) is very successful for removing artifacts if they are not stimulus-related, but artifact residues due to imperfect decompositions can add up if the artifacts are related to the stimulus. The use of other algorithms such as FastICA (Hyvarinen, 1999) or AMICA (Adaptive Mixture ICA) - a newly developed algorithm which is proposed to supersede Infomax - may prove better choices, but the quality and amount of input data will always determine the quality of the ICA, as well as computational power and time available.

Further to interference from EOG from the VOR, there is also the possibility of EMG interference caused by the VCR to counteract acceleration. The use of ICA to separate EMG artifacts is generally less successful in practise than for EOG - interfering EOG activity comes from the vertical and horizontal extraocular muscles (Croft and Barry, 2000), and comprises low-frequency activations due to blinking or saccades. More generally, EMG is a complex signal, being a mix of a greater number of muscle units with activation in a broad band of frequencies (Konrad, 2005), in EEG parlance sometimes ranging from delta up to high gamma or beyond. This is often seen to be difficult to remove from ICA; the EMG simulation tests performed in the FASTER methods section proved too simplistic to represent real-life situations. Therefore, even after FASTER correction, the possibility of contamination by EMG remained. Again the use of different ICA algorithms may be beneficial.

Using time-frequencies measures, the time periods of high EMG contribution were identified using the power increase in the gamma band (Goncharova et al., 2003).

Interestingly, these periods were not the same as the peaks of the acceleration profile - the EMG profile manifested as a tri-phasic profile, with peaks both leading and lagging the ERP peaks. As discussed, two possible reasons for this profile appearing are an onset burst followed by a lagging VCR (Keshner, 2003), or a tri-phasic VCR driven by expectation (Blouin et al., 2003; Cooke and Brown, 1990) and/or related to the jerk signal. Further investigation in this area would be necessary to definitively determine the cause of this unexpected effect. What can be seen is that the peaks of high-frequency EMG activity do not correspond to the main ERP peaks - this is fortuitous for the purposes of validation of the nature of the ERPs recorded, as the ERP peaks can then be considered to be mainly produced by neural sources. Source analyses were able to again back up this assertion, with sLORETA output from the broadband ERP showing some significant activation at the occipital extreme, but mainly activation in areas which have concordance with literature on their involvement in vestibular or motion processing. There remains a possibility that some low-frequency EMG activity overlapped with the ERPs, but the amplitude appeared to be small, and its shape different from that seen in the ERPs, thus any influence it has appears to be relatively small. Thus the argument for the validity of the ERPs as cortically based recordings was systematically constructed over the course of Chapters 4 - 7.

## 8.3 Vestibular Electrophysiology using EEG

There are various methods for dealing with EEG data - a number of the most common and informative are time-series analysis, time-frequency analysis, and source analysis. The application of these analyses to the EEG recordings made during vestibular true motion stimulation is discussed throughout Chapters 6 and 7. Vestibular processing of true motion stimuli was seen to elicit a P3 ERP component in Chapter 6, which is an ERP component studied in other stimulus modalities. In one respect, this result is unsurprising - the P3 is generally considered to be generated independent of modality, and has been elicited by stimuli ranging from visual, auditory, somatosensory, olfactory and even cross-modal stimulation. However, the use of vestibular stimulation to evoke cognitive responses such as the P3 has little precedence. Furthermore, the late response peak at 600ms with button responses around 875ms is unusual; this is interesting as it points to the slow cortical processing of vestibular stimuli, something which has been seen in behavioural studies (Barnett-Cowan and Harris, 2009; Baxter and Travis, 1938).

The processing of vestibular information in the cognitive representation of the experimental environment was investigated using the P3 ERP component in the study described in Chapter 6. The results from this study show that the P3 is easily identifiable, and is statistically detectable in >90% of individual cases. The number of epochs necessary for single-subject significance was determined. The P3 waveform also appears to coincide with a decrease in power the alpha band. Response times and latencies appear to be linked, and have a higher intra-subject variability than inter-subject variability, indicating differences in detection threshold between people.

The neural responses to forwards and backwards linear acceleration stimuli were investigated and classified in Chapter 7. A wide range of results, hypotheses and conclusions can be made, based upon classification of the ERP components. An initial onset peak shows a wide spread in the grand average, but is smaller in individuals; this implies that the grand average is comprised of temporally distinct peaks. This peak may therefore represent an objective method of indexing the individual's vestibular detection threshold. This is a weakness of the grand averaging method. There is a cortical representation of the acceleration stimulus. This representation is modulated across time, and leads the EOG waveform while sharing a similar, but not identical, temporal profile. Thus, the neural response recorded may be partially representative of the maintenance of fixation and suppression of the VOR. Integrating the horizontal EOG channels yields very close approximations to the input acceleration profile; this would imply that the linear VOR in the horizontal plane is dependent on jerk, the derivative of acceleration. This has been proposed before (Angelaki, 1992; Angelaki et al., 1993; Angelaki and Hess, 1996), although (Raphan et al., 1996) disagrees in the discussion that jerk coding is necessary. Vertical EOG channels display this property, but with more mixed results, indicating they are also driven by other motion properties. This response is more evident in the backward waveform than the forward; a number of observations hint that the neural response to forward motion recruits more visual areas than backward, and that backward motion by contrast recruits more somatosensory areas – as people cannot see behind them, this may be a direction-based sensory reweighting related to e.g. collision detection (Regan and Vincent, 1995). Activity at peaks localises ERP sources to a number of areas which have been identified in fMRI and PET literature as vestibular processing areas. This includes the temporo-parietal insular junction, identified by two recent meta-analyses as the convergent area common to all methods of vestibular stimulation seen in literature (Lopez et al., 2012; zu Eulenburg et al.,

2012), and can thus be reasonably confidently considered the human analogue of the macaque parieto-insular vestibular cortex. A decrease in power in the alpha frequency band is seen to coincide with the first main peak of both backward and forward ERPs; this decrease follows approximately the same time-course as the modulation of the acceleration response amplitude, and may therefore be related to areas involved in VOR suppression. The EMG profile displays a tri-phasic profile which exhibits peaks that are out of phase with the main ERP's peak; this could be due to stimulus expectation - there is a possible CNV in the summed waveform, or it may indicate that the VCR is related to the jerk signal. The possibility of expectation is interesting in the context of ageing - as discussed above, in elderly adults the low-frequency VOR exhibits an increase in phase lead in a number of different experimental studies. This increase may be related to a higher reliance on cortical internal representation or interpolation of the signal due to decreased reliability of the vestibular input. The reliability-based reweighting principle is reviewed in (Fetsch et al., 2010), but its application to internal signals has yet to be investigated.

Some comparable results can be seen in both Chapter 6 and Chapter 7. One interesting phenomenon which is seen in both chapters is the inter-subject temporal variation in the initial peak and the P3 peak; this would seem to be related to a variation among subjects in the detection threshold of vestibular stimuli. This threshold seems quite wide among an otherwise unremarkable set of subjects; if this is representative of the general population, then this may be a predictive factor in phenomena such as motion-sickness which is known to affect a large percentage of people (Oman, 1990); if a person has a low vestibular threshold, they may be more likely to experience spurious motion cues from e.g. a bumpy car ride, which is at odds with their visual/proprioceptive input. This may also thus be a factor in vasovagal syncope, as discussed above. The decrease in alpha band power during the ERP is also seen in both the vestibular evoked potential and the vestibular P3. The P3 is known to be associated with an alpha power decrease (Yordanova et al., 2001), which would appear to be an attentional effect, as there is no difference in stimuli that would induce exogenous excitation, due to left-right balancing. The alpha power decrease in the motion-response ERP cannot be specifically pinned down as exogenous or endogenous; however the high magnitude of the alpha changes points to a side-effect of vestibular stimulation over a long period in a dark environment, which is tiredness. Most subjects reported the sensation as that of being rocked to sleep, and two fully fell asleep for a few moments (although none missed any responses). Regular breaks, light and water were given

to reduce this effect, but this may nonetheless have resulted in a high baseline level of alpha power which could increase the magnitude of these alpha effects.

Both studies also point to a methodological difference when comparing these results to those of other sensory modalities - the stimulus length and profile. Here, a 1.25s sinusoidal stimulus was used. This is quite disparate from the type of stimuli frequently used in visual, auditory or somatosensory studies. These are step profiles with high amplitudes and short lengths of approximately 10-50ms, used to approximate a discrete delta function so that the recorded ERP is near to an impulse response (Comerchero and Polich, 1999). For safety reasons, a high-amplitude step function or approximation thereof should not be performed with human subjects. Furthermore, these types of profiles are less usual in everyday motion than continuous stimuli. There is little information available on the effect of stimulus length on the common sensory evoked potentials; if further visual-vestibular experiments are performed, this will need to be considered. As is discussed above, they may also be useful for determining perception thresholds.

That such a range of information can be exploited from a single set of experiments is a promising indication for future research into vestibular processing. Note, however, that a few of these observations were not statistically significant, but were approaching a traditional significance level using the stringent conditions; furthermore, some proposed explanations for results were only hypothetical. These results therefore present opportunities for future research and investigation.

## 8.4 Vestibular Function and Ageing

As discussed in Chapter 2, vestibular information is a key factor in maintaining balance, posture and gait. Disorders of the vestibular system are often investigated using nystagmus and eye movement during head movements to target different VOR components (Baloh and Honrubia, 1979; Dix and Hallpike, 1952). This is useful for conditions such as BPPV (Hughes and Proctor, 1997) or damage to the vestibular organs, which are peripheral problems. Vestibular decline with aging is also a peripheral problem, as the number of cilia reduces with age; however this is gradual and compensation occurs over time (Matheson et al., 1999). The link between aging, falls and vestibular decline thus involves both central and peripheral components, and so neuroimaging methods could be beneficial for further investigation. The paradigms and methods developed in this thesis allow for neuroimaging

during true motion, which provides more ecologically valid responses than other stimuli. The onset responses in the ERPs discussed above may be useful for detecting vestibular thresholds, and ERP components such as P3 amplitude and latency are known to be affected by processing difficulty (Kiiski et al., 2011b).

Sensory processing is known to change during aging (Stevens et al., 1998). Multisensory integration is seen to be enhanced, perhaps as a consequence of decreased reliability of unisensory input (Laurienti et al., 2006; Diederich et al., 2008). The benefit of multisensory integration increases with age, enhancing response-times more than in younger groups, and a temporal window of integration (TWI) model analysis indicates that the temporal window for multisensory integration is wider for older adults. The TWI is the period of time in which two discrete events are perceptually fused together and experienced as a single event. As discussed in Mozolic et al., (2012), this may be due to increased variability and slowing in unisensory processing requiring a longer time for multisensory integration, rather than a top-down change. In a recent audio-visual multisensory integration study, older adults prone to falls were seen to have an extended window of multisensory integration for an audio-visual illusion which was nearly four times as long as non-fallers (Setti et al., 2011). Interestingly, it was seen that the unisensory variability of the elderly fallers and non-fallers was not significantly different. This does not fit the explanation of increased variability of unisensory processing as an explanation of the discrepancy, and so may be a top-down change. This could provide new insight into falling – if this finding is generalizable beyond audio-visual to visual-vestibular integration, it could be that quick vestibular changes are not processed properly within an appropriate timeframe to adjust or correct for falling. The experiments described in this thesis provide a good basis for the investigation of multisensory integration using ERP methods – time-domain analyses of EEG data are common in making observations about multisensory processing, e.g. (Busse et al., 2005; Giard and Peronnet, 1999; Molholm et al., 2002; Santangelo et al., 2008; Stanford and Stein, 2007). Such analyses were not possible using previous methods of vestibular imaging such as fMRI or PET due to their low temporal resolution.

The decline of the vestibular system over age happens due to changes and loss which occur within the cilia and neurons (Anniko, 1983; Bergstrom, 1973; Park et al., 2001; Rauch et al., 2001; Rosenhall and Rubin, 1975) making vestibular inputs less sensitive and reliable. In studies of traumatic vestibular loss, vestibular compensation has been studied and described in animals and humans (Curthoys and Halmagyi, 1995; Pfaltz, 1983; Sadeghi et

al., 2011; Zennou-Azogui et al., 1996). The prevailing opinion is that compensation for the loss of vestibular input comes from multisensory substitution, predominantly based on visual and proprioceptive input. While it may not be necessarily valid to assume that this model can be extended from traumatic vestibular loss to slow age-related vestibular loss, the majority of evidence available comes from such studies. Literature review revealed only a small number study of compensation during ageing, the most relevant of which shows that proprioception compensates sufficiently for vestibular loss in a dark room (Schweigart et al., 2002). This may implicate proprioception plays a larger role for compensation during the ageing process, or may be driven by reweighting due to the lack of visual input. Other studies investigate compensation during ageing at the level of neurotransmitters and brainstem structures (Alvarez et al., 2000; Drago et al., 1996; Giardino et al., 2002); these are not informative at the appropriate level for this discussion.

The implications of an elongated multisensory TWI on a system using multisensory compensation could be viewed as a reduction of the sampling rate of the system, which leads to a reduced bandwidth, reducing the ability to respond appropriately to high-frequency stimuli. A sudden shift in vestibular information could occur due to a change in incline or discontinuity of the floor, or muscular instability, both of which could lead to falls unless quickly compensated. The possibility of loss of high-frequency response has some behavioural correspondence in literature - Hirvonen et al., (1997) showed an increase in gain at high frequencies (>2 Hz), with associated poor tracking, which could be a compensatory increase. The test required high-frequency neck movements, however, which may be a confounding factor in an ageing population due to muscle stiffness. Conversely, a longitudinal study (Baloh et al., 2003) reported that low frequency (0.2Hz) VOR responses have lower gain in older adults, while faster responses (0.8Hz) do not. Interestingly, a phase lead is also noted at low frequencies, which may indicate prediction and thus a higher reliance on internal representation to enact compensation. A further comprehensive study (Paige, 1994) investigates the VOR from 0.025Hz - 4Hz, showing an increase in phase lead and a decrease in gain at low frequencies in elderly people compared to younger. No changes in VOR at high frequencies were observed; however in smooth pursuit tasks and VOR suppression, elderly and middle aged subjects displayed significantly slower pursuit (increased lag) and decreased gain in higher frequencies. Furthermore, while unisensory VOR and pursuit responses showed considerable differences between age groups, use of visual enhancement in the VOR task reduced the differences between old and young groups

considerably. The causes for increased multisensory integration may have a peripheral basis if also seen in unisensory modalities, but are likely to reside in the domain of higher cognitive functions if they are confined to multisensory integration. A study on the auditory TWI in elderly and young subjects indicates that the TWI itself is unchanged with age, but that frequency discrimination is impaired (Horváth et al., 2007). One study of visual integration also showed that temporal integration is not affected with age (Andersen and Ni, 2008). Thus this finding may be generalizable to other senses. The vestibular evoked potentials detailed in Chapter 7 provide an interesting method for investigation, as the acceleration-following component of the ERPs could determine whether the stimulus is being processed, and where in the brain this is happening. Frequency analysis of ERPs could be informative of changes or breakdown of processing. The mismatch negativity protocol, as employed in the Horváth study, could also be adapted to vestibular and multimodal stimuli.

Certainly, further investigation into these mechanisms is necessary, and in particular to understand why the integration window in people who fall is longer than in those who do not fall. Moreover, it first needs to be investigated whether this enhanced integration window is seen in the vestibular system, or whether it is specific to audio-visual integration, which is the most prevalent multisensory combination examined in literature. The vestibular P3 methodology described in Chapter 6 could potentially be adapted to investigate this by using progressively shorter time-courses of small motions to determine the threshold at which a P3 response is not elicited by an oddball stimulus. This may however necessitate high-amplitude stimuli to reach the detection threshold at very short time intervals, which could present the danger of whiplash. Other tasks may therefore be more applicable - determining the window of perception of simultaneity for e.g. visual-vestibular or audio-vestibular stimuli may be useful. The unisensory ERP described in Chapter 7 could be compared to the multisensory ERP evoked using such a paradigm, and the integration time-course could be investigated.

The time difference necessary between the onsets of such stimuli for the perception of simultaneity has been investigated previously (Barnett-Cowan and Harris, 2009), and it is seen that the onset of the vestibular stimulus needs to be considerably earlier than either visual, auditory or somatosensory stimuli to be perceived as simultaneous. This may be due to the Gaussian time-course of the vestibular stimuli used in this experiment - detection threshold may not have been reached instantly. These thresholds are seen in Chapters 6 and 7 of this thesis to vary significantly between individuals. However, response-times were also compared to a square-wave signal, and were not seen to vary significantly, so this is less likely

to be a simple factor – it appears that cognitive responses to vestibular stimulation are slow in comparison to other stimuli. In Chapter 7, the lag at the maximum cross-correlation value of the EEG and EOG time-courses was used to infer that the EEG responses preceded the EOG. This approach can also be used to determine the lag between the acceleration time-course and the EEG response, which is a measure of processing time and thus could be useful to explore this response disparity. On computing the lag between the difference ERP and the acceleration time-course, the maximum cross-correlation value appears at a time-lag of 147ms (average across all electrodes). This is a prediction of cortical processing time of vestibular stimuli based on the assumption of a linear response to acceleration, which is discussed and justified in Chapter 7. This time value is less than that shown in the response-time study; however, the time taken to react is also a factor. This is seen in Chapter 6 – the average peak latency for the P3 is 600ms, while the average response time is 875ms. Thus the average time to respond after processing is approximately 275ms – adding this to the 147ms of cortical processing, the result is 422ms, which is very close to the mean, and well within the confidence interval of the mean response time for vestibular stimuli recorded in the response-time study. This shows that using the neuroimaging methods described in the thesis, both time for processing and time for reaction can be separated using neuroimaging methods and related to behavioural measures. Applying this to the questions of sensory processing changes with ageing could be informative of whether it is sensory processing, executive function or both that contributes to multisensory enhancement. However, it remains to be determined whether these are relevant on an individual level, and the application to clinical and ageing populations may not be straightforward – for example, clinical conditions or age-related peripheral deterioration of the motor can delay response times.

The TWI model discussed before is a two-stage model: the first stage is a "race" stage, where the first sensory stimulus to be received determines the outcome of the percept. With this view, the long stimulus asynchrony which appears necessary for perception of vestibular stimuli as simultaneous may be relevant. The onset potentials evoked and detailed in Chapter 7 may provide a manner in which to study the neural substrates of such perceptions. As it must be true that in everyday life, vestibular sensation and visual flow present concurrent sensory inputs with no stimulus asynchrony, the use of galvanic stimulation or high-intensity visual stimuli in the Barnett-Cowan study may highlight cognitive

aspects of vestibular perception which require further investigation, or it may highlight the need for more appropriate comparisons between stimuli of a similar nature and saliency.

The methods developed to ensure the quality of the EEG data were also applied to clinical EEG data for investigation of syncope, a cause of falling in the elderly which often overlaps with orthostatic hypotension (Atkins et al., 1991; Sarasin et al., 2002). Results showed that the use of such measures was informative, but the limited spatial resolution of the system along with other technical issues leaves room for improvement in the results. Syncope would initially seem disparate from vestibular function; however there is a growing body of knowledge on the vestibulosympathetic reflex (Holstein et al., 2011; Ray, 2000; Ray and Monahan, 2002b), which is a vestibular reflex that affects the sympathetic nervous system. This normally modifies blood pressure in different head positions and during motion in response to otolith stimulation. However, as with vestibular functional changes during aging, this reflex may not maintain sufficient blood pressure, and contribute to hypotensive episodes and phenomena such as syncope (Monahan and Ray, 2002; Ray and Monahan, 2002a). Furthermore, the vestibular system is also seen to have interaction with the vagus nerve, the abnormal function of which is the cause of vasovagal syncope as investigated in Chapter 8 (Akert and Gernandt, 1962; Molinari, 1975; Ruggiero et al., 1996). A recent retrospective study and follow-up experimental study also determined a relationship between motion sickness susceptibility and vasovagal syncope (Bosser et al., 2006; Bosser et al., 2007); as motion sickness is strongly affected by sensory conflict between visual and vestibular systems (Bles et al., 1998), this would imply a sensory sensitivity to vestibular or vestibular-visual stimuli could be implicated in vasovagal syncope. Indeed, a recent study showed that the use of galvanic vestibular stimulation was successful in eliciting vasovagal syncope in a rat (Cohen et al., 2011), showing proof of this concept. As discussed above, the enhanced multisensory facilitation experienced during ageing could therefore be a factor in syncope when elderly people are presented with vestibular stimulation. This underscores the importance of further investigation into vestibular function in ageing, as it points to a convergent aspect in the understanding of falls which underlies two seemingly separate areas of research. It was unfortunate that recording of vestibular responses was impossible during this study, as they may have provided further results to inform this issue.

## 8.5 Future Work inspired by the Thesis

The experiments described in this thesis demonstrate that the use of EEG enables insight into vestibular function. The experiments performed in this thesis both bring new knowledge and add evidence to issues at the forefront of the field of research, over which there is discussion and controversy. A number of specific questions of basic research arise from the results, particularly those of Chapter 7, which opens a wide avenue of investigation:

- **What are the characteristics of ERPs elicited by left/right stimuli?** The results found for backward and forward motion could be complemented by comparing leftward vs. rightward translations, as there is no confound of visual expectation as is seen in forward vs. backward translations. There is some potential to use the left and right standard ERPs from the P3 experiment for this task, but the context of the cognitive P3 task makes comparison with the forward/backward ERPs less straightforward. Furthermore the angular difference is 90° for the standards, as compared to 180° for the forward/backward paradigm. Pilot analyses of the left vs. right standards alone did not reveal as much as the motion-response ERPs, and so a full analysis was not pursued.
- **What produces the attenuation evident in the vestibular evoked potential?** A number of possible explanations for this attenuation were discussed in Chapter 7. Further insight could be gained by examining continuous translation, rather than single sinusoids, to investigate whether the attenuation of ERP responses is due to habituation / adaptation, or if it is seen to happen on a similar timescale to rotational motion as reported in (St George and Fitzpatrick, 2011). Furthermore, the inter-stimulus interval could be varied more to reduce effects of habituation.
- **Do ERP responses recorded during true motion relate to fixation suppression?** Changing fixation requirements, to investigate the hypothesis that the ERP is representative of VOR modulation, could provide answers to the questions about fixation arising from Chapter 7. The use of a set fixation point (i.e. variable distance from the subject), rather than set fixation distance, would enable more comparison with literature as this is a more common setup (Angelaki, 2004; Barnes and Paige, 2004; Paige and Seidman, 1999). Removing the requirement for fixation entirely may also show interesting ERP results.
- **Are there differences in relative contribution of visual and somatosensory information in forward and backward motion?** A potentially interesting avenue of

research would be investigating whether any changes in visual or somatosensory tests are evident comparing backward to forward motion. This could be performed using perhaps evoked potential or P3 tasks, to determine whether either sensory modality is affected by spatial attention and the available sensory information during motion as is hinted in Figure 7.8; this may also have implications for locomotion (Zelenin et al., 2011).

- **How do these results relate to visual motion cues?** Vestibular information is integrated with other sensory information at a very early stage of processing (Angelaki and Cullen, 2008). In particular, the integration of visual and vestibular sensory information is involved in motion perception, (e.g. Butler et al., 2010; Cardin and Smith, 2009; Fetsch et al., 2010; Fetsch et al., 2009; MacNeilage et al., 2010; Smith et al., 2011). In Chapter 7, this relationship is seen tangentially in the analysis of VOR and the hypothesis of fixation suppression. However, a more appropriate type of investigation would involve the use of visual motion stimuli in conjunction with true motion stimuli, with perhaps manipulations of congruence. Investigating this relationship using ERP analysis could reveal the cortical regions involved in this process, and timescales or temporal features heretofore unknown. A pilot study recording with a vection stimulus with a similar motion profile as that used in the thesis experiments was begun; however, due to time constraints, the data has not been fully analysed yet.
- **How can the P3 paradigm be extended?** The P3 paradigm provides a number of manipulable parameters. Manipulating the heading angle, for example, it would be possible to find the point at which change can no longer be detected. This could be beneficial for people with communication difficulties or young children. This paradigm could also be used for investigating differences in directional sensitivities to motion, to investigate conditions such as unilateral vestibular dysfunction. The P3 has been seen to have use in numerous clinical contexts (Ito et al., 1995; Juckel et al., 2008; Kiiski et al., 2011a; Polich, 1998).
- **How are discrete and continuous ERP responses related?** Performing a set of experiments to compare discrete and continuous stimulus ERPs for well-known ERPs would be informative and may lead to inferential models such that the discrete vestibular ERP could be estimated. A deconvolution-based method has been developed for continuous auditory and visual stimuli (visual/auditory evoked spread spectrum potential, VESPA and AESPA) (Lalor et al., 2006;

Lalor et al., 2009) but while these methods provide estimates of steady-state activity, they are somewhat different, as they effectively estimate the instantaneous discrete ERP at each point of a continuous stimulus. As potentials such as the visual and auditory evoked potentials have been well-studied over many years, it would be informative to vary stimulus lengths and compare their morphology. Finding a relationship may give insight into approximating a discrete linear motion ERP without performing dangerous high-acceleration experiments.

Some technical questions are also posed based on the methods developed and described in Chapter 4:

- **Could AMICA or other ICA methods be used to improve FASTER?** The FASTER algorithm may benefit from adaptation to include the newly developed AMICA method of ICA decomposition. Once this has been published and made available within the EEGLAB framework, FASTER can be tested to determine whether it provides a more accurate decomposition. This would be beneficial for further experiments, and for the EEG community in general – as the software is available freely, it is already being used in a number of studies. Since its release in late 2010, it has been downloaded over 2000 times, and has thus far gathered 34 citations.
- **How does the time-domain ICA rescaling method perform in quantitative tests?** Full development and testing of the work-in-progress method described in Appendix 4C would determine its suitability for application to general EEG datasets; initial tests appear visually promising, and its use in EEG-fMRI data seems successful, but objective testing is necessary.
- **How can these measures be deployed more practically?** Any practical use of these measures in a clinical or larger-scale study would greatly benefit from the derivation of a simpler, cheaper and more user-friendly method of producing linear motion stimuli. The Stewart platform has very good controllability, but requires a considerable investment, and a dedicated support team. Solutions such as motorised chairs on a linear track could be explored, or even motorised wheelchairs may be useable with some modification. More traditional methods such as sleds (Baloh et al., 1988; Seidman, 2008; Walsh, 1961) may also be

useful if a sufficient amount of controllability and repeatability was maintained. Furthermore, the number of trials used here required subjects to be in the platform for a long time - each experiment took approximately one hour in the platform, plus 20 - 30 minutes setup time for the EEG cap. As discussed above, this may have affected the results obtained by decreasing alertness and hence increasing alpha power. Reducing the number of trials necessary would make this a more viable option.

- **Is the grand averaging method appropriate?** A recent report by (Matysiak et al., 2013) suggests that rescaling of grand-average ERPs by subject before combining them increases uniformity and reliability of the estimate. This could be easily implemented as an option into FASTER, and could then be evaluated over a larger set of real-life data to evaluate the claim.

The protocols of the experiments describe a flexible method of investigation of the vestibular system under real motion conditions, which poses a number of questions for further research and application in the field of age-related vestibular decline:

- **Can changes in vestibular function as measured by EEG investigation be used to measure age-related vestibular compensation and identify elderly adults at risk of falls?** The results presented in the thesis present a strong case for using EEG to examine vestibular function. This is particularly appealing for use in ageing to examine how processing changes in the cortex affect the tendency to fall. A quite simple study would be to use one of the experiments described in Chapters 6 or 7 to compare cohorts of younger subjects, older subjects with history of falls and older subjects without history of falls. This would allow detection of any change associated with age, and any change associated with falls. If such changes are evident, testing may show their presence or early development, enabling early warning signs of instability. Further investigation into the comparability of individual responses to group average would also be very useful here.
- **What is the effect of ageing and fall-risk on the vestibular TWI?** As discussed above, the temporal window of integration may be wider in older adults. Moreover, it may be different in adults at risk of falls. A very important question is whether this result can be seen in visual-vestibular or proprioceptive-vestibular

multisensory integration along with audio-visual integration where it was already demonstrated. The temporal window lengths for these sensory interactions would have to be determined first, and then the test for an extended window in fallers could be performed. An analogue of the Shams illusion could be developed, or a simple temporal order judgement task may suffice. The addition of neuroimaging may be helpful in detecting cortical areas involved in the fusion task and thus those whose function is compromised in fallers. Furthermore, the effect of temporal window changes on frequency discrimination and high-frequency perception could be determined by modulating the stimulus frequency.

- **Can the disparity between vestibular decline and balance performance be clarified?** It is well-established that decline in the vestibular organs is associated with age; yet a number of studies have found that the relationship between caloric test changes and performance in gait and balance tests is not straight-forward. Thus it would be useful to investigate compensation strategies to determine why some people are affected more than others by peripheral decline.
- **Can a link between vestibular decline and orthostatic or vasovagal syncope be found?** The links between vestibular processing, cardiac function and vasovagal syncope are discussed above, and a possible relationship is hypothesised. Vestibular testing using standard or neuroimaging tests, or tests of multisensory integration as discussed above, would give further insight into this matter.

These questions and experiments pave the way for future advancements in the area of ageing and falls, vestibular electrophysiology and EEG data processing.

## 8.6 Conclusion

The research questions posed have been answered during the course of four experiments and one methodological development. Recording the neural correlates of vestibular processing of true linear motion using EEG on a Stewart platform produces viable results from the brain with interesting temporal features and comparable spatial localisation to literature. This enables further investigation of vestibular function, in particular the assessment of neuro-plastic changes of cortical vestibular processing and compensation associated with ageing and cognitive function. Using automated EEG processing makes the

process more objective and efficient. The conclusions drawn from the experiments are informative with regard to topics of recent debate in the scientific community, concur with recent analyses of human cortical vestibular function, and have potential clinical relevance in the area of age-related sensory decline, and suggest potential links between these areas which may be investigated. Further research is proposed on extending the framework developed for vestibular neuroimaging during true motion, and in applications to the field of vestibular deline.

# Bibliography


Agrawal, Y., Carey, J.P., Della Santina, C.C., Schubert, M.C., Minor, L.B., 2010. Diabetes, Vestibular Dysfunction, and Falls: Analyses From the National Health and Nutrition Examination Survey. Otology & Neurotology 31, 1445-1450 1410.1097/MAO.1440b1013e3181f1442f1035.

Akbarian, S., Grüsser, O.J., Guldin, W.O., 1992. Thalamic connections of the vestibular cortical fields in the squirrel monkey (Saimiri sciureus). The Journal of Comparative Neurology 326, 423-441.

Akert, K., Gernandt, B.E., 1962. Neurophysiological study of vestibular and limbic influences upon vagal outflow. Electroencephalography and Clinical Neurophysiology 14, 904-914.

Allen, P.J., Josephs, O., Turner, R., 2000. A Method for Removing Imaging Artifact from Continuous EEG Recorded during Functional MRI. Neuroimage 12, 230-239.

Alvarez, J.C., Dí az, C., Suárez, C., Fernández, J.A., González del Rey, C., Navarro, A., Tolivia, J., 2000. Aging and the human vestibular nuclei: morphometric analysis. Mechanisms of Ageing and Development 114, 149-172.

Amat, J., 1982. Input to the vestibulo cerebellum and triceps brachii motoneurons during natural vestibular stimulation in frog. Neuroscience 7, 1665-1671.

Aminoff, M.J., Goodin, D.S., 1994. Visual Evoked Potentials. Journal of Clinical Neurophysiology 11, 493-499.

Anastasio, T.J., 2001. A pattern correlation model of vestibulo-ocular reflex habituation. Neural Networks 14, 1-22.

Andersen, G.J., Ni, R., 2008. Aging and visual processing: Declines in spatial not temporal integration. Vision Research 48, 109-118.

Angelaki, D., 1992. Two-dimensional coding of linear acceleration and the angular velocity sensitivity of the otolith system. Biological Cybernetics 67, 511-521.

Angelaki, D., Bush, G., Perachio, A., 1993. Two-dimensional spatiotemporal coding of linear acceleration in vestibular nuclei neurons. The Journal of Neuroscience 13, 1403-1417.

Angelaki, D.E., 2004. Eyes on Target: What Neurons Must do for the Vestibuloocular Reflex During Linear Motion. J Neurophysiol 92, 20-35.

Angelaki, D.E., Cullen, K.E., 2008. Vestibular System: The Many Facets of a Multimodal Sense. Annual Review of Neuroscience 31, 125-150.

Angelaki, D.E., Hess, B.J.M., 1996. Organizational Principles of Otolith- and Semicircular Canal-Ocular Reflexes in Rhesus Monkeysa. Annals of the New York Academy of Sciences 781, 332-347.

Angelaki, D.E., Klier, E.M., Snyder, L.H., 2009. A Vestibular Sensation: Probabilistic Approaches to Spatial Perception. Neuron 64, 448-461.

Anniko, M., 1983. The aging vestibular hair cell. American Journal of Otolaryngology 4, 151-160.

Atkins, D., Hanusa, B., Sefcik, T., Kapoor, W., 1991. Syncope and orthostatic hypotension. The American Journal of Medicine 91, 179-185.

Baker, R., Highstein, S.M., 1978. Vestibular projections to medial rectus subdivision of oculomotor nucleus. Journal of Neurophysiology 41, 1629-1646.

Baloh, R.W., Beykirch, K., Honrubia, V., Yee, R.D., 1988. Eye movements induced by linear acceleration on a parallel swing. Journal of Neurophysiology 60, 2000-2013.

Baloh, R.W., Enrietto, J., Jacobson, K.M., Lin, A., 2001. Age-Related Changes in Vestibular Function. Annals of the New York Academy of Sciences 942, 210-219.

Baloh, R.W., Honrubia, V., 1979. Clinical Evaluation of the Vestibular System. Clinical Neurophysiology of the Vestibular System. FA Davis Company, Philadelphia, pp. 112-113.

Baloh, R.W., Ying, S.H., Jacobson, K.M., 2003. A Longitudinal Study of Gait and Balance Dysfunction in Normal Older People. Archives of Neurology 60, 835-839.

Bardet, J.-M., Lang, G., Oppenheim, G., Philippe, A., Stoev, S., Taqqu, M.S., 2003. Semi-parametric estimation of the long-range dependence parameter: a survey. In: Birkhäuser (Ed.), Theory and applications of long-range dependence, pp. 557-577.

Barnes, G.R., Paige, G.D., 2004. Anticipatory VOR Suppression Induced by Visual and Nonvisual Stimuli in Humans. Journal of Neurophysiology 92, 1501-1511.

Barnett-Cowan, M., Harris, L., 2009. Perceived timing of vestibular stimulation relative to touch, light and sound. Experimental Brain Research 198, 221-231.

Barnett-Cowan, M., Nolan, H., Butler, J.S., Foxe, J.J., Reilly, R.B., Bülthoff, H.H., 2010. Reaction time and event-related potentials to visual, auditory and vestibular stimuli. Journal of Vision 10, 1400.

Baxter, B., Travis, R.C., 1938. The reaction time to vestibular stimuli. Journal of Experimental Psychology 22, 277-282.

Beauchamp, M.S., Cox, R.W., Deyoe, E.A., 1997. Graded Effects of Spatial and Featural Attention on Human Area MT and Associated Motion Processing Areas. Journal of Neurophysiology 78, 516-520.

Bell, A.J., Sejnowski, T.J., 1995. An Information-Maximization Approach to Blind Separation and Blind Deconvolution. Neural Computation 7, 1129-1159.

Belouchrani, A., Abed-Meraim, K., Cardoso, J.F., Moulines, E., 1997. A blind source separation technique using second-order statistics. Signal Processing, IEEE Transactions on 45, 434-444.

Bénar, C.-G., Aghakhani, Y., Wang, Y., Izenberg, A., Al-Asmi, A., Dubeau, F., Gotman, J., 2003. Quality of EEG in simultaneous EEG-fMRI for epilepsy. Clinical Neurophysiology 114, 569-580.

Benjamini, Y., Hochberg, Y., 1995. Controlling the False Discovery Rate: A Practical and Powerful Approach to Multiple Testing. Journal of the Royal Statistical Society. Series B (Methodological), 289-300.

Bense, S., Stephan, T., Yousry, T.A., Brandt, T., Dieterich, M., 2001. Multisensory Cortical Signal Increases and Decreases During Vestibular Galvanic Stimulation (fMRI). Journal of Neurophysiology 85, 886-899.

Berard, J.R., Fung, J., McFadyen, B.J., Lamontagne, A., 2009. Aging affects the ability to use optic flow in the control of heading during locomotion. Exp Brain Res 194, 183-190.

Berger, D.R., Bülthoff, H.H., 2009. The role of attention on the integration of visual and inertial cues. Exp Brain Res 198, 287-300.

Bergstrom, B., 1973. Morphology of the vestibular nerve. II. The number of myelinated vestibular nerve fibers in man at various ages. Acta Oto-laryngologica 76, 173-179.

Bertolini, G., Ramat, S., 2011. Velocity storage in the human vertical rotational vestibulo-ocular reflex. Experimental Brain Research 209, 51-63.

Bian, N.-Y., Wang, B., Cao, Y., Zhang, L., 2006. Automatic Removal of Artifacts from EEG Data Using ICA and Exponential Analysis. Advances in Neural Networks - ISNN 2006, pp. 719-726.

Blanke, O., Perrig, S., Thut, G., Landis, T., Seeck, M., 2000. Simple and complex vestibular responses induced by electrical cortical stimulation of the parietal cortex in humans. Journal of Neurology, Neurosurgery & Psychiatry 69, 553-556.

Bles, W., Bos, J.E., de Graaf, B., Groen, E., Wertheim, A.H., 1998. Motion sickness: Only one provocative conflict? Brain Research Bulletin 47, 481-487.

Blouin, J.-S., Descarreaux, M., Bélanger-Gravel, A., Simoneau, M., Teasdale, N., 2003. Attenuation of human neck muscle activity following repeated imposed trunk-forward linear acceleration. Experimental Brain Research 150, 458-464.

Blum, P.S., Abraham, L.D., Gilman, S., 1979. Vestibular, auditory, and somatic input to the posterior thalamus of the cat. Experimental Brain Research 34, 1-9.

Bonmassar, G., Purdon, P.L., Jääskeläinen, I.P., Chiappa, K., Solo, V., Brown, E.N., Belliveau, J.W., 2002. Motion and Ballistocardiogram Artifact Removal for Interleaved Recording of EEG and EPs during MRI. Neuroimage 16, 1127-1141.

Bosser, G., Caillet, G., Gauchard, G., Marçon, F., Perrin, P., 2006. Relation between motion sickness susceptibility and vasovagal syncope susceptibility. Brain Research Bulletin 68, 217-226.

Bosser, G., Gauchard, G.C., Brembilla-Perrot, B., Marçon, F., Perrin, P.P., 2007. Experimental evaluation of a common susceptibility to motion sickness and vasovagal syncope in children. Brain Research Bulletin 71, 485-492.

Bottini, G., Sterzi, R., Paulesu, E., Vallar, G., Cappa, S.F., Erminio, F., Passingham, R.E., Frith, C.D., Frackowiak, R.S.J., 1994. Identification of the central vestibular projections in man: a positron emission tomography activation study. Experimental Brain Research 99, 164-169.

Brandt, T., Bartenstein, P., Janek, A., Dieterich, M., 1998. Reciprocal inhibitory visual-vestibular interaction. Visual motion stimulation deactivates the parieto-insular vestibular cortex. Brain 121, 1749-1758.

Brandt, T., Botzel, K., Yousry, T., Dieterich, M., Schulze, S., 1995. Rotational vertigo in embolic stroke of the vestibular and auditory cortices. Neurology 45, 42-44.

Brandt, T., Dieterich, M., 1999. The Vestibular Cortex: Its Locations, Functions, and Disorders. Annals of the New York Academy of Sciences 871, 293-312.

Brandt, T., Schautzer, F., Hamilton, D.A., Brüning, R., Markowitsch, H.J., Kalla, R., Darlington, C., Smith, P., Strupp, M., 2005. Vestibular loss causes hippocampal atrophy and impaired spatial memory in humans. Brain 128, 2732-2741.

Brázdil, M., Dobsík, M., Mikl, M., Hlustík, P., Daniel, P., Pazourková, M., Krupa, P., Rektor, I., 2005. Combined event-related fMRI and intracerebral ERP study of an auditory oddball task. Neuroimage 26, 285-293.

Bremmer, F., Duhamel, J.R., Ben Hamed, S., Graf, W., 2002a. Heading encoding in the macaque ventral intraparietal area (VIP). Eur J Neurosci 16, 1554-1568.

Bremmer, F., Klam, F., Duhamel, J.R., Ben Hamed, S., Graf, W., 2002b. Visual-vestibular interactive responses in the macaque ventral intraparietal area (VIP). Eur J Neurosci 16, 1569-1586.

Bremmer, F., Kubischik, M., Pekel, M., Lappe, M., Hoffmann, K.P., 1999a. Linear vestibular self-motion signals in monkey medial superior temporal area. Ann N Y Acad Sci 871, 272-281.

Bremmer, F., Kubischik, M., Pekel, M., Lappe, M., Hoffmann, K.P., 1999b. Linear Vestibular Self-Motion Signals in Monkey Medial Superior Temporal Area. Annals of the New York Academy of Sciences 871, 272-281.

Britten, K.H., van Wezel, R.J., 1998. Electrical microstimulation of cortical area MST biases heading perception in monkeys. Nat Neurosci 1, 59-63.

Britten, K.H., Van Wezel, R.J., 2002. Area MST and heading perception in macaque monkeys. Cereb Cortex 12, 692-701.

Busse, L., Roberts, K.C., Crist, R.E., Weissman, D.H., Woldorff, M.G., 2005. The spread of attention across modalities and space in a multisensory object. Proceedings of the National Academy of Sciences of the United States of America 102, 18751-18756.

Butler, J.S., Smith, S.T., Campos, J.L., Bulthoff, H.H., 2010. Bayesian integration of visual and vestibular signals for heading. J Vis 10, 23.

Cardin, V., Smith, A.T., 2009. Sensitivity of Human Visual and Vestibular Cortical Regions to Egomotion-Compatible Visual Stimulation. Cereb. Cortex, bhp268.

CDC, 2006. Fatalities and Injuries from Falls Among Older Adults -- United States, 1993--2003 and 2001--2005. Morbidity and Mortality Weekly Report 55, 1221-1224.

Chen, A., Deangelis, G.C., Angelaki, D.E., 2010. Macaque parieto-insular vestibular cortex: responses to self-motion and optic flow. J Neurosci 30.

Chen, Y.-C., Duann, J.-R., Lin, C.-L., Chuang, S.-W., Jung, T.-P., Lin, C.-T., 2009. Motion-Sickness Related Brain Areas and EEG Power Activates. pp. 348-354.

Chiappa, K.H., 1997. Evoked Potentials in Clinical Medicine. Lippincroft-Raven, New York.

Clark, V.P., Fannon, S., Lai, S., Benson, R., Bauer, L., 2000. Responses to Rare Visual Target and Distractor Stimuli Using Event-Related fMRI. Journal of Neurophysiology 83, 3133-3139.

Cohen, H., Cohen, B., Raphan, T., Waespe, W., 1992. Habituation and adaptation of the vestibuloocular reflex: a model of differential control by the vestibulocerebellum. Experimental Brain Research 90, 526-538.

Cohen, B., Martinelli, G., Ogorodnikov, D., Xiang, Y., Raphan, T., Holstein, G., Yakushin, S., 2011. Sinusoidal galvanic vestibular stimulation (sGVS) induces a vasovagal response in the rat. Experimental Brain Research 210, 45-55.

Comerchero, M.D., Polich, J., 1999. P3a and P3b from typical auditory and visual stimuli. Clinical Neurophysiology 110, 24-30.

Cooke, J.D., Brown, S.H., 1990. Movement-related phasic muscle activation. II. Generation and functional role of the triphasic pattern. Journal of Neurophysiology 63, 465-472.

Corby, J.C., Kopell, B.S., 1972. Differential Contributions of Blinks and Vertical Eye Movements as Artifacts in EEG Recording. Psychophysiology 9, 640-644.

Croft, R.J., Barry, R.J., 2000. Removal of ocular artifact from the EEG: a review. Neurophysiologie Clinique/Clinical Neurophysiology 30, 5-19.

Curthoys, I.S., Halmagyi, G.M., 1995. Vestibular compensation: a review of the oculomotor, neural, and clinical consequences of unilateral vestibular loss. Journal of vestibular research : equilibrium & orientation 5, 67-107.

David, O., Kilner, J.M., Friston, K.J., 2006. Mechanisms of evoked and induced responses in MEG/EEG. Neuroimage 31, 1580-1591.

de Winkel, K.N., Weesie, J., Werkhoven, P.J., Groen, E.L., 2010. Integration of visual and inertial cues in perceived heading of self-motion. J Vis 10, 1.

Deecke, L., Schwarz, D.W.F., Fredrickson, J.M., 1974. Nucleus ventroposterior inferior (VPI) as the vestibular thalamic relay in the rhesus monkey I. Field potential investigation. Experimental Brain Research 20, 88-100.

Delorme, A., Makeig, S., 2004. EEGLAB: an open source toolbox for analysis of single-trial EEG dynamics including independent component analysis. Journal of Neuroscience Methods 134, 9-21.

Delorme, A., Sejnowski, T.J., Makeig, S., 2007. Enhanced detection of artifacts in EEG data using higher-order statistics and independent component analysis. Neuroimage 34, 1443–1449.

Demêmes, D., Wenthold, R.J., Moniot, B., Sans, A., 1990. Glutamate-like immunoreactivity in the peripheral vestibular system of mammals. Hearing Research 46, 261-269.

Di Russo, F., Martínez, A., Hillyard, S.A., 2003. Source Analysis of Event-related Cortical Activity during Visuo-spatial Attention. Cerebral Cortex 13, 486-499.

Diederich, A., Colonius, H., Schomburg, A., 2008. Assessing age-related multisensory enhancement with the time-window-of-integration model. Neuropsychologia 46, 2556-2562.

Dierks, T., Jelic, V., Pascual-Marqui, R.D., Wahlund, L.-O., Julin, P., Linden, D.E.J., Maurer, K., Winblad, B., Nordberg, A., 2000. Spatial pattern of cerebral glucose metabolism (PET) correlates with localization of intracerebral EEG-generators in Alzheimer's disease. Clinical Neurophysiology 111, 1817-1824.

Dieterich, M., Bartenstein, P., Spiegel, S., Bense, S., Schwaiger, M., Brandt, T., 2005. Thalamic infarctions cause side-specific suppression of vestibular cortex activations. Brain 128, 2052-2067.

Dieterich, M., Bense, S., Lutz, S., Drzezga, A., Stephan, T., Bartenstein, P., Brandt, T., 2003. Dominance for Vestibular Cortical Function in the Non-dominant Hemisphere. Cereb. Cortex 13, 994-1007.

Dieterich, M., Brandt, T., 2008. Functional brain imaging of peripheral and central vestibular disorders. Brain 131, 2538-2552.

Dix, M.R., Hallpike, C.S., 1952. The pathology symptomatology and diagnosis of certain common disorders of the vestibular system. Proc R Soc Med 45, 341-354.

Drago, F., Nardo, L., Rampello, L., Raffaele, R., 1996. Vestibular Compensation in Aged Rats with Unilateral Labyrinthectomy Treated with Dopaminergic Drugs. Pharmacological Research 33, 135-140.

Duffy, C.J., 1998. MST Neurons Respond to Optic Flow and Translational Movement. Journal of Neurophysiology 80, 1816-1827.

Duffy, C.J., Wurtz, R.H., 1991a. Sensitivity of MST neurons to optic flow stimuli. I. A continuum of response selectivity to large-field stimuli. J Neurophysiol 65, 1329-1345.

Duffy, C.J., Wurtz, R.H., 1991b. Sensitivity of MST neurons to optic flow stimuli. II. Mechanisms of response selectivity revealed by small-field stimuli. J Neurophysiol 65, 1346-1359.

Dutia, M.B., Price, R.F., 1987. Interaction between the vestibulo-collic reflex and the cervico-collic stretch reflex in the decerebrate cat. The Journal of Physiology 387, 19-30.

Eickhoff, S.B., Weiss, P.H., Amunts, K., Fink, G.R., Zilles, K., 2006. Identifying human parieto-insular vestibular cortex using fMRI and cytoarchitectonic mapping. Human Brain Mapping 27, 611-621.

Ellingson, M.L., Liebenthal, E., Spanaki, M.V., Prieto, T.E., Binder, J.R., Ropella, K.M., 2004. Ballistocardiogram artifact reduction in the simultaneous acquisition of auditory ERPS and fMRI. Neuroimage 22, 1534-1542.

Englander, F., Hodson, T.J., Terregrossa, R.A., 1996. Economic dimensions of slip and fall injuries. J Forensic Sci 41, 733-746.

Evans, A., Collins, D., MIlls, S., Brown, E., Kelly, R., Peters, T., 1993. 3D statistical neuroanatomical models from 305 MRI volumes. Proceedings of IEEE-Nuclear Science Symposium and Medical Imaging Conference, pp. 1813–1817.

Fasold, O., von Brevern, M., Kuhberg, M., Ploner, C.J., Villringer, A., Lempert, T., Wenzel, R., 2002. Human Vestibular Cortex as Identified with Caloric Stimulation in Functional Magnetic Resonance Imaging. Neuroimage 17, 1384-1393.

Ferber-Viart, C., Duclaux, R., Colleaux, B., Dubreuil, C., 1997. Myogenic Vestibular-Evoked Potentials in Normal Subjects: A Comparison Between Responses Obtained from Sternomastoid and Trapezius Muscles. Acta Oto-laryngologica 117, 472-481.

Ferree, T.C., Clay, M.T., Tucker, D.M., 2001. The spatial resolution of scalp EEG. Neurocomputing 38-40, 1209-1216.

Fetsch, C.R., DeAngelis, G.C., Angelaki, D.E., 2010. Visual–vestibular cue integration for heading perception: applications of optimal cue integration theory. European Journal of Neuroscience 31, 1721-1729.

Fetsch, C.R., Turner, A.H., DeAngelis, G.C., Angelaki, D.E., 2009. Dynamic Reweighting of Visual and Vestibular Cues during Self-Motion Perception. J. Neurosci. 29, 15601-15612.

Fetsch, C.R., Wang, S., Gu, Y., Deangelis, G.C., Angelaki, D.E., 2007. Spatial reference frames of visual, vestibular, and multimodal heading signals in the dorsal subdivision of the medial superior temporal area. J Neurosci 27, 700-712.

Fetter, M., Aw, S., Haslwanter, T., Heimberger, J., Dichgans, J., 1998. Three-Dimensional Eye Movement Analysis During Caloric Stimulation Used to Test Vertical Semicircular Canal Function. Otology & Neurotology 19, 180-187.

Freeman, W.J., Holmes, M.D., Burke, B.C., Vanhatalo, S., 2003. Spatial spectra of scalp EEG and EMG from awake humans. Clinical Neurophysiology 114, 1053-1068.

Friberg, U., Stahle, J., Svedberg, A., 1983. The Natural Course of Meniere's Disease. Acta Oto-laryngologica 96, 72-77.

Frissen, I., Campos, J., Souman, J., Ernst, M., 2011. Integration of vestibular and proprioceptive signals for spatial updating. Experimental Brain Research 212, 163-176.

Friston, K.J., Buchel, C., 2003. Statistical Parametric Mapping: The Analysis of Functional Brain Images. Academic Press.

Furman, J.M., Müller, M.L.T.M., Redfern, M.S., Jennings, J.R., 2003. Visual-vestibular stimulation interferes with information processing in young and older humans. Experimental Brain Research 152, 383-392.

Garrido, M.I., Friston, K.J., Kiebel, S.J., Stephan, K.E., Baldeweg, T., Kilner, J.M., 2008. The functional anatomy of the MMN: A DCM study of the roving paradigm. Neuroimage 42, 936-944.

Gerson, A.D., Parra, L.C., Sajda, P., 2005. Cortical origins of response time variability during rapid discrimination of visual objects. Neuroimage 28, 342-353.

Giard, M.H., Peronnet, F., 1999. Auditory-Visual Integration during Multimodal Object Recognition in Humans: A Behavioral and Electrophysiological Study. Journal of Cognitive Neuroscience 11, 473-490.

Giardino, L., Zanni, M., Fernandez, M., Battaglia, A., Pignataro, O., Calzà, L., 2002. Plasticity of GABA(a) system during ageing: focus on vestibular compensation and possible pharmacological intervention. Brain Research 929, 76-86.

Gibbons, H., Stahl, J., 2007. Response-time corrected averaging of event-related potentials. Clinical Neurophysiology 118, 197-208.

Goncharova, I.I., McFarland, D.J., Vaughan, T.M., Wolpaw, J.R., 2003. EMG contamination of EEG: spectral and topographical characteristics. Clinical Neurophysiology 114, 1580-1593.

Grabherr, L., Cuffel, C., Guyot, J.-P., Mast, F., 2011. Mental transformation abilities in patients with unilateral and bilateral vestibular loss. Experimental Brain Research 209, 205-214.

Gramann, K., Gwin, J.T., Bigdely-Shamlo, N., Ferris, D.P., Makeig, S., 2010. Visual evoked responses during standing and walking. Frontiers in Human Neuroscience 4.

Graziano, M.S.A., 1999. Where is my arm? The relative role of vision and proprioception in the neuronal representation of limb position. Proceedings of the National Academy of Sciences 96, 10418-10421.

Green, A.M., Angelaki, D.E., 2003. Resolution of Sensory Ambiguities for Gaze Stabilization Requires a Second Neural Integrator. The Journal of Neuroscience 23, 9265-9275.

Greenblatt, R.E., Ossadtchi, A., Pflieger, M.E., 2005. Local Linear Estimators for the Bioelectromagnetic Inverse Problem. Trans. Sig. Proc. 53, 3403-3412.

Grefkes, C., Fink, G.R., 2005. REVIEW: The functional organization of the intraparietal sulcus in humans and monkeys. Journal of Anatomy 207, 3-17.

Grüsser, O.J., Pause, M., Schreiter, U., 1990. Localization and responses of neurones in the parieto-insular vestibular cortex of awake monkeys (Macaca fascicularis). The Journal of Physiology 430, 537-557.

Gu, Y., Angelaki, D.E., DeAngelis, G.C., 2008. Neural correlates of multisensory cue integration in macaque MSTd.

Gu, Y., DeAngelis, G.C., Angelaki, D.E., 2007. A functional link between area MSTd and heading perception based on vestibular signals. Nat Neurosci 10, 1038-1047.

Gu, Y., Watkins, P.V., Angelaki, D.E., DeAngelis, G.C., 2006. Visual and nonvisual contributions to three-dimensional heading selectivity in the medial superior temporal area. J Neurosci 26, 73-85.

Guzman-Lopez, J., Silvanto, J., Yousif, N., Nousi, S., Quadir, S., Seemungal, B.M., 2011. Probing V5/MT excitability with transcranial magnetic stimulation following visual motion adaptation to random and coherent motion. Annals of the New York Academy of Sciences 1233, 200-207.

Gwin, J.T., Gramann, K., Makeig, S., Ferris, D.P., 2010. Removal of Movement Artifact From High-Density EEG Recorded During Walking and Running. Journal of Neurophysiology 103, 3526-3534.

Halgren, E., Baudena, P., Clarke, J.M., Heit, G., Liegeois, C., Chauvel, P., Musolino, A., 1995. Intracerebral potentials to rare target and distractor auditory and visual stimuli. I. Superior temporal plane and parietal lobe. Electroencephalogr Clin Neurophysiol 94, 191-220.

Handy, T.C., Grafton, S.T., Shroff, N.M., Ketay, S., Gazzaniga, M.S., 2003. Graspable objects grab attention when the potential for action is recognized. Nat Neurosci 6, 421-427.

Harris, L.R., Jenkin, M., Zikovitz, D.C., 2000. Visual and non-visual cues in the perception of linear self-motion. Exp Brain Res 135, 12-21.

Heinrich, S., Rapp, K., Rissmann, U., Becker, C., König, H.H., 2010. Cost of falls in old age: a systematic review. Osteoporosis International 21, 891-902.

Highstein, S.M., Fay, R.R., Popper, A.N., 2004. The Vestibular System.

Highstein, S.M., McCrea, R.A., 1988. The anatomy of the vestibular nuclei. Rev Oculomot Res 2, 177-202.

Hirvonen, T.P., Aalto, H., Pyykkö, I., Juhola, M., Jänttil, P., 1997. Changes in Vestibulo-ocular Reflex of Elderly People. Acta Oto-laryngologica 117, 108-110.

Hofferberth, B., 1983. Evoked Potentials to Rotatory Stimulation: Preliminary Results. Acta Oto-laryngologica 96, 134-136.

Hofferberth, B., 1995. The Clinical Significance of Vestibular Evoked Potentials (REP). Acta Oto-laryngologica 115, 124-125.

Hoffmann, S., Falkenstein, M., 2008. The Correction of Eye Blink Artefacts in the EEG: A Comparison of Two Prominent Methods. PLoS ONE 3, e3004.

Holstein, G.R., Martinelli, G.P., Friedrich, V.L., 2011. Anatomical observations of the caudal vestibulo-sympathetic pathway. Journal of Vestibular Research 21, 49-62.

Hood, J.D., Kayan, A., 1985. Observations upon the evoked responses to natural vestibular stimulation. Electroencephalography and Clinical Neurophysiology/Evoked Potentials Section 62, 266-276.

Horn, H., Syed, N., Lanfermann, H., Maurer, K., Dierks, T., 2003. Cerebral networks linked to the event-related potential P300. European Archives of Psychiatry and Clinical Neuroscience 253, 154-159.

Horváth, J., Czigler, I., Winkler, I., Teder-Sälejärvi, W.A., 2007. The temporal window of integration in elderly and young adults. Neurobiology of Aging 28, 964-975.

Hughes, C.A., Proctor, L., 1997. Benign Paroxysmal Positional Vertigo. The Laryngoscope 107, 607-613.

Huang, N.E., Shen, Z., Long, S.R., Wu, M.C., Shih, H.H., Zheng, Q., Yen, N.-C., Tung, C.C., Liu, H.H., 1998. The empirical mode decomposition and the Hilbert spectrum for nonlinear and non-stationary time series analysis. Proceedings of the Royal Society of London. Series A: Mathematical, Physical and Engineering Sciences 454, 903-995.

Huiskamp, G.J., 2005. Reduction of the Ballistocardiogram Artifact in Simultaneous EEG-fMRI using ICA. Conf Proc IEEE Eng Med Biol Soc 4, 3691-3694.

Hyvarinen, A., 1999. Fast and robust fixed-point algorithms for independent component analysis. Neural Networks, IEEE Transactions on 10, 626-634.

Ilgin, N., Olgunturk, R., Kula, S., Turan, L., Tunaoglu, S., Temiz, H., Gokcora, N., Gucuyener, K., 2005. Brain perfusion assessed by 99mTc-ECD SPECT imaging in pediatric patients with neurally mediated reflex syncope. Pacing Clin Electrophysiol 28, 534-539.

Israel, I., Rivaud, S., Gaymard, B., Berthoz, A., Pierrotdeseilligny, C., 1995. Cortical Control of Vestibular-Guided Saccades in Man. Brain 118, 1169-1183.

Ito, J., Takamatsu, N., Kitagawa, J., Kimura, J., 1995. Somatosensory P3 and auditory P3 components of event-related potentials (ERPs) in healthy subjects and patients with dementia. Pathophysiology 2, 61-66.

Jeka, J.J., Allison, L.K., Kiemel, T., 2010. The Dynamics of Visual Reweighting in Healthy and Fall-Prone Older Adults. Journal of Motor Behavior 42, 197-208.

Jeong, S.-H., Oh, S.-Y., Kim, H.-J., Koo, J.-W., Kim, J., 2010. Vestibular dysfunction in migraine: effects of associated vertigo and motion sickness. Journal of Neurology 257, 905-912.

Juckel, G., Clotz, F., Frodl, T., Kawohl, W., Hampel, H., Pogarell, O., Hegerl, U., 2008. Diagnostic Usefulness of Cognitive Auditory Event-Related P300 Subcomponents in Patients With Alzheimers Disease? Journal of Clinical Neurophysiology June 25, 147-152.

Jung, T.-P., Humphries, C., Lee, T.-W., Makeig, S., McKeown, M.J., Iragui, V., Sejnowski, T.J., 1998. Extended ICA removes artifacts from electroencephalographic recordings. Proceedings of the 1997 conference on Advances in neural information processing systems 10. MIT Press, Denver, Colorado, United States.

Jung, T.-P., Makeig, S., Humphries, C., Lee, T.-W., McKeown, M.J., Iragui, V., Sejnowski, T.J., 2000. Removing electroencephalographic artifacts by blind source separation. Psychophysiology 37, 163-178.

Junghöfer, M., Elbert, T., Tucker, D.M., Rockstroh, B., 2000. Statistical control of artifacts in dense array EEG / MEG studies. Psychophysiology 37, 523–532.

Jurgens, R., Becker, W., 2006. Perception of angular displacement without landmarks: evidence for Bayesian fusion of vestibular, optokinetic, podokinesthetic, and cognitive information. Exp Brain Res 174, 528-543.

Kappenman, E.S., Luck, S.J., 2010. The effects of electrode impedance on data quality and statistical significance in ERP recordings. Psychophysiology 47, 888-904.

Kast, R., Lankford, J.E., 1986. Otolithic Evoked Potentials: A New Technique for Vestibular Studies. Acta Oto-laryngologica 102, 175-178.

Katayama, J., Polich, J., 1996. P300 from one-, two-, and three-stimulus auditory paradigms. International Journal of Psychophysiology 23, 33-40.

Katayama, J.i., Polich, J., 1999. Auditory and visual P300 topography from a 3 stimulus paradigm. Clinical Neurophysiology 110, 463-468.

Kenny, R.A., 2003. Syncope in the Elderly. Journal of Cardiovascular Electrophysiology 14, S74-S77.

Keshner, E., Baker, J., Banovetz, J., Peterson, B., 1992. Patterns of neck muscle activation in cats during reflex and voluntary head movements. Experimental Brain Research 88, 361-374.

Keshner, E.A., 2003. Head-Trunk Coordination During Linear Anterior-Posterior Translations. Journal of Neurophysiology 89, 1891-1901.

Kiiski, H., Lonergan, R., Whelan, R., Nolan, H., Kinsella, K., O'Brien, M., Reilly, R.B., Hutchinson, M., N., T., 2009. P3 Abnormalities in Multiple Sclerosis as a Function of Oligoadenylate Synthetase Genotype. Neuroscience Ireland, Dublin, Ireland, p. 87.

Kiiski, H., Reilly, R., Lonergan, R., Kelly, S., O'Brien, M., Kinsella, K., Bramham, J., Burke, T., O'Donnchadha, S., Nolan, H., 2011a. Change in PASAT performance correlates with change in P3 ERP amplitude over a 12-month period in multiple sclerosis patients. Journal of the neurological sciences.

Kiiski, H., Whelan, R., Lonergan, R., Nolan, H., Kinsella, K., Hutchinson, M., Tubridy, N., Reilly, R., 2011b. Preliminary evidence for correlation between PASAT performance and P3a and P3b amplitudes in progressive multiple sclerosis. European Journal of Neurology 18, 792-795.

Kiiski, H., Whelan, R., Lonergan, R., Nolan, H., Kinsella, K., Hutchinson, M., Tubridy, N., Reilly, R.B., 2010. Preliminary evidence for correlation between PASAT performance and P3a and P3b amplitudes in progressive multiple sclerosis. European Journal of Neurology, no-no.

Kleine, J.F., Guldin, W.O., Clarke, A.H., 1999. Variable otolith contribution to the galvanically induced vestibulo-ocular reflex. NeuroReport 10, 1143-1148.

Klimesch, W., Sauseng, P., Hanslmayr, S., 2007. EEG alpha oscillations: The inhibition–timing hypothesis. Brain Research Reviews 53, 63-88.

Kluge, M., Beyenburg, S., Fernández, G., Elger, C.E., 2000. Epileptic vertigo: Evidence for vestibular representation in human frontal cortex. Neurology 55, 1906-1908.

Knight, R.T., Scabini, D., Woods, D.L., Clayworth, C.C., 1989. Contributions of temporal-parietal junction to the human auditory P3. Brain Research 502, 109-116.

Kolchev, C., 1995. Vestibular Late Evoked Potentials (VbEP) Processed by Means of Brain Electrical Activity Mapping (BEAM). Acta Oto-laryngologica 115, 130-133.

Konrad, P., 2005. The ABC of EMG. Noraxon INC. USA.

Kosma, A., Nazarpour, K., Sanei, S., 2009. Removal of ballistocardiogram artifact from electroencephalograms exploiting heart rate variability. Proceedings of the 16th

international conference on Digital Signal Processing. IEEE Press, Santorini, Greece, pp. 272-275.

Kovacs, G., Raabe, M., Greenlee, M.W., 2007. Neural Correlates of Visually Induced Self-Motion Illusion in Depth. Cereb. Cortex, bhm203.

Kovacs, G., Raabe, M., Greenlee, M.W., 2008. Neural correlates of visually induced self-motion illusion in depth. Cerebral Cortex 18, 1779-1787.

Kozlowski, D., Byrdziak, P., Krupa, W., Gawrysiak, M., Piwko, G., Kubica, J., Swiatecka, G., 2003. Left ventricle systolic volume in vasovagal syncope patients. Folia Morphol (Warsz) 62, 175-178.

Kristinsdottir, E.K., Jarnlo, G.B., Magnusson, M., 2000. Asymmetric vestibular function in the elderly might be a significant contributor to hip fractures. Scandinavian journal of rehabilitation medicine 32, 56-60.

Kuramochi, R., Kimura, T., Nakazawa, K., Akai, M., Torii, S., Suzuki, S., 2004. Anticipatory modulation of neck muscle reflex responses induced by mechanical perturbations of the human forehead. Neuroscience Letters 366, 206-210.

Lagae, L., Maes, H., Raiguel, S., Xiao, D.K., Orban, G.A., 1994. Responses of macaque STS neurons to optic flow components: a comparison of areas MT and MST. Journal of Neurophysiology 71, 1597-1626.

Lalor, E.C., Pearlmutter, B.A., Reilly, R.B., McDarby, G., Foxe, J.J., 2006. The VESPA: A method for the rapid estimation of a visual evoked potential. Neuroimage 32, 1549-1561.

Lalor, E.C., Power, A.J., Reilly, R.B., Foxe, J.J., 2009. Resolving Precise Temporal Processing Properties of the Auditory System Using Continuous Stimuli. Journal of Neurophysiology 102, 349-359.

Lappe, M., Bremmer, F., Pekel, M., Thiele, A., Hoffmann, K.P., 1996. Optic flow processing in monkey STS: a theoretical and experimental approach. J Neurosci 16, 6265-6285.

Lappe, M., Grigo, A., 1999. How stereovision interacts with optic flow perception: neural mechanisms. Neural Netw 12, 1325-1329.

Lau, K.L., Glover, R.G., Linkenhoker, B., Wylie, D.R.W., 1998. Topographical organization of inferior olive cells projecting to translation and rotation zones in the vestibulocerebellum of pigeons. Neuroscience 85, 605-614.

Laurienti, P.J., Burdette, J.H., Maldjian, J.A., Wallace, M.T., 2006. Enhanced multisensory integration in older adults. Neurobiology of Aging 27, 1155-1163.

Lehmann, D., Skrandies, W., 1980. Reference-free identification of components of checkerboard-evoked multichannel potential fields. Electroencephalography and Clinical Neurophysiology 48, 609-621.

Liedgren, S.R.C., Schwarz, D.W.F., 1976. Vestibular Evoked Potentials in Thalamus and Basal Ganglia of the Squirrel Monkey (Saimiri Sciureus). Acta Oto-laryngologica 81, 73-82.

Lin, C.-T., Ko, L.-W., Lin, Y.-H., Jung, T.-P., Liang, S.-F., Hsiao, L.-S., 2007. EEG Activities of Dynamic Stimulation in VR Driving Motion Simulator. Engineering Psychology and Cognitive Ergonomics, pp. 551-560.

Linden, D.E.J., Prvulovic, D., Formisano, E., Völlinger, M., Zanella, F.E., Goebel, R., Dierks, T., 1999. The Functional Neuroanatomy of Target Detection: An fMRI Study of Visual and Auditory Oddball Tasks. Cerebral Cortex 9, 815-823.

Lobel, E., Kleine, J.F., Bihan, D.L., Leroy-Willig, A., Berthoz, A., 1998. Functional MRI of Galvanic Vestibular Stimulation. Journal of Neurophysiology 80, 2699-2709.

Lopez, C., Halje, P., Blanke, O., 2008. Body ownership and embodiment: Vestibular and multisensory mechanisms. Neurophysiologie Clinique/Clinical Neurophysiology 38, 149-161.

Lopez, C., Blanke, O., 2011. The thalamocortical vestibular system in animals and humans. Brain Research Reviews 67, 119-146.

Lopez, C., Blanke, O., Mast, F.W., 2012. The human vestibular cortex revealed by coordinate-based activation likelihood estimation meta-analysis. Neuroscience 212, 159-179.

Macias, J.D., Massingale, S., Gerkin, R.D., 2005. Efficacy of Vestibular Rehabilitation Therapy in Reducing Falls. Otolaryngology - Head and Neck Surgery 133, 323-325.

MacNeilage, P.R., Banks, M.S., DeAngelis, G.C., Angelaki, D.E., 2010. Vestibular Heading Discrimination and Sensitivity to Linear Acceleration in Head and World Coordinates. The Journal of Neuroscience 30, 9084-9094.

Maeda, M., Shimazu, H., Shinoda, Y., 1972. Nature of synaptic events in cat abducens motoneurons at slow and quick phase of vestibular nystagmus. Journal of Neurophysiology 35, 279-296.

Mallinson, A.I., Longridge, N.S., 2004. Caloric response does not decline with age. Journal of Vestibular Research 14, 393-396.

Manchester, D., Woollacott, M., Zederbauer-Hylton, N., Marin, O., 1989. Visual, Vestibular and Somatosensory Contributions to Balance Control in the Older Adult. Journal of Gerontology 44, M118-M127.

Matheson, A.J., Darlington, C.L., Smith, P.F., 1999. Dizziness in the elderly and age-related degeneration of the vestibular system. NZ J Psychol 28, 10-16.

Matysiak, A., Kordecki, W., Sieluzycki, C., Zacharias, N., Heil, P., Konig, R., 2013. Variance stabilization for computing and comparing grand mean waveforms in MEG and EEG. Psychophysiology 50, 627-639.

McIntosh, S., Costa, D.D., Kenny, R.A., 1993. Outcome of an Integrated Approach to the Investigation of Dizziness, Falls and Syncope, in Elderly Patients Referred to a 'Syncope' Clinic. Age and Ageing 22, 53-58.

Meng, H., May, P.J., Dickman, J.D., Angelaki, D.E., 2007. Vestibular Signals in Primate Thalamus: Properties and Origins. J. Neurosci. 27, 13590-13602.

Menzies, J.R.W., Porrill, J., Dutia, M., Dean, P., 2010. Synaptic Plasticity in Medial Vestibular Nucleus Neurons: Comparison with Computational Requirements of VOR Adaptation. PLoS ONE 5, e13182.

Merfeld, D.M., Zupan, L.H., 2002. Neural Processing of Gravitoinertial Cues in Humans. III. Modeling Tilt and Translation Responses. Journal of Neurophysiology 87, 819-833.

Merfeld, D.M., Park, S., Gianna-Poulin, C., Black, F.O., Wood, S., 2005. Vestibular Perception and Action Employ Qualitatively Different Mechanisms. I. Frequency Response of VOR and Perceptual Responses During Translation and Tilt. Journal of Neurophysiology 94, 186-198.

Mergner, T., Glasauer, S., 1999. A Simple Model of Vestibular Canal-Otolith Signal Fusion. Annals of the New York Academy of Sciences 871, 430-434.

Mergner, T., Rosemeier, T., 1998. Interaction of vestibular, somatosensory and visual signals for postural control and motion perception under terrestrial and microgravity conditions—a conceptual model. Brain Research Reviews 28, 118-135.

Mielniczuk, J., Wojdy, P., 2007. Estimation of Hurst exponent revisited. Comput. Stat. Data Anal. 51, 4510-4525.

Min, B.K., Busch, N.A., Debener, S., Kranczioch, C., Hanslmayr, S., Engel, A.K., Herrmann, C.S., 2007. The best of both worlds: phase-reset of human EEG alpha activity and additive power contribute to ERP generation. Int J Psychophysiol 65, 58-68.

Mobascher, A., Brinkmeyer, J., Warbrick, T., Musso, F., Wittsack, H.J., Stoermer, R., Saleh, A., Schnitzler, A., Winterer, G., 2009. Fluctuations in electrodermal activity reveal variations in single trial brain responses to painful laser stimuli – A fMRI/EEG study. Neuroimage 44, 1081-1092.

Molholm, S., Ritter, W., Murray, M.M., Javitt, D.C., Schroeder, C.E., Foxe, J.J., 2002. Multisensory auditory–visual interactions during early sensory processing in humans: a high-density electrical mapping study. Cognitive Brain Research 14, 115-128.

Molinari, G.A., Mingrino, S., 1974. Cortical evoked responses to vestibular stimulation in man. The Journal of Laryngology & Otology 88, 515-521.

Molinari, G.A., 1975. Vagal responses to vestibular stimulation in the cat. ORL J Otorhinolaryngol Relat Spec 37, 129-137.

Monahan, K.D., Ray, C.A., 2002. Vestibulosympathetic reflex during orthostatic challenge in aging humans. Am J Physiol Regul Integr Comp Physiol 283, R1027-1032.

Montant, M., Romaiguère, P., Roll, J.-P., 2009. A new vibrator to stimulate muscle proprioceptors in fMRI. Human Brain Mapping 30, 990-997.

Moretti, D.V., Babiloni, F., Carducci, F., Cincotti, F., Remondini, E., Rossini, P.M., Salinari, S., Babiloni, C., 2003. Computerized processing of EEG-EOG-EMG artifacts for multi-centric studies in EEG oscillations and event-related potentials. International Journal of Psychophysiology 47, 199-216.

Morgan, C.D., Geisler, M.W., Covington, J.W., Polich, J., Murphy, C., 1999. Olfactory P3 in young and older adults. Psychophysiology 36, 281-287.

Morgan, C.D., Murphy, C., 2002. Olfactory event-related potentials in Alzheimer's disease. J Int Neuropsychol Soc 8, 753-763.

Mozolic, J.L., Hugenschmidt, C.E., Peiffer, A.M., Laurienti, P.J., 2012. Multisensory Integration and Aging. In: Murray MM, MT, W. (Eds.), The Neural Bases of Multisensory Processes. CRC Press, Boca Raton, Florida.

Mulert, C., Jäger, L., Schmitt, R., Bussfeld, P., Pogarell, O., Möller, H.-J., Juckel, G., Hegerl, U., 2004. Integration of fMRI and simultaneous EEG: towards a comprehensive understanding of localization and time-course of brain activity in target detection. Neuroimage 22, 83-94.

Muller, M., 1994. Semicircular Duct Dimensions and Sensitivity of the Vertebrate Vestibular System. Journal of Theoretical Biology 167, 239-256.

Naito, Y., Tateya, I., Hirano, S., Inoue, M., Funabiki, K., Toyoda, H., Ueno, M., Ishizu, K., Nagahama, Y., Fukuyama, H., Ito, J., 2003. Cortical correlates of vestibulo-ocular reflex modulation: a PET study. Brain 126, 1562-1578.

Negishi, M., Abildgaard, M., Nixon, T., Todd Constable, R., 2004. Removal of time-varying gradient artifacts from EEG data acquired during continuous fMRI. Clinical Neurophysiology 115, 2181-2192.

Newlands, S.D., Lin, N., Wei, M., 2009. Response Linearity of Alert Monkey Non-Eye Movement Vestibular Nucleus Neurons During Sinusoidal Yaw Rotation. Journal of Neurophysiology 102, 1388-1397.

Niazy, R.K., Beckmann, C.F., Iannetti, G.D., Brady, J.M., Smith, S.M., 2005. Removal of FMRI environment artifacts from EEG data using optimal basis sets. Neuroimage 28, 720-737.

Nichols, T., Hayasaka, S., 2003. Controlling the familywise error rate in functional neuroimaging: a comparative review. Statistical Methods in Medical Research 12, 419-446.

Nichols, T.E., Holmes, A.P., 2002. Nonparametric permutation tests for functional neuroimaging: A primer with examples. Human Brain Mapping 15, 1-25.

Niven, J.I., Hixson, W.C., Correia, M.J., 1966. Elicitation of Horizontal Nystagmus by Periodic Linear Acceleration. Acta Oto-laryngologica 62, 429-441.

Nutt, J.G., Bloem, B.R., Giladi, N., Hallett, M., Horak, F.B., Nieuwboer, A., 2011. Freezing of gait: moving forward on a mysterious clinical phenomenon. The Lancet Neurology 10, 734-744.

Ohmi, M., 1996. Egocentric perception through interaction among many sensory systems. Brain Res Cogn Brain Res 5, 87-96.

Okuma, Y., 2006. Freezing of gait in Parkinson's disease. Journal of Neurology 253, vii27-vii32.

Olbrich, S., Mulert, C., Karch, S., Trenner, M., Leicht, G., Pogarell, O., Hegerl, U., 2009. EEG-vigilance and BOLD effect during simultaneous EEG/fMRI measurement. Neuroimage 45, 319-332.

Oman, C.M., 1990. Motion sickness: a synthesis and evaluation of the sensory conflict theory. Canadian Journal of Physiology and Pharmacology 68, 294-303.

Oman, C.M., Lichtenberg, B.K., Money, K.E., McCoy, R.K., 1986. M.I.T./Canadian vestibular experiments on the Spacelab-1 mission: 4. Space motion sickness: symptoms, stimuli, and predictability. Experimental Brain Research 64, 316-334.

Onton, J., Makeig, S., Christa, N., Wolfgang, K., 2006. Information-based modeling of event-related brain dynamics. Progress in Brain Research. Elsevier, pp. 99-120.

Oostenveld, R., Praamstra, P., 2001. The five percent electrode system for high-resolution EEG and ERP measurements. Clinical Neurophysiology 112, 713-719.

Paige, G.D., 1994. Senescence of human visual-vestibular interactions: smooth pursuit, optokinetic, and vestibular control of eye movements with aging. Experimental Brain Research 98, 355-372.

Paige, G.D., Seidman, S.H., 1999. Characteristics of the VOR in Response to Linear Acceleration. Annals of the New York Academy of Sciences 871, 123-135.

Palmer, J.A., Makeig, S., Delgado, K.K., Rao, B.D., 2008. Newton method for the ICA mixture model. Acoustics, Speech and Signal Processing, 2008. ICASSP 2008. IEEE International Conference on, pp. 1805-1808.

Park, J.J., Tang, Y., Lopez, I., Ishiyama, A., 2001. Age-related change in the number of neurons in the human vestibular ganglion. The Journal of Comparative Neurology 431, 437-443.

Pascual-Marqui, R.D., 2002. Standardized low-resolution brain electromagnetic tomography (sLORETA): technical details. Methods Find Exp Clin Pharmacol 24 Suppl D, 5-12.

Pascual-Marqui, R.D., 2007. Discrete, 3D Distributed, Linear Imaging Methods of Electric Neuronal Activity. Part 1: Exact, Zero Error Localization. arXiv:0710.3341 [math-ph].

Pascual-Marqui, R.D., 2009. Theory of the EEG Inverse Problem, Chapter 5. In: Tong, S., Thakor, N.V. (Eds.), Quantitative EEG Analysis: Methods and Clinical Applications. Artech House, Boston.

Pascual-Marqui, R.D., Michel, C.M., Lehmann, D., 1994. Low resolution electromagnetic tomography: a new method for localizing electrical activity in the brain. International Journal of Psychophysiology 18, 49-65.

Paulin, M.G., Nelson, M.E., Bower, J.M., 1989. Dynamics of Compensatory Eye Movement Control: An Optimal Estimation Analysis of the Vestibulo-Ocular Reflex. International Journal of Neural Systems 1, 23 - 29.

Peterka, R.J., Black, F.O., Schoenhoff, M.B., 1990. Age-related changes in human vestibulo-ocular reflexes: sinusoidal rotation and caloric tests. J Vestib Res 1, 49-59.

Peuskens, H., Sunaert, S., Dupont, P., Van Hecke, P., Orban, G.A., 2001. Human Brain Regions Involved in Heading Estimation. The Journal of Neuroscience 21, 2451-2461.

Pfaltz, C.R., 1983. Vestibular Compensation: Physiological und Clinical Aspects. Acta Oto-laryngologica 95, 402-406.

Pizzagalli, D.A., Oakes, T.R., Fox, A.S., Chung, M.K., Larson, C.L., Abercrombie, H.C., Schaefer, S.M., Benca, R.M., Davidson, R.J., 2003. Functional but not structural subgenual prefrontal cortex abnormalities in melancholia. Mol Psychiatry 9, 393-405.

Polich, J., 1993. Cognitive Brain Potentials. Current Directions in Psychological Science 2, 175-179.

Polich, J., 1998. P300 Clinical Utility and Control of Variability. Journal of Clinical Neurophysiology 15, 14-33.

Polich, J., 2007. Updating P300: An integrative theory of P3a and P3b. Clinical Neurophysiology 118, 2128-2148.

Presacco, A., Goodman, R., Forrester, L., Contreras-Vidal, J.L., 2011. Neural decoding of treadmill walking from noninvasive electroencephalographic signals. Journal of Neurophysiology 106, 1875-1887.

Pyykkö, I., Aalto, H., Grönfors, T., Starck, J., Ishizaki, H., 1995. Vestibular Evoked Responses in Man: Methodological Aspects. Acta Oto-laryngologica 115, 117-119.

Ramat, S., Straumann, D., Zee, D.S., 2005. Interaural Translational VOR: Suppression, Enhancement, and Cognitive Control. Journal of Neurophysiology 94, 2391-2402.

Ramat, S., Bertolini, G., 2009. Estimating the time constants of the rVOR. A model-based study. Ann N Y Acad Sci 1164, 140-146.

Raphan, T., Cohen, B., 2002. The vestibulo-ocular reflex in three dimensions. Experimental Brain Research 145, 1-27.

Raphan, T., Wearne, S., Cohen, B., 1996. Modeling the Organization of the Linear and Angular Vestibulo-Ocular Reflexesa. Annals of the New York Academy of Sciences 781, 348-363.

Rauch, S.D., Velazquez-VillaseÑOr, L., Dimitri, P.S., Merchant, S.N., 2001. Decreasing Hair Cell Counts in Aging Humans. Annals of the New York Academy of Sciences 942, 220-227.

Rausch, M., Spengler, F., Eysel, U.T., 1998. Proprioception acts as the main source of input in human S-I activation experiments: a functional MRI study. NeuroReport 9, 2865-2868.

Ray, C.A., 2000. Interaction of the vestibular system and baroreflexes on sympathetic nerve activity in humans. American Journal of Physiology - Heart and Circulatory Physiology 279, H2399-H2404.

Ray, C.A., Monahan, K.D., 2002a. Aging Attenuates the Vestibulosympathetic Reflex in Humans. Circulation 105, 956-961.

Ray, C.A., Monahan, K.D., 2002b. The Vestibulosympathetic Reflex In Humans: Neural Interactions Between Cardiovascular Reflexes. Clinical and Experimental Pharmacology and Physiology 29, 98-102.

Redfern, M.S., Jennings, J.R., Martin, C., Furman, J.M., 2001. Attention influences sensory integration for postural control in older adults. Gait & Posture 14, 211-216.

Regan, D., Vincent, A., 1995. Visual processing of looming and time to contact throughout the visual field. Vision Research 35, 1845-1857.

Rinne, T., Bronstein, A.M., Rudge, P., Gresty, M.A., Luxon, L.M., 1998. Bilateral loss of vestibular function: clinical findings in 53 patients. Journal of Neurology 245, 314-321.

Ris, L., de Waele, C., Serafin, M., Vidal, P.P., Godaux, E., 1995. Neuronal activity in the ipsilateral vestibular nucleus following unilateral labyrinthectomy in the alert guinea pig. Journal of Neurophysiology 74, 2087-2099.

Robinson, D.A., 1981. The Use of Control Systems Analysis in the Neurophysiology of Eye Movements. Annual Review of Neuroscience 4, 463-503.

Rodionov, V., Elidan, J., Sohmer, H., 1996. Analysis of the middle latency evoked potentials to angular acceleration impulses in man. Electroencephalography and Clinical Neurophysiology/Evoked Potentials Section 100, 354-361.

Rosenblad, A., 2009. B. F. J. Manly: Randomization, bootstrap and Monte Carlo methods in biology, third edition. Computational Statistics 24, 371-372.

Rosenhall, U., Rubin, W., 1975. Degenerative Changes in the Human Vestibular Sensory Epithelia. Acta Oto-laryngologica 79, 67-80.

Roy, J.E., Cullen, K.E., 1998. A neural correlate for vestibulo-ocular reflex suppression during voluntary eye-head gaze shifts. Nat Neurosci 1, 404-410.

Roy, J.E., Cullen, K.E., 2003. Brain Stem Pursuit Pathways: Dissociating Visual, Vestibular, and Proprioceptive Inputs During Combined Eye-Head Gaze Tracking. Journal of Neurophysiology 90, 271-290.

Ruggiero, D.A., Mtui, E.P., Otake, K., Anwar, M., 1996. Vestibular afferents to the dorsal vagal complex: substrate for vestibular-autonomic interactions in the rat. Brain Research 743, 294-302.

Rullmann, M., Anwander, A., Dannhauer, M., Warfield, S.K., Duffy, F.H., Wolters, C.H., 2009. EEG source analysis of epileptiform activity using a 1 mm anisotropic hexahedra finite element head model. Neuroimage 44, 399-410.

Russo, F.D., Martínez, A., Sereno, M.I., Pitzalis, S., Hillyard, S.A., 2002. Cortical sources of the early components of the visual evoked potential. Human Brain Mapping 15, 95-111.

Sadeghi, S.G., Minor, L.B., Cullen, K.E., 2011. Multimodal Integration After Unilateral Labyrinthine Lesion: Single Vestibular Nuclei Neuron Responses and Implications for Postural Compensation. Journal of Neurophysiology 105, 661-673.

Salisbury, D.F., Rutherford, B., Shenton, M.E., McCarley, R.W., 2001. Button-pressing affects P300 amplitude and scalp topography. Clinical Neurophysiology 112, 1676-1684.

Santangelo, V., Van der Lubbe, R., Olivetti Belardinelli, M., Postma, A., 2008. Multisensory integration affects ERP components elicited by exogenous cues. Experimental Brain Research 185, 269-277.

Sarasin, F.P., Louis-Simonet, M., Carballo, D., Slama, S., Junod, A.-F., Unger, P.F., 2002. Prevalence of orthostatic hypotension among patients presenting with syncope in the ED. The American Journal of Emergency Medicine 20, 497-501.

Schlack, A., Hoffmann, K.P., Bremmer, F., 2002. Interaction of linear vestibular and visual stimulation in the macaque ventral intraparietal area (VIP). Eur J Neurosci 16, 1877-1886.

Schlindwein, P., Mueller, M., Bauermann, T., Brandt, T., Stoeter, P., Dieterich, M., 2008. Cortical representation of saccular vestibular stimulation: VEMPs in fMRI. Neuroimage 39, 19-31.

Schlögl, A., Keinrath, C., Zimmermann, D., Scherer, R., Leeb, R., Pfurtscheller, G., 2007. A fully automated correction method of EOG artifacts in EEG recordings. Clinical Neurophysiology 118, 98-104.

Schneider, D., Kolchev, C., Constantinescu, L., C.-F. Claussen, 1996. Vestibular Evoked Potentials and Brain Electrical Activity Mapping - A Test of Vestibular Function - A Review. International Tinnitus Journal 2, 27 - 43.

Schweigart, G., Chien, R.-D., Mergner, T., 2002. Neck proprioception compensates for age-related deterioration of vestibular self-motion perception. Experimental Brain Research 147, 89-97.

Seemungal, B.M., Guzman-Lopez, J., Arshad, Q., Schultz, S.R., Walsh, V., Yousif, N., 2013. Vestibular activation differentially modulates human early visual cortex and V5/MT excitability and response entropy. Cereb Cortex 23, 12-19.

Seidman, S.H., 2008. Translational motion perception and vestiboocular responses in the absence of non-inertial cues. Exp Brain Res 184, 13-29.

Seiss, E., Hesse, C.W., Drane, S., Oostenveld, R., Wing, A.M., Praamstra, P., 2002. Proprioception-Related Evoked Potentials: Origin and Sensitivity to Movement Parameters. Neuroimage 17, 461-468.

Seiss, E.S., Praamstra, P.P., Hesse, C.H., Rickards, H.R., 2003. Proprioceptive sensory function in Parkinson's disease and Huntington's disease: evidence from proprioception-related EEG potentials. Experimental Brain Research 148, 308-319.

Sekihara, K., Sahani, M., Nagarajan, S.S., 2005. Localization bias and spatial resolution of adaptive and non-adaptive spatial filters for MEG source reconstruction. Neuroimage 25, 1056-1067.

Serrador, J.M., Lipsitz, L.A., Gopalakrishnan, G.S., Black, F.O., Wood, S.J., 2009. Loss of otolith function with age is associated with increased postural sway measures. Neuroscience Letters 465, 10-15.

Setti, A., Burke, K., Kenny, R., Newell, F., 2011. Is inefficient multisensory processing associated with falls in older people? Experimental Brain Research 209, 375-384.

Séverac Cauquil, A., Faldon, M., Popov, K., Day, B.L., Bronstein, A.M., 2003. Short-latency eye movements evoked by near-threshold galvanic vestibular stimulation. Experimental Brain Research 148, 414-418.

Sharpe, J.A., Johnston, J.L., 1990. Vertigo and nystagmus. Current Opinion in Neurology 3, 789-795.

Sheliga, B.M., Yakushin, S.B., Silvers, A., Raphan, T., Cohen, B., 1999. Control of Spatial Orientation of the Angular Vestibulo-Ocular Reflex by the Nodulus and Uvula of the Vestibulocerebellum. Annals of the New York Academy of Sciences 871, 94-122.

Shenton, J.T., Schwoebel, J., Coslett, H.B., 2004. Mental motor imagery and the body schema: evidence for proprioceptive dominance. Neuroscience Letters 370, 19-24.

Shigemasu, H., Miyawaki, Y., Kamitani, Y., Kitazaki, M., 2007. Decoding heading directions from human cortical activity. Journal of Vision 7, 752.

Shlens, J., 2005. A Tutorial on Principal Component Analysis.

Siegler, I., Viaud-Delmon, I., Israel, I., Berthoz, A., 2000. Self-motion perception during a sequence of whole-body rotations in darkness. Experimental Brain Research 134, 66-73.

Simpson, J.I., Precht, W., Llinás, R., 1974. Sensory separation in climbing and mossy fiber inputs to cat vestibulocerebellum. Pflügers Archiv European Journal of Physiology 351, 183-193.

Sloane, P.D., Baloh, R.W., Honrubia, V., 1989. The vestibular system in the elderly: Clinical implications. American Journal of Otolaryngology 10, 422-429.

Smith, A.T., Wall, M.B., Thilo, K.V., 2011. Vestibular Inputs to Human Motion-Sensitive Visual Cortex. Cerebral Cortex.

Sousa, R.F.d., Gazzola, J.M., Ganança, M.M., Paulino, C.A., 2011. Correlação entre equilíbrio corporal e capacidade funcional de idosos com disfunções vestibulares crônicas. Brazilian Journal of Otorhinolaryngology 77, 791-798.

Srivastava, G., Crottaz-Herbette, S., Lau, K.M., Glover, G.H., Menon, V., 2005. ICA-based procedures for removing ballistocardiogram artifacts from EEG data acquired in the MRI scanner. Neuroimage 24, 50-60.

St George, R.J., Fitzpatrick, R.C., 2011. The sense of self-motion, orientation and balance explored by vestibular stimulation. The Journal of Physiology 589, 807-813.

Stanford, T.R., Stein, B.E., 2007. Superadditivity in multisensory integration: putting the computation in context. NeuroReport 18, 787-792 710.1097/WNR.1090b1013e3280c1091e1315.

Stephan, T., Deutschländer, A., Nolte, A., Schneider, E., Wiesmann, M., Brandt, T., Dieterich, M., 2005. Functional MRI of galvanic vestibular stimulation with alternating currents at different frequencies. Neuroimage 26, 721-732.

Stevens, A.A., Skudlarski, P., Gatenby, J.C., Gore, J.C., 2000. Event-related fMRI of auditory and visual oddball tasks. Magnetic Resonance Imaging 18, 495-502.

Stevens, J.A., Corso, P.S., Finkelstein, E.A., Miller, T.R., 2006. The costs of fatal and non-fatal falls among older adults. Injury Prevention 12, 290-295.

Stevens, J.C., Cruz, L.A., Marks, L.E., Lakatos, S., 1998. A Multimodal Assessment of Sensory Thresholds in Aging. The Journals of Gerontology Series B: Psychological Sciences and Social Sciences 53B, P263-P272.

Stewart, D., 1966. A Platform with Six Degrees of Freedom. Proceedins of the Institution of Mechanical Engineers 180, 371-386.

Straka, H., Dieringer, N., 1993. Electrophysiological and Pharmacological Characterization of Vestibular Inputs to Identified Frog Abducens Motoneurons and Internuclear Neurons In Vitro. European Journal of Neuroscience 5, 251-260.

Straka, H., Vibert, N., Vidal, P.P., Moore, L.E., Dutia, M.B., 2005. Intrinsic membrane properties of vertebrate vestibular neurons: Function, development and plasticity. Progress in Neurobiology 76, 349-392.

Suzuki, M., Kitano, H., Ito, R., Kitanishi, T., Yazawa, Y., Ogawa, T., Shiino, A., Kitajima, K., 2001. Cortical and subcortical vestibular response to caloric stimulation detected by functional magnetic resonance imaging. Cognitive Brain Research 12, 441-449.

Takahashi, K., Gu, Y., May, P.J., Newlands, S.D., DeAngelis, G.C., Angelaki, D.E., 2007. Multimodal coding of three-dimensional rotation and translation in area MSTd: comparison of visual and vestibular selectivity. J Neurosci 27, 9742-9756.

Teasdale, N., Simoneau, M., 2001. Attentional demands for postural control: the effects of aging and sensory reintegration. Gait & Posture 14, 203-210.

Telford, L., Howard, I.P., Ohmi, M., 1995. Heading judgments during active and passive self-motion. Exp Brain Res 104, 502-510.

Todd, N.P.M., Rosengren, S.M., Colebatch, J.G., 2008. A source analysis of short-latency vestibular evoked potentials produced by air- and bone-conducted sound. Clinical Neurophysiology 119, 1881-1894.

Tootell, R., Reppas, J., Kwong, K., Malach, R., Born, R., Brady, T., Rosen, B., Belliveau, J., 1995. Functional analysis of human MT and related visual cortical areas using magnetic resonance imaging. The Journal of Neuroscience 15, 3215-3230.

Tootell, R.B.H., Taylor, J.B., 1995. Anatomical Evidence for MT and Additional Cortical Visual Areas in Humans. Cerebral Cortex 5, 39-55.

Toulotte, C., Thevenon, A., Watelain, E., Fabre, C., 2006. Identification of healthy elderly fallers and non-fallers by gait analysis under dual-task conditions. Clinical Rehabilitation 20, 269-276.

van Wassenhove, V., Buonomano, D.V., Shimojo, S., Shams, L., 2008. Distortions of Subjective Time Perception Within and Across Senses. PLoS ONE 3, e1437.

Vitacco, D., Brandeis, D., Pascual-Marqui, R., Martin, E., 2002. Correspondence of event-related potential tomography and functional magnetic resonance imaging during language processing. Human Brain Mapping 17, 4-12.

Vitte, E., Derosier, C., Caritu, Y., Berthoz, A., Hasboun, D., Soulié, D., 1996. Activation of the hippocampal formation by vestibular stimulation: a functional magnetic resonance imaging study. Experimental Brain Research 112, 523-526.

Volpe, U., Mucci, A., Bucci, P., Merlotti, E., Galderisi, S., Maj, M., 2007. The cortical generators of P3a and P3b: A LORETA study. Brain Research Bulletin 73, 220-230.

von der Heyde, M., 2001. A Distributed Virtual Reality System for Spatial Updating: Concepts, Implementation, and Experiments. Technische Fakultät. Universität Bielefeld.

Vorobyov, S., Cichocki, A., 2002. Blind noise reduction for multisensory signals using ICA and subspace filtering, with application to EEG analysis. Biological Cybernetics 86, 293-303.

Wagner, M., Fuchs, M., Kastner, J., 2004. Evaluation of sLORETA in the Presence of Noise and Multiple Sources. Brain Topography 16, 277-280.

Wallis, G., Chatziastros, A., Bülthoff, H., 2002. An unexpected role for visual feedback in vehicle steering control. Curr Biol 12, 295-299.

Walsh, E.G., 1961. Role of the vestibular apparatus in the perception of motion on a parallel swing. The Journal of Physiology 155, 506-513.

Wardman, D.L., Fitzpatrick, R.C., 2002. What Does Galvanic Vestibular Stimulation Stimulate?

Sensorimotor Control of Movement and Posture. In: Gandevia, S.C., Proske, U., Stuart, D.G. (Eds.). Springer US, pp. 119-128.

Warren, W.H., Blackwell, A.W., Morris, M.W., 1989. Age Differences in Perceiving the Direction of Self-Motion From Optical Flow. Journal of Gerontology 44, P147-P153.

Warren, W.H., Jr., Morris, M.W., Kalish, M., 1988. Perception of translational heading from optical flow. J Exp Psychol Hum Percept Perform 14, 646-660.

Welch, P.D., 1967. The Use of Fast Fourier Transform for the Estimation of Power Spectra: A Method Based on Time Averaging Over Short, Modified Periodograms. IEEE Trans. Audio Electroacoustics, 70-73.

Whelan, R., Lonergan, R., Kiiski, H., Nolan, H., Kinsella, K., Bramham, J., O'Brien, M., Reilly, R., Hutchinson, M., Tubridy, N., 2010a. A high-density ERP study

reveals latency, amplitude, and topographical differences in multiple sclerosis patients versus controls. Clinical Neurophysiology 121, 1420-1426.

Whelan, R., Lonergan, R., Kiiski, H., Nolan, H., Kinsella, K., Hutchinson, M., Tubridy, N., Reilly, R., 2010b. Impaired information processing speed and attention allocation in multiple sclerosis patients versus controls: A high-density EEG study. Journal of the neurological sciences 293, 45-50.

Whelan, R., Lonergan, R., Kiiski, H., Nolan, H., Kinsella, K., Hutchinson, M., Tubridy, N., Reilly, R.B., 2010c. Impaired information processing speed and attention allocation in multiple sclerosis patients versus controls: A high-density EEG study. Journal of the neurological sciences 293, 45-50.

Wilson, V.J., 1991. Vestibulospinal and neck reflexes: interaction in the vestibular nuclei. Arch Ital Biol 129, 43-52.

Wilson, V.J., Boyle, R., Fukushima, K., Rose, P.K., Shinoda, Y., Sugiuchi, Y., Uchino, Y., 1995. The Vestibulocollic Reflex. J Vestib Res 5, 147-170.

Wilson, V.J., Yoshida, M., 1969. Monosynaptic inhibition of neck motoneurons by the medial vestibular nucleus. Experimental Brain Research 9, 365-380.

Wolfgang, K., 1999. EEG alpha and theta oscillations reflect cognitive and memory performance: a review and analysis. Brain Research Reviews 29, 169-195.

Worrell, G.A., Lagerlund, T.D., Sharbrough, F.W., Brinkmann, B.H., Busacker, N.E., Cicora, K.M., O'Brien, T.J., 2000. Localization of the Epileptic Focus by Low-Resolution Electromagnetic Tomography in Patients with a Lesion Demonstrated by MRI. Brain Topography 12, 273-282.

Worsley, K.J., Taylor, J.E., Tomaiuolo, F., Lerch, J., 2004. Unified univariate and multivariate random field theory. Neuroimage 23, Supplement 1, S189-S195.

Yagi, T., Kurosaki, S., Yamanobe, S., Morizono, T., 1992. Three-Component Analysis of Caloric Nystagmus in Humans. Archives of Otolaryngology–Head & Neck Surgery 118, 1077-1080.

Yandong, L., Zhongwei, M., Wenkai, L., Yanda, L., 2006. Automatic removal of the eye blink artifact from EEG using an ICA-based template matching approach. Physiological Measurement, 425.

Yen Pik Sang, F., Jáuregui-Renaud, K., Green, D.A., Bronstein, A.M., Gresty, M.A., 2006. Depersonalisation/derealisation symptoms in vestibular disease. Journal of Neurology, Neurosurgery & Psychiatry 77, 760-766.

Yordanova, J., Kolev, V., Polich, J., 2001. P300 and alpha event-related desynchronization (ERD). Psychophysiology 38, 143-152.

Yoshiura, T., Zhong, J., Shibata, D.K., Kwok, W.E., Shrier, D.A., Numaguchi, Y., 1999. Functional MRI study of auditory and visual oddball tasks. NeuroReport 10, 1683-1688.

Zelenin, P.V., Deliagina, T.G., Orlovsky, G.N., Karayannidou, A., Stout, E.E., Sirota, M.G., Beloozerova, I.N., 2011. Activity of motor cortex neurons during backward locomotion. Journal of Neurophysiology 105, 2698-2714.

Zennou-Azogui, Y., Xerri, C., Leonard, J., Tighilet, B., 1996. Vestibular compensation: role of visual motion cues in the recovery of posturo-kinetic functions in the cat. Behavioural Brain Research 74, 65-77.

Zhang, T., Heuer, H.W., Britten, K.H., 2004. Parietal Area VIP Neuronal Responses to Heading Stimuli Are Encoded in Head-Centered Coordinates. Neuron 42, 993-1001.

Zink, R., Bucher, S.F., Weiss, A., Brandt, T., Dieterich, M., 1998. Effects of galvanic vestibular stimulation on otolithic and semicircular canal eye movements and perceived vertical. Electroencephalography and Clinical Neurophysiology 107, 200-205.

zu Eulenburg, P., Caspers, S., Roski, C., Eickhoff, S.B., 2012. Meta-analytical definition and functional connectivity of the human vestibular cortex. Neuroimage 60, 162-169.

Zumsteg, D., Friedman, A., Wieser, H.G., Wennberg, R.A., 2006a. Propagation of interictal discharges in temporal lobe epilepsy: Correlation of spatiotemporal mapping with intracranial foramen ovale electrode recordings. Clinical neurophysiology : official journal of the International Federation of Clinical Neurophysiology 117, 2615-2626.

Zumsteg, D., Lozano, A.M., Wennberg, R.A., 2006b. Depth electrode recorded cerebral responses with deep brain stimulation of the anterior thalamus for epilepsy. Clinical neurophysiology : official journal of the International Federation of Clinical Neurophysiology 117, 1602-1609.

Zumsteg, D., Lozano, A.M., Wieser, H.G., Wennberg, R.A., 2006c. Cortical activation with deep brain stimulation of the anterior thalamus for epilepsy. Clinical neurophysiology : official journal of the International Federation of Clinical Neurophysiology 117, 192-207.

Zumsteg, D., Wennberg, R.A., Treyer, V., Buck, A., Wieser, H.G., 2005. H215O or 13NH3 PET and electromagnetic tomography (LORETA) during partial status epilepticus. Neurology 65, 1657-1660.

# Published Works